Università degli Studi di Cagliari

PHD DEGREE

PHD COURSE IN EARTH AND ENVIRONMENTAL SCIENCES AND TECHNOLOGIES (EEST)

Cycle XXXII

TITLE OF THE PHD THESIS

Numerical modeling of the pollutant spread and a web application for environmental monitoring to support mine reclamation activities

Scientific Disciplinary Sector(s)

GEO/06

PhD Student:	Pier Andrea Marras
Coordinator of the PhD Programme	Prof. Aldo Muntoni
Tutor	Prof. Giovanni de Giudici
Co-tutors	Dr. Pierluigi Cau

Final exam. Academic Year 2018 – 2019
Thesis defence: January-February 2020 Session

La tesi è stata prodotta durante la frequenza del corso di dottorato in Scienze e Tecnologie della Terra e dell'Ambiente dell'Università degli Studi di Cagliari, XXXII ciclo, con il supporto di una borsa di studio finanziata nell'ambito del Progetto Centro di Eccellenza per la Sostenibilità Ambientale – CESA

SUMMARY

Abstract

Heavy metal pollution is a serious and urgent issue of integrated watershed management in Sardinia and worldwide. To determine the effective management strategies for pollution control, it is essential to quantify the input and output fluxes of metal by analyzing the environmental system in all its main components. Numerical physically-based models can simulate the behavior of a system, such as a river's watershed, starting from the knowledges of the physical processes that occur in the studied area. In this work, the Rio San Giorgio basin was studied, due to the mining activities in the Iglesias Mine District, that caused severe pollution in the area. This area is in fact characterized by several mining areas, wastes and tailings, abandoned after centuries of intense mining activity, that mainly exploited minerals of Zn and Pb. SWAT hydrological model (Arnold et al., 1998) and SWAT Heavy Metal (HM) module (Meng et al., 2018) were used to simulate the fate and the transport of the Zn and Pb in the different mediums of the watershed system. Moreover, future simulations were run using Regional Climate Models of the Euro-CORDEX experiment (Giorgi et al., 2009) as climate forcing for the watershed models. This toolset allowed to simulate transport of Zn and Pb in the surface waters of Rio San Giorgio for a historical and a future period, with evaluation of some waste management scenarios. The general decrease of mean rainfall and the increase of extreme precipitation events projected by the RCMs for the future is well reflected in the results of the SWAT and SWAT-HM modellization. In fact, the mean loads of Zn and Pb in the river tend to a decrease, but extreme loads are projected for the future in occurrence of intense precipitations predicted by the RCMs models. A web-application (CESApp) Decision Support System (DSS) was also developed to share the results of the modeling, such as models' inputs, outputs and the different scenarios of the metals spread with researchers and stakeholders.

Chapter 1: Introduction

The increase in metals and pollutants in our environment is a main concern debated by the scientific community. Particularly, no threshold values are given at the global scale (Rockstrom et al. 2009) for chemical pollution to define a safe operating space for the humanity. Among the main challenges encountered in evaluating the effect of industrial activities on the environment, the reconstruction of recent increase in metals and pollutants related to industrial revolution is one of the points to be elucidated. National and EU regulations define thresholds for metals in environmental matrix. The threshold values given by the Italian decree 152/2006, are the chemical concentrations of elements that can be, as a first approximation, considered the safe conditions depending on the specific use of the areas. These chemical concentration values are often referred as the "environmental pressures" that the law can admit. However, environmental systems are complex systems where many different compartments co participate to the environmental processes that, definitively, define the impact of elements and pollutants on our environment. This holistic view of different environmental factors such as the weather conditions, the slope of the hills, the riverbed morphology, the vegetation of the land, the water quality and the presence of pollutant sources is part of the complexity science. Considering mine polluted areas, the interaction among the different factors of the environment should be studied at both watershed scale or at the microscopic scale (De Giudici et al. 2017; De Giudici et al. 2018; De Giudici et al. 2019). Moreover, these processes can be studied with a holistic approach by numerical simulations.

A numerical model is a combination of a large number of mathematical equations that can simulate the behavior of a system, such as a river's watershed, starting from the knowledges of the physical processes that occur in the studied area. To better understand the environmental behavior of heavy metals and the associated risks, watershed-scale, process-based numerical models are increasingly used (Meng et al., 2018; Velleux et al., 2006; Vink and Peters, 2003). Furthermore, spatially distributed models can provide an estimation of the simulated values all over the area, overcoming the problem of having spotted and spread measures that only describe specific site characteristics and make difficult to describe the whole system. Moreover, numerical simulation can be useful to calculate values for future weather conditions that cannot be given by other means. Using of numerical simulations can also be useful to simulate remediation actions or prevent pollutant dispersal processes. In fact, often, remediation technologies cannot be probed at a large scale, but

simulation can provide important lacking information about the applying conditions and the results of remediation actions. Fast and reliable estimates of the damages on the water quality due to pollution could play essential role in establishing governmental regulations for environmental protection (Kachiashvili et al., 2005).

In this work, the investigated study area was the Rio San Giorgio river's basin (southwest Sardinia). This area is characterized by several mining areas, wastes and tailings, abandoned after centuries of intense mining activity, that mainly exploited minerals of Pb and Zn. These mining residues contain significantly high concentrations of heavy metals such as Pb, Zn, Cd, Hg, As, generally with values above the Italian decree limits in soils, water, stream sediments and air (D.Lgs 152/2006). Although mining activities ceased almost 30 years ago, no remediation actions were carried out and the wastes are continuously exposed to weathering.

The purpose of this study was to create a toolkit, composed by numerical models and a user-friendly web interface, that can provide a long-term estimation of heavy metal dispersion, in particular Zn and Pb, in surface waters of the Rio San Giorgio watershed.

This toolkit is a Decision Support System (DSS) to support researcher and stakeholder in devising remediation activities and waste treatment. In detail, three kind of models were implemented: Soil and Water Assessment Tool (SWAT) hydrological model (Arnold et al., 1998), SWAT-Heavy Metal (SWAT-HM) metal module (Meng et al., 2018) and a set of Regional Climate Models (RCM) of the Euro-CORDEX experiment (Giorgi et al., 2009) in order to provide to the SWAT and SWAT-HM models the climate forcing for future projections.

This thesis is divided into four chapters. After the introduction, follows the materials and methods chapter. The third chapter is a paper entitled "Future precipitation in Sardinia and streamflow changes for a small basin using EURO-CORDEX regional climate simulations and the SWAT model" to be submitted. This paper focuses on application of numerical simulations on climate changes for the investigated area. The four chapter describes SWAT-HM numerical simulations: the approach, the results and how can these be used. The web based general tool, CESApp, is presented in the appendix, also this was part of my Ph.D project.

Study area

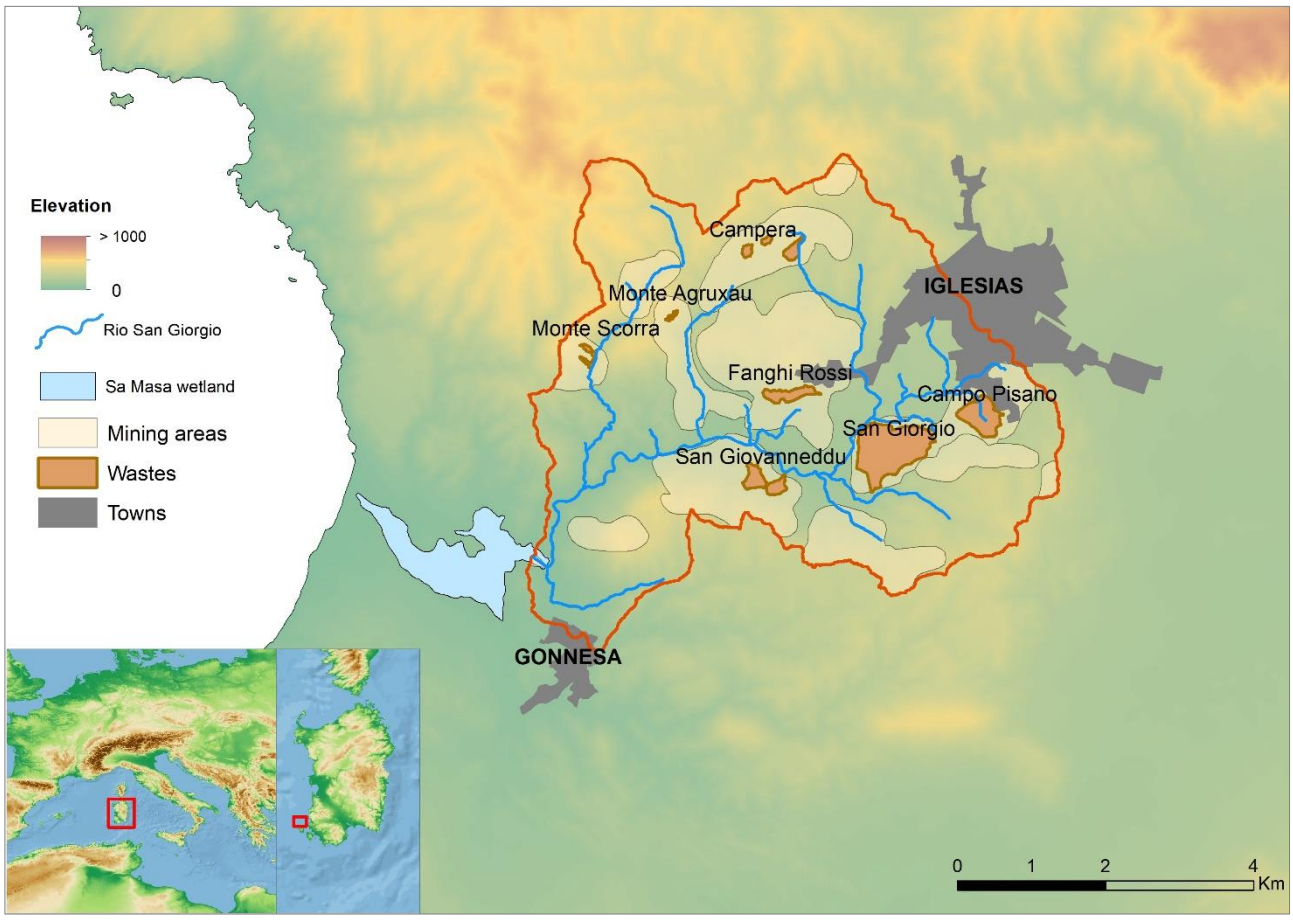

Figure 1 - Study area

Figure 2 - View of the Rio San Giorgio basin nearby the town of Iglesias

Geography and geomorphology

The study area is the catchment of the Rio San Giorgio (FIGURE 2), nearby the town of Iglesias (SW Sardinia) that has an area of around 3082 hectares (30,82 Km^2), with a maximum elevation of 630 m a.s.l. and an average of 320 m a.s.l. The landscape is strongly influenced by the tectonic structures of the area, in particular a huge synclinal called "Sinclinale di Iglesias", with high slopes in the northern portion of the basins and rounded hills in the southern part. Limestone rocks, that surround the basin due to the Sinclinale di Iglesias, interrupt the rounded hills with steeper slopes nearby San Giovanni Mine. Rio San Giorgio main flow path riverbed is set in the axial area of the fold.

Figure 3 - Campo Pisano waste

Sixteen abandoned mines occur in the Rio San Giorgio catchment area (IGEA, De Giudici et al., 2017) with hundreds of kilometers of tunnels and 5 main tailing dams: Campo Pisano (FIGURE 3), San Giorgio, San Giovanni, Monteponi Red Muds ("Fanghi Rossi") FIGURE 4 and Monti Agruxau. The Rio San Giorgio outlet is located in a wetland, Sa Masa, that has an area of around 75 ha.

Figure 4 - "Fanghi Rossi" dump at Monteponi abandoned mine

Geology

The Iglesiente area, located in the southwest Sardinia, has complex and important geological features with the oldest outcrops of the whole island that hosted rich metal deposits, among ones of the most important in Europe several years ago. Two main tectonic units were identified in the area: an “autochthonous” unit and a “allochtonous” unit, both involved in the Ercinic orogenesis. The autochthonous unit is mostly composed by Cambrian tidal carbonates (Bechstädt et al., 1988; Pillola et al., 1991), the allochthonous unit, instead, is mostly composed by terrigenous rocks that overthrusted the autochthonous unit from north-east to south-west during Hercynian orogeny (Carmignani et al., 1982). Tectonic features make difficult to reconstruct a detailed paleogeography of this area, due to different compressional phases and interferences. The Rio San Giorgio basin is mostly set on Paleozoic rocks ranging from lower Cambrian to upper Ordovician.

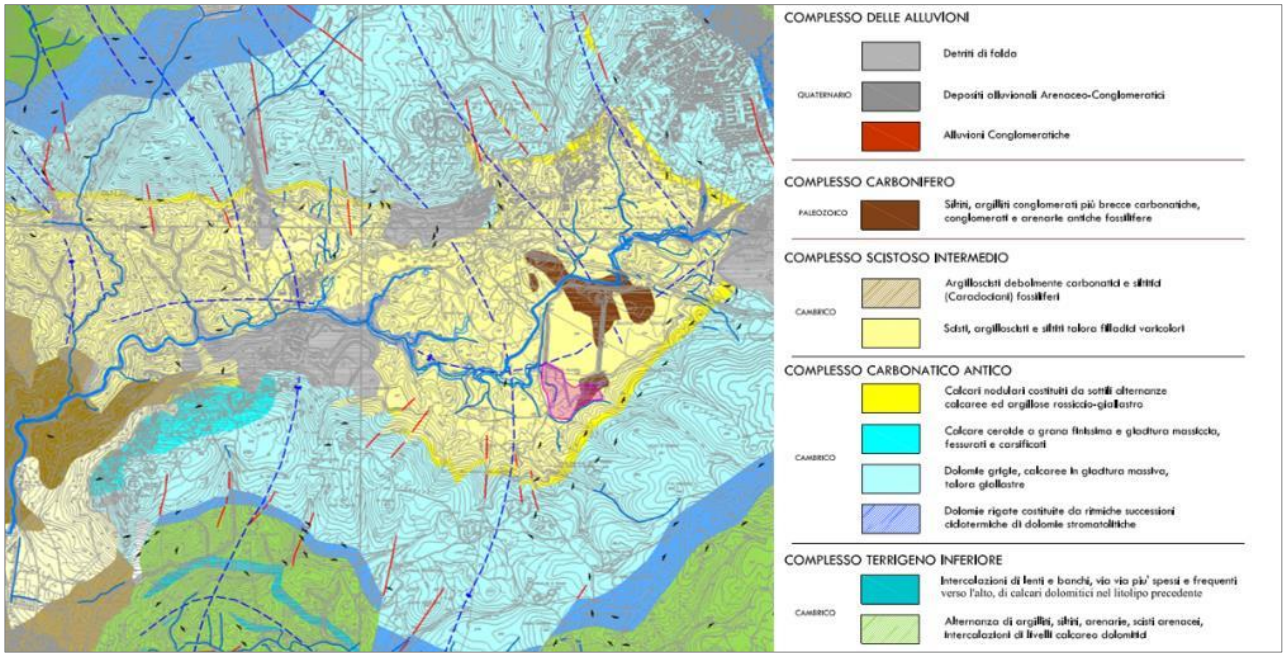

Figure 5 - Geological map of the Rio San Giorgio area

Pillola (Pillola et al, 1994) recognizes this series comprising three groups: Nebida Group, Gonnesa Group and Iglesias Group. The Nebida Group has a thickness of about 500 meters and is mainly composed by sandstones, with limestones and marl pockets, and is divided in Mattoppa Formation and Punta Manna formation (Pillola, 1994). Gonnesa Group is composed by shallow water platform carbonates, overlayed by the nodular limestones and slates of the Iglesias Group. During the intra Ordovician "Fase Sarda" tectonic phase, sediments of Cambrian to Lower Ordovician underwent an extensive deformation phase (Boni, 1999). After this, erosion and deposition of Upper Ordovician sediments occurred with angular unconformity. These deposits consist of thick successions of continental conglomerates and sandstones (‘Puddinga’ AUCT.), overlayed by marine slates, lasting until Late Ordovician–Silurian time. The Variscan orogeny produced at least two compressional phases and one extensional phase of deformation (Carmignani et al., 1997). The Variscan deformation also produced low-grade metamorphism and several phases of magmatic intrusion, which affected the deformed Paleozoic successions (Boni et al., 1999). Permian and Carbonifer sediments are quite scarce and Triassic rocks are represented by some outcrops in the western area of Nebida, while no other Mesozoic rocks are reported. Eocenic sediments are well known in this area, due to the carbon mines activity. In the Oligo-Miocene era, the entire Island was interested by tectonic activity and volcanism along fractures, especially on the sides of the Campidano, in the nearby Cixerri graben and in the Sant’Antioco and San Pietro islands.

Ore deposits and history of mining activities

Main mineralization in the Rio San Giorgio basin are dated to lower Cambrian. They consist in stratiform or strata bound deposits with massive sulphides (Sedimentary Exhalative) and lower grade sulphides (Mississippi Valley type). Most common minerals are sphalerite, galena, pyrite, barite and As-pyrite. Fe, Cd and Ag are associated with strata-bound galena. By products were Ag, Bi, Cd and other metals. Also non sulphidic ores, that were exploited until the sixties, smithsonite ($ZnCO_3$), hydrozincite($Zn_5(CO_3)_2(OH)_6$), monteponite (CdO), hemimorphite ($Zn_4Si_2O_7(OH)_2 \cdot (H_2O)$), pyromorphite ($Zn_4Si_2O_7(OH)_2 \cdot (H_2O)$), anglesite ($PbSO_4$) and cerussite ($PbCO_3$), were found in oxidized bodies

First mining exploitation in this area dates back to Nuragic Sardinians, Phoenicians and Carthaginian and first underground activities were carried out by the Romans, that dig until 100 meters of depth at Is Cungiaus due to the presence of Ag rich galena and barite. After Roman Empire, Pisans started a new phase of intense exploitation, founding the town of Iglesias in the 1324. During Aragonese kingdom, mining activities were limited and scarce, rising again during Savoy's conquest. In this period the exploitation increased, and industrialization take place in the area. In 1829 the Monte San Giovanni deposit was discovered and in 1850 the "Società di Monteponi" company became leader in the extraction field, due to the use of new technologies and machineries. During the two world wars the activities slowly decreased. After the wars, in the reconstruction period, a big reprise of the exploitation occurred again, until the end of the 70's when a crisis began until the definitive closure in 1996, due to high operating costs. Nowadays the area is the main part of the "Parco Geominerario storico e ambientale della Sardegna", a national park, previously recognized by UNESCO, that includes all the abandoned mining sites of the Island.

During exploitation activities, no prevention measures were taken and only after definitive closure the areas are still claiming for remediation. 17 million cubic meters of open pit excavations, 12 million cubic meters of dump and tailings (RAS, 2003; http://www.sardegnaambiente.it/) are exposed to weathering and degradation. Zavattero et al. (2006) analyzed the change of the natural landscape with mining activity in the last century: from 1955 to 1977 the extraction was strongly intensified due to the post-war reconstruction and the mine dumps increased from 109 ha to 147 ha, and flotation ponds increased from 34 to 77 ha. After 1977 mine activities gradually decreased, until the end of the extraction in the 90's, and vegetation (shrubs) partially cover these areas.

Metals in the study area

Trace metals, particularly Zn, are nutrients for living organisms, however, when present in the environment in high concentrations, trace metals can pose a serious threat to ecosystem and human health. Despite the presence of several mine residuals such as wastes and tailings, exposed to weathering, De Giudici et al. (2017) reported Zn and Pb concentrations in stream water lower than other streams affected by acid mine drainage in Sardinia (Cidu and Fanfani, 2002; Cidu et al., 2011; Frau et al., 2015). In fact, Zn concentration values range from 49 µg/l to 2500 µg/l and Pb from 0.63 µg/l to 16 µg/l (De Giudici et al., 2017) thanks to the presence of natural biogeochemical barriers, mainly represented by Phragmites Australis and and Juncus Acutus (Bacchetta et al., 2015), that retain and accumulate metals through complex processes taking place in the hyporheic zone (De Giudici et al. 2017). Previous water sampling campaigns conducted by IGEA s.p.a. between December 2006 and April 2007, reported significantly higher concentrations (*Piano di investigazione dell'asta fluviale del Rio San Giorgio*, 2009, internal report) reported values of Zn in stream water ranging from 160 µg/l to 676900 µg/l, nearby Fanghi Rossi dump, and Pb ranging from 10 µg/l to 2180 µg/l. De Giudici et al. (2017) conducted a hydrological tracer campaign, collecting river water samples from upstream to downstream and reporting concentrations between 49 and 2500 ug/l for Zn and between 1.6 ug/l and 12 ug/l for Pb.

Several measures of metals in soils are reported by IGEA s.p.a. for the study area, with an extremely varying range of concentrations. Extreme values were measured at San Giorgio mine, such as 106130 mg/kg of Zn and 48420 mg/kg for Pb in 2007 in 2007. Lower values, like 364 mg/kg for Zn, nearby San Giovanni mine, and 97 mg/kg for Pb close to Monte Agruxau mine, were measured respectively in 2006 and 2009.

In Rio San Giorgio riverbed, stream sediments were sampled in different points along the main path by IGEA in 2006, revealing very high concentrations of Zn and Pb (respectively 131304 mg/kg and 40059 mg/kg) upstream San Giovanni mine. Samples collected nearby the river's outlet, show a big decrease of concentration, probably due to the contribution of the tributaries to the streamflow, with 37668 mg/kg for Zn and 10739 mg/kg.

Stream sediments play a fundamental role in water pollution, as metals tend to be assimilated in sediment with organic matter, Fe/Mn oxides, sulphides, and clay thus forming several reactive components, which are harmful to the environment (Lim et al., 2012). Under different physical and chemical conditions, metals in sediment may leach out into the water column as free ions. In turn,

contaminated sediments also act as sources of heavy metals when released into the river water (Lim et al., 2012).

In streams affected by mining, the interaction between biosphere and geosphere is often responsible for natural attenuation of heavy metal loads (Akob et al., 2014; De Giudici et al., 2014). This takes place via a complex set of processes often occurring in the hyporheic zone where water, sediments and biosphere interact (Byrne et al., 2013; De Giudici et al., 2009, 2014). Hyporheic exchange is the flow of stream water in and out of the shallow subsurface and the river/banks riparian zone. The stream water, temporarily in the subsurface, may undergo reactions altering the biogeochemical signature of that water as it returns to the stream (Bencala, 2011). Thus, within the streambed sediments there is an interface between surface and groundwater where many biogeochemical reactions take place, such as ion adsorption, biopolymer diffusion, mineral dissolution, and (bio)mineral precipitation (Bencala, 2011; Bencala et al., 2011; Byrne et al., 2010; Runkel et al., 2003). The groundwater - surface water interface is actually a biologically driven redox interface (Byrne et al., 2014). Mass exchange in the hyporheic zone and its biogeochemical reactions depend on streambed hydrologic connectivity, patterns of hyporheic-exchange flow that control the mixing, and transport of redox-sensitive species (Kaser et al., 2009). In this thesis, the toolkit comprises a heavy-metal module. This module is starting to allow us modelling of complex systems such as Rio San Giorgio polluted site.

Bibliography

Akob, D.M., Bohu, T., Beyer, A., Schäffner, F., Händel, M., Johnson, C.A., Merten, D., Büchel, G., Totsche, K.U., Küsel, K., 2014. Identification of Mn(II)-oxidizing bacteria from a Low-pH contaminated former uranium mine. Appl. Environ. Microbiol. 80, 5086–5097.

Arnold, J.G., Srinivasan, R., Muttiah, R.S., Williams, J.R., 1998. Large Area Hydrologic Modeling and Assessment Part I: Model Development1. Wiley Online Library.

Bacchetta, G., Cappai, G., Carucci, A., Tamburini, E., 2015. Use of native plants for the remediation of abandoned mine sites in mediterranean semiarid environments. Bull. Environ. Contam.Toxicol 94, 326e333.

Bechstädt T., Schledding T., Selg M., 1988. Rise and fall of an isolated, unstable carbonate platform: The Cambrian of Southwestern Sardinia. Geologische Rundschau Volume 77, Issue 2, Pages 389-416.

Bencala K.E., 2011. Stream–Groundwater Interactions. Treatise on Water Science (book). DOI: 10.1016/B978-0-444-53199-5.00115-9

Bencala K.E., Gooseff M.N., Kimball B.A., 2011. Rethinking hyporheic flow and transient storage to advance understanding of stream-catchment connections. Water Resources Research 47-3. https://doi.org/10.1029/2010WR010066

Byrne P., Binley A., Heathwaite A.L., Ullah S., Heppell C., Lansdown K., Zhang H., Trimmer M., Keenan., Control of river stage on the reactive chemistry of the hyporheic zone. Hydrological Processes 28(17). DOI: 10.1002/hyp.9981

Carmignani L., Cocozza T., Gandin A., Pertusati P.C., 1982. VI. Lineamenti della geologia dell'Iglesiente-Sulcis. Guida alla Geologia del Paleozoico Sardo. Società Geologica Italiana: 65-67.

Caruso, B., Cox, T., Runkel, R.L., Velleux, M., Bencala, K.E., Nordstrom, D.K., et al., 2008. Metals fate and transport modelling in streams and watersheds: state of the science and USEPA workshop review. Hydrol. Process. 22, 4011–4021.

Cidu, R., Fanfani, L., 2002. Overview of the environmental geochemistry of mining districts in southwestern Sardinia. Italy. Environ. Geol. 2, 243e251.

Cidu, R., Frau, F., Da Pelo, S., 2011. Drainage at abandoned mine sites: natural attenuation of contaminants in different seasons. Mine Water Environ. 30, 113e126.

De Giudici G., Podda F., Sanna R., Musu E., Tombolini R., Cannas C., Musinu A., Casu M., 2009. Structural properties of biologically controlled hydrozincite: An HRTEM and NMR spectroscopic study. merican Mineralogist 94(11):1698-1707. DOI: 10.2138/am.2009.3181

De Giudici G., Wanty R.B., Podda F., Kimball B.A., Verplanck P.L., Lattanzi P.F., Cidu R., Medas D., 2014. Quantifying Biomineralization of Zinc in the Rio Naracauli (Sardinia, Italy), Using a Tracer Injection and Synoptic Sampling. Chemical Geology 384. DOI: 10.1016/j.chemgeo.2014.07.002

De Giudici G., Pusceddu C., Medas D., Meneghini C., Gianoncelli A., Rimondi V., Podda F., Cidu R., Lattanzi P.F., Wanty R.B., and Kimball B.A., 2017. The role of natural biogeochemical barriers in limiting metal loading to a stream affected by mine drainage. Applied Geochemistry 76. DOI: 10.1016/j.apgeochem.2016.11.020

De Giudici G., Medas D., Cidu R., Lattanzi P.F., Podda F., Frau F., Rigonat N., Da Pelo, S., Pusceddu C., Onnis P., Marras P.A., Wanty R.B., and Kimball B.A., 2018. Application of hydrologic-tracer techniques to the Casargiu adit and Rio Irvi (SW-Sardinia, Italy): Using enhanced natural attenuation to reduce extreme metal loads. Applied Geochemistry. Volume 96, September 2018, Pages 42-54. DOI: https://doi.org/10.1016/j.apgeochem.2018.06.004

De Giudici G., Medas D., Cidu R., Lattanzi P.F., Podda F., Rigonat N., Marras P.A., Wanty R.B., and Kimball B.A., 2019. Assessment of origin and fate of contaminants along mining-affected Rio Montevecchio (SW Sardinia, Italy): A hydrologic-tracer and environmental mineralogy study. Applied Geochemistry 109:104420. DOI: 10.1016/j.apgeochem.2019.104420.

Frau, F., Medas, D., Da Pelo, S., Wanty, R.B., Cidu, R., 2015. Environmental effects on the aquatic system and metal discharge to the Mediterranean Sea from a near neutral zinc-ferrous sulfate mine drainage. Water Air Soil Poll. 226, 55.

Giorgi F, Jones C, Asrar GR (2009) Addressing climate information needs at the regional level: The CORDEX framework. WMO Bull 58:175–183

Kachiashvili K., Gordenzani D., Lazarov R., Melikdzhanian D., 2005. Modeling and simulation of pollutants transport in rivers. Applied Mathematical Modelling 31 (2007) 1371–1396

Kaser, D.H., Binley, A., Heathwaite, A.L., Krause, S., 2009. Spatio-temporal variation of hyporheic flow in a riffle-step-pool sequence. Hydrol. Process 23, 2138e2149.

Lim W.Y., Aris A.Z., Zakaria M.P. Spatial Variability of Metals in Surface Water and Sediment in the Langat River and Geochemical Factors That Influence Their Water-Sediment Interactions. Sci. World J. 2012 doi: 10.1100/2012/652150

Marras P., Muroni D., Manca S., Soru C., Pusceddu G., Marrocu M., Cau P., 2014. The SWAT model and a web-based information system to assess the water balance of Sardinia (Italy), SWAT International Conference, Pernambuco, Brazil, 21-33.

Meng Y., Zhou L., He S., et al., 2018. A heavy metal module coupled with the SWAT model and its preliminary application in a mine-impacted watershed in China. Science of The Total Environment, 613-614:1207-1219.

Pillola G.L., 1994. The Cambro-Ordovician of Southwestern Sardinia: Trilobites biostratigraphy and paleobiogeographical affinities. In: Bechstädt T. & Boni M. (EDS)- Sedimentological, stratigraphical and ore deposits field guide of the autochtonous Cambro-Ordovician of SW Sardinia, 49(1): 19-28

Pillola G.L., 1994. The Iglesias group in the type area of Campo Pisano-Cabitza. In: Bechstädt T. & Boni M. (EDS)- Sedimentological, stratigraphical and ore deposits field guide of the autochtonous Cambro-Ordovician of SW Sardinia, 49(2): 304-306

Runkel R.L., Diane M. Mcknight, Rajaram H., 2003. Modeling Hyporheic Zone Processes. Advances in Water Resources 26(9):901-905. DOI: 10.1016/S0309-1708(03)00079-4.

Velleux M. L., Julien P. Y., Sanchez R. R., Clements W. H., England J. F., 2006. Simulation of Metals Transport and Toxicity at a Mine-Impacted Watershed: California Gulch, Colorado *Environ*. Sci. Technol. 2006,40, 22, 6996-7004. https://doi.org/10.1021/es0608592

Vink R., Peters S., 2003. Modelling point and diffuse heavy metal emissions and loads in the Elbe basin.
Zavattero L., Casti M., Bacchetta G., Di Pietro R., 2006. Analisi multitemporale del paesaggio del distretto minerario di Monteponi (Sardegna sud-occidentale), Rivista Italiana di Telerilevamento, 37:137-146.

Chapter 2: Materials and methods

This chapter is divided in two main sections: the first section is dedicated to the SWAT model implementation, the second one describes the SWAT-Heavy metals (HM) model. For both models I will explain the main theoretical basis, the input data processing and the calibration procedure.

Numerical models

Water-quality numerical models are a promising tool to predict the changes in surface water quality for environmental management at a large scale (Wang et al., 2013). Heavy metal fate and transport models are increasingly used as an effective tool (Meng et al, 2017) to better understand the environmental behavior of heavy metals and the associated risks. Many types of numerical models for the simulation of the pollutant transport are in use, with different degrees of complexity and different simulated processes. According to Caruso et al. (2008), models can be classified into four types:

- equilibrium model,
- stream model,
- soil model
- watershed model.

Watershed models take into account both upland and in-stream processes, allowing for the description of the behavior of metals for environmental management at regional scale (Velleux et al., 2006).
Depending on the aim of the study, different model can be used. Model choice factors are the study scale, data availability/quality, model documentation and previous applications, time and money constraints, the payment of license, and so on. This study aims at understanding metals dispersion in Rio San Giorgio watershed. Thus, watershed models were used to simulate the fate and transport of Zn and Pb within the investigated area.

In this study multi-model approach was assumed in order to deal with the complexity of the system. The core of our multi model approach is the SWAT model. SWAT is one of the most used hydrological models in the world, thanks to its capabilities to reproduce water cycle for long-term periods and under different conditions. SWAT simulates water cycle and quality, with different land management practices, is physically based and parametric, is open source and well-tested by a large community that constantly develops new features to improve its efficiency. Different options are provided by the model to simulate processes such as runoff, infiltration, evapotranspiration, lateral flow, etc. These are the main reasons that leaded to the choice of this model. Moreover SWAT was used in previous studies (Marras et al., 2014; Perra et al., 2018;) conducted to assess the water balance in Sardinia with good results in terms of reliability of the model. Limitations of SWAT model is that it is only able to reproduce heavy metals transport in 1-D river channel through a simple mass balance. Thus, SWAT-Heavy Metal experimental module (Meng et al., 2018) was also implemented, allowing to reproduce complex reactions that generate the heavy metals fate and transport. The mechanisms and reactions that can be simulated by SWAT-HM are leaching, slow reaction, adsorption, desorption and upward migration.

Hereafter, SWAT will be described and then HM module will be described. Focus will be on description of the implementation and calibration of the models, as well the input datasets and their pre-processing. At the end of this chapter, the use of SWAT-HM for simulate features simulation will be described.

SWAT Model

The Soil and Water Assessment Tool (SWAT) is a long term and physically based numerical model that simulates hydrology, sediments, nutrients and pesticide cycle in a continuous timestep. SWAT operates at basin scale on daily time step (Arnold *et al*., 1998, 2000; Neitsh *et al*., 2001).

It was developed from an earlier continuous time step model named Simulator for Water Resources in Rural Basins (SWRRB) (Williams *et al.,*1985, Arnold *et al.,* 1990) with the purpose to simulate non-point source loadings from watershed.

SWAT is widely used to model hydrology at watershed scale and to predict the impact of land management practices on water, agricultural chemical yields and sediments in small or large

complex basins with varying land use land cover conditions and soil type over long periods of time.

Model descritpion

In the SWAT model, the watershed is first divided into sub-basins based on topographic criteria, then a further sub-division into Hydrological Response Units (HRU) is done on the basis of unique overlays of soil type, slope class and land use/cover that the user provides to the model as primary input. Simulated processes are divided in two macro phases: *upland phase* and *channel phase.*
The *upland phase* is the land phase of the hydrological cycle is the simulation of the loads of water, sediments, nutrients or pesticides coming from each sub-basin that are then routed to the rivers in the *channel phase* of the hydrological cycle. The processes simulated in the *upland phase* are:

Weather
Hydrology
Sedimentation
Plant growth
Nutrient cycling
Pesticide dynamics
Management

Once the processes in the *upland phase* are simulated, everything (water, sediments, nutrients etc.) is transferred to the channel (channel phase), and the following processes are simulated:

Flood routing
Transmission losses and evaporation
Sediment routing
Nutrient routing
Pesticide routing

The core of the SWAT model is based on the water balance equation:

$$SW_t = SW_0 + \sum_{i=1}^{n} (R_{day} + Q_{surf} - E_a - w_{seep} - Q_{gw})$$

in which SW_t is the final soil water content (mm), SW_0 is initial soil water content on day i (mm), t is the time (days), R_{day} is the amount of precipitation on day i (mm), Q_{surf} is the amount of surface runoff on day i (mm), E_a is the amount of evapotranspiration on day i (mm), w_{seep} is the amount of water entering the vadose zone from the soil profile on day i (mm), and Q_{gw} is the amount of return flow on day i (mm). Surface runoff from daily rainfall is estimated using a modified SCS curve number method, which estimates the amount of runoff based on local land use, soil type, and antecedent moisture condition (Schuol & Abbaspour, 2006). Peak runoff predictions are based on a modification of the Rational Formula (Chow et al., 1988).

SWAT is parametric, meaning that every simulated process is controlled by specific parameters, such as Curve Number, permeability, soil porosity, depth of plant roots, etc., that can be changed and adjusted based on meaningful values. Parameters are directly associated to soils and land cover and the model calculates the balance for each HRU separately, giving the possibility to have a very detailed reproduction of the real conditions of the watershed with a precise spatial distribution of the features.

The soil profile is subdivided into multiple layers that support soil water processes including infiltration, evaporation, plant uptake, lateral flow, and percolation to lower layers. The soil percolation component of SWAT uses a water storage capacity technique to predict flow through each soil layer in the root zone.

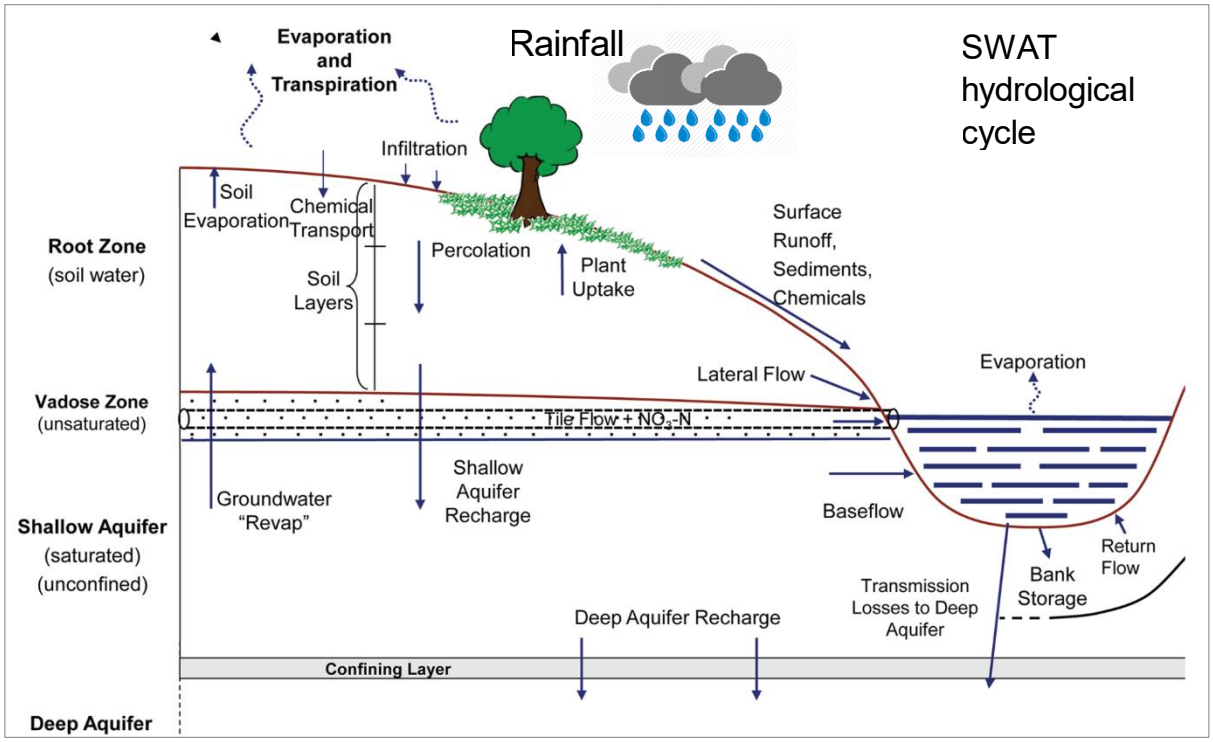

Figure 6 Schematic of the hydrologic cycle and the sediment and chemical transport pathways (from Moriasi et al., 2013).

Downward flow occurs when field capacity of a soil layer is exceeded and the layer below is not saturated. Percolation from the bottom of the soil profile recharges the shallow aquifer. Daily average soil temperature is simulated as a function of the maximum and minimum air temperature. If the temperature in a particular layer reaches less than or equal to 0 ◦C, no percolation is allowed from that layer. Lateral sub-surface flow in the soil profile is calculated simultaneously with percolation. Groundwater flow contribution to total stream flow is simulated by routing a shallow aquifer storage component to the stream (Arnold and Allen, 1996). The model computes evaporation from soils and plants separately. Potential evapotranspiration can be modelled with the Penman–Monteith (Monteith, 1965), Priestley–Taylor (Priestley and Taylor, 1972), or Hargreaves methods (Hargreaves and Samani, 1985), depending on the availability of data. Potential soil water evaporation is estimated as a function of potential ET and leaf area index (area of plant leaves relative to the soil surface area). Actual soil evaporation is estimated by using exponential functions of soil depth and water content. Plant water evaporation is simulated as a linear function of potential ET, leaf area index and root depth and can be limited by soil water content. Sediment yield in SWAT is estimated with the modified soil loss equation (MUSLE) developed by Williams and Berndt (1977). The sediment routing model consists of two components operating simultaneously: deposition and degradation. The deposition in the channel and floodplain from the sub-watershed

to the watershed outlet is based on the sediment particle settling velocity. The settling velocity is determined using Stoke's law (Chow et al., 1988) and is calculated as a function of particle diameter squared. The depth of fall through a reach is the product of settling velocity and the reach travel time. The delivery ratio is estimated for each particle size as a linear function of fall velocity, travel time, and flow depth. Degradation in the channel is based on Bagnold's stream power concept (Bagnold, 1977; Williams, 1980). Channel routing is simulated using the variable storage or Muskingum method.

For further model details, equations and theory please consult Neitsch et al., 2011. The input data and its processing, necessary to delineate the basin, define the soils, the land cover/use and the climate forcing to simulate the water cycle, is described in the following paragraphs.

SWAT model implementation

SWAT model offers different Graphic User Interfaces (GUI) that allow users to delineate the physical characteristics of the watershed, such as boundaries, accumulation zones, river channels, slope, soils and land cover. Additional features, like point sources and reservoirs, can be add to the basin. The main study area is Rio San Giorgio basin, but also Rio Mannu di Fluminimaggiore catchment was modeled due to the presence of a streamflow measurement gauge that allowed to calibrate the model for the simulation of the hydrologic cycle.

The input data used in this study will be described in detail. In this research ArcSWAT for ArcGIS was used to pre-process the input data and build the model.

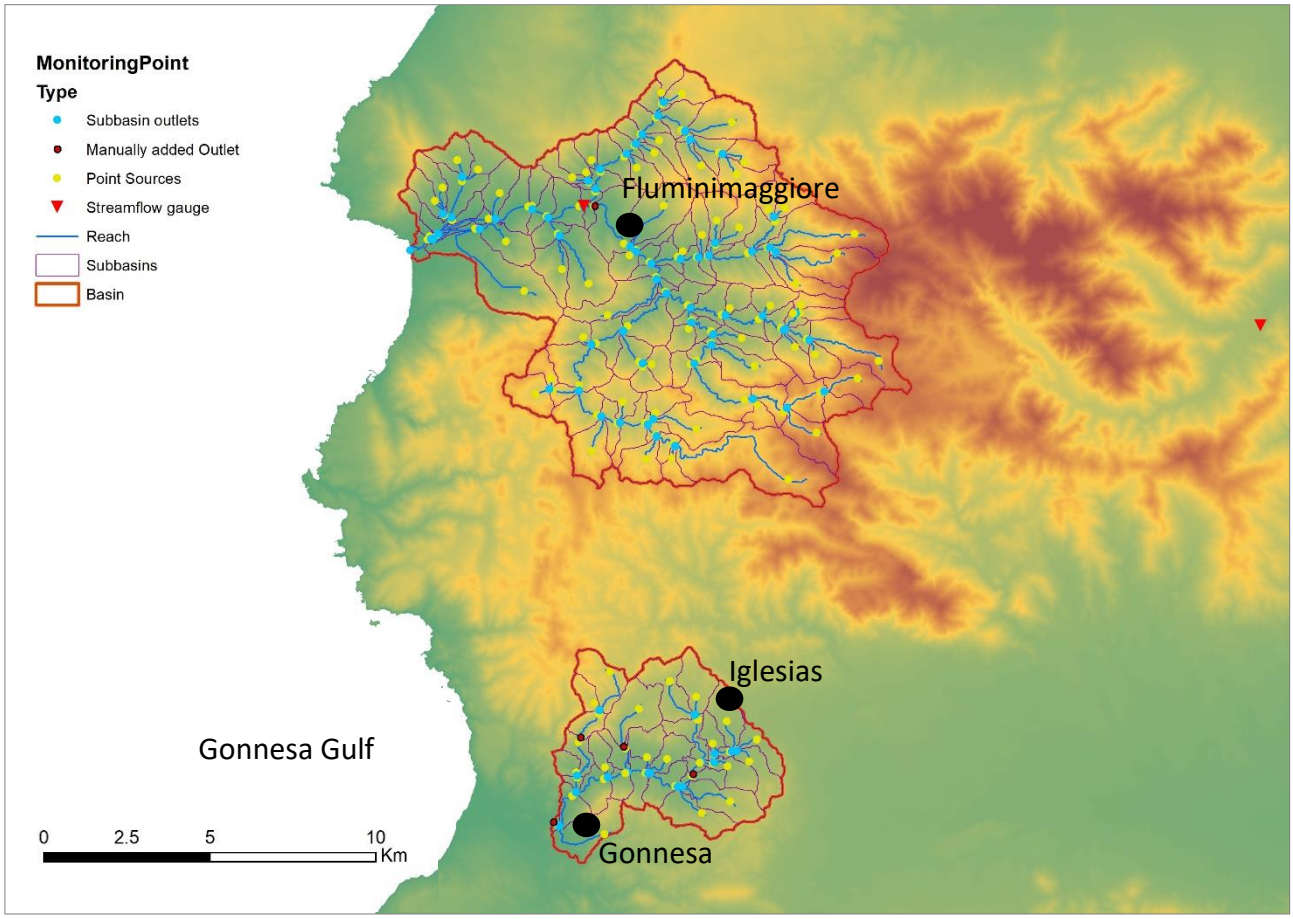

Figure 7 - SWAT model domain: upper catchement is Rio Mannu di Fluminimaggiore with its measurement station (red inverted triangle)

Delineation of the watershed

The delineation of the watershed was carried out starting from Digital Elevation Model (DEM) provided by the local government offices of "Regione Autonoma della Sardegna" (RAS, 2011, http://webgis2.regione.sardegna.it/catalogodati/card.jsp?uuid=R_SARDEG:QIEUH). It is a regular grid dataset with an elementary cell of 10m x 10m resolution. Based on the DEM, ArcSWAT delineates the boundaries of the watershed, calculates the flow direction and the accumulation zones. River network was then delineated, and watershed was divided in sub-watershed or sub-basins, based on the minimum drained area, set at 50 hectares. As the SWAT model produces the outputs at the sub-basin scale, some additional outlets were defined in strategic sites, like measurement stations, point sources and wastewater treatment plants, to better control the model results. Two point-sources (FIGURE 8) release urban wastewater in the Rio San Giorgio: the first one is located in the outskirts of Iglesias town and discharges around 900.000 m^3/year of non-treated water, the second one is located in Bindua and inputs a yearly amount of around 110.000 m3. Point

sources have been modeled using the option “constant daily amount” of SWAT, and daily values were obtained by simple division of the annual discharge.

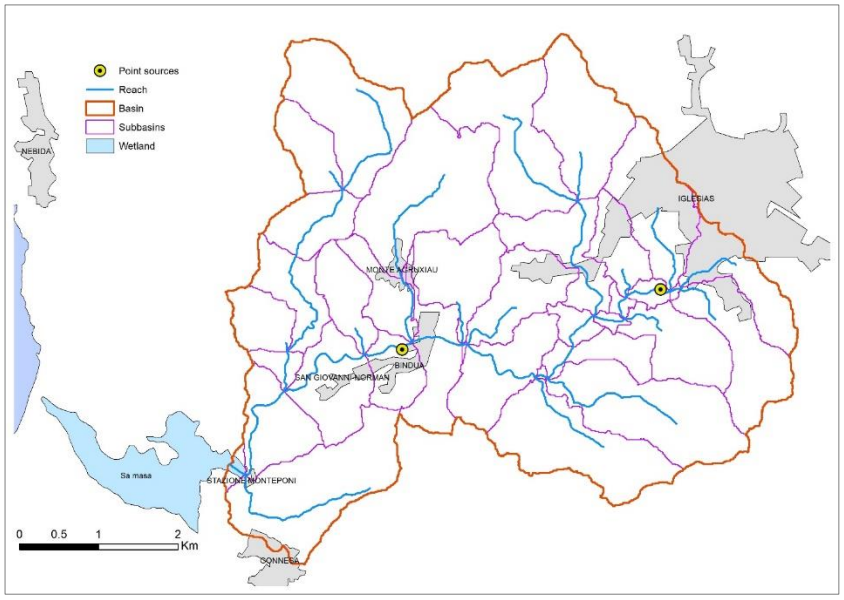

Figure 8 - Point sources position within Rio San Giorgio catchement

Delineation of the Hydrologic Response Units

The Hydrologic Response Units are homogeneous portions of the basin, given by the different combinations of soil, land cover and slope, that have the same hydrologic behavior. In ArcSWAT these areas are obtained by the overlay of soil map, land cover map and slope map. Each map is linked to a database that contains the values of the physical parameters associated to these features, like Curve Number, permeability, porosity, classification of the land cover and many other parameters that regulate the water cycle within the soil profile and in the surface. HRUs can be defined as a single dominant combination for each sub-basin or as all the possible combinations of the three features (soil, land use and slope class) for each sub-basin. In this study, all the possible combinations of soils, land use and slope were identified for each sub-basin. Each dataset will be described in detail.

Land Cover dataset.

The Land Cover dataset, that was retrieved from the local government offices (RAS, 2008, http://webgis2.regione.sardegna.it/catalogodati/card.jsp?uuid=R_SARDEG:WBMEW), is based on the CORINE Land Cover (CLC) standard and it has been converted into the SWAT standard in a

previous study (Marras et al., 2014). The CLC dataset has a scale of 1:25000 and a resolution of 0,5 ha for urban areas and 0,75 for extra-urban areas. Main land cover is represented by the class “Garigue”, that corresponds to Mediterranean scrub, and evergreen forest. Since the abandoned mining areas are partially covered by vegetation, the areas classified as “UIDU” (Industrial) do not match with the “Mining areas” perimeter that is represented in Figure 9.

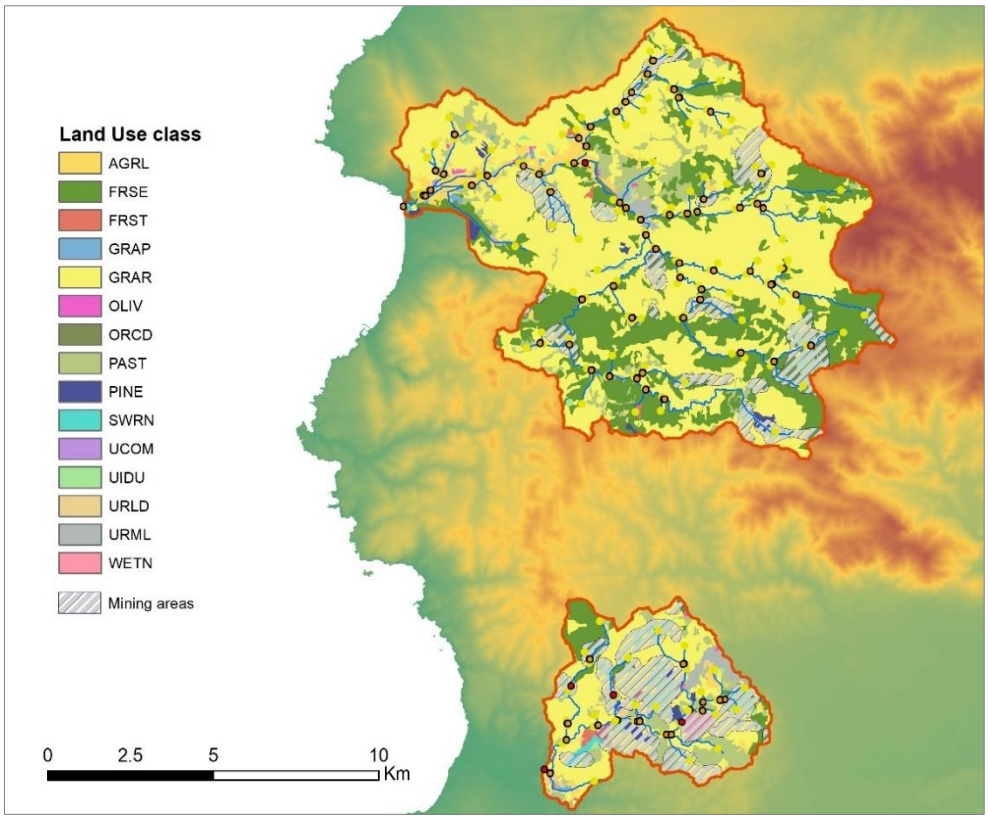

Figure 9 - Land use/cover distribution in the modeled area

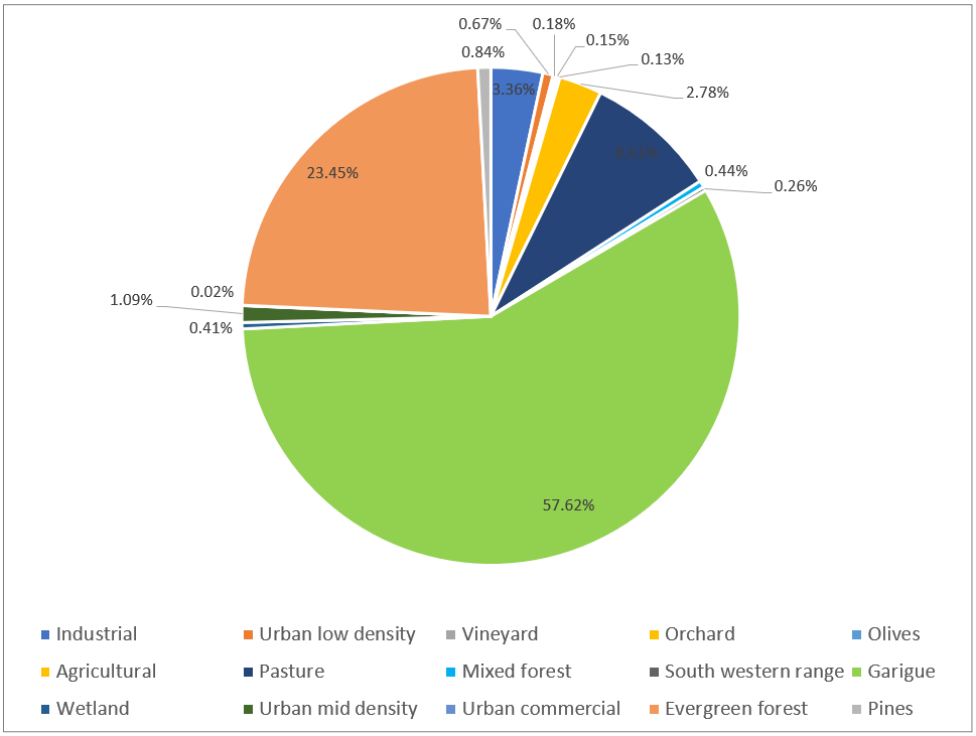

Figure 10 - Land use coverage

Soil dataset.

Soil database was developed by the researchers of the CRS4 Research Center (Cadeddu e Lecca, 2003) using the SWAT standard based on previous pedologic studies (Arangino, et al., 1986; Aru et al.,1991; Montanarella, 1999; Righini et al., 2001). The map in Figure 11 shows the distribution of the soils within the watersheds.

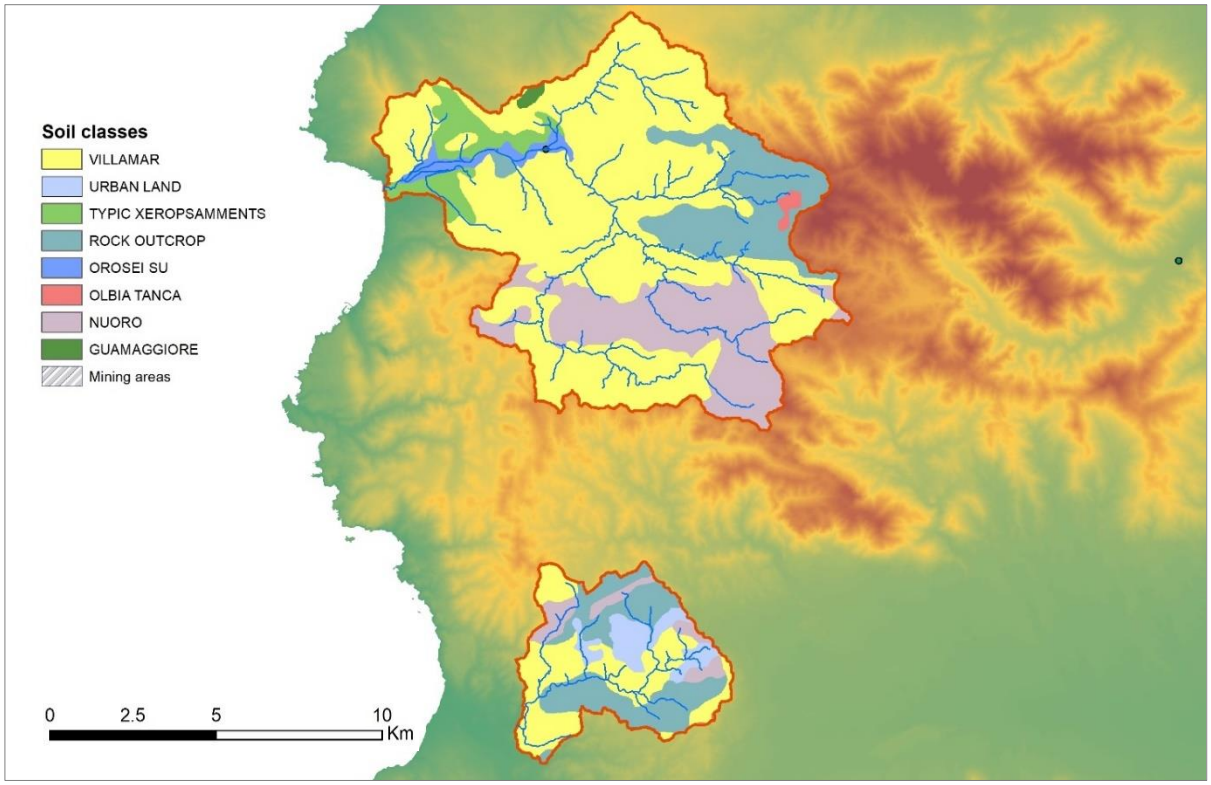

Figure 11 - Soil distribution map

Each soil class is related to specific parameters contained in the soil database and can be sub-divided up to ten layers with different characteristics. For each layer the following parameters (Table 1) are specified in the database:

Table 1 - Soil parameters meaning and measure units. The * can be a number from 1 to 10 that indicates the soil layer in order of depth.

NLAYERS	Number of layers
HYDGRP	Hydrologic group
SOL_ZMX	Maximum rooting depth of soil profile (mm)
ANION_EXCL	Fraction of porosity (void space) from which anions are excluded
SOL_CRK	Potential or maximum crack volume of the soil profile expressed as fraction of total soil volume
SOL_Z*	Depth from soil surface to bottom of layer (mm)
SOL_BD*	Moist bulk density (Mg/m^3 or g/cm^3)
SOL_AWC*	Available water capacity of soil layer (mm H_2O/mm soil)
SOL_K*	Saturated hydraulic conductivity (mm/hr)
SOL_CBN*	Organic Carbon content (% in soil weight)
CLAY*	Clay content (% in soil weight)
SILT*	Silt content (% in soil weight)
SAND*	Sand content (% in soil weight)
ROCK*	Rock fragment content (% in soil weight)
SOL_ALB*	Moist soil albedo (fraction)

USLE_K*	USLE equation soil erodibility (metric ton m^2 hr)

Specific values for each parameter and for each soil layer are then shown in

Table 2

Table 2 - Soil parameter values

PARAMETER	GUAMAGGIORE2	VILLAMAR	ROCK OUTCROP	TYPIC XEROP.	OROSEI SU	OLBIA TANCA	NUORO	URBAN LAND
NLAYERS	3	4	3	4	3	3	3	3
HYDGRP	B	B	C	B	C	B	C	C
SOL_ZMX	1651.00	736.60	482.60	787.40	457.20	1320.80	1651.00	1651.00
ANION_EXCL	0.50	0.50	0.50	0.50	0.50	0.50	0.50	0.50
SOL_CRK	0.50	0.50	0.50	0.50	0.50	0.50	0.50	0.50
SOL_Z1	177.80	279.40	203.20	101.60	76.20	101.60	127.00	152.40
SOL_BD1	1.13	1.25	1.25	1.10	1.25	1.25	1.30	1.10
SOL_AWC1	0.17	0.19	0.16	0.11	0.17	0.16	0.21	0.12
SOL_K1	270.00	26.00	33.00	5.40	70.00	800.00	12.00	24.00
SOL_CBN1	3.20	3.49	2.33	0.00	2.33	3.20	2.03	2.03
CLAY1	6.50	11.50	18.50	13.00	5.50	3.00	7.00	7.00
SILT1	30.37	56.14	38.54	56.26	58.02	16.70	71.07	58.99
SAND1	63.13	32.36	42.96	30.74	36.48	80.30	21.93	34.01
ROCK1	11.75	7.51	10.29	40.00	11.74	7.51	0.00	40.00
SOL_ALB1	0.01	0.01	0.01	0.23	0.01	0.01	0.01	0.01
USLE_K1	0.24	0.32	0.32	0.28	0.32	0.17	0.49	0.20
SOL_EC1	0.00	0.00	0.00	0.00	0.00	0.00	0.00	0.00
SOL_Z2	482.60	457.20	457.20	558.80	431.80	965.20	711.20	508.00
SOL_BD2	1.23	1.35	1.35	1.30	1.35	1.40	1.30	1.38
SOL_AWC2	0.11	0.14	0.13	0.15	0.09	0.04	0.17	0.14
SOL_K2	260.00	15.00	23.00	6.00	37.00	450.00	90.00	22.00
SOL_CBN2	1.07	0.29	0.78	0.00	0.29	1.07	0.68	0.68
CLAY2	5.00	11.50	18.50	13.00	5.50	2.50	6.00	7.00
SILT2	30.69	56.14	38.54	56.26	58.02	1.52	40.57	58.99
SAND2	64.31	32.36	42.96	30.74	36.48	95.98	53.43	34.01
ROCK2	31.01	20.93	17.44	11.92	50.84	45.77	0.00	20.72
SOL_ALB2	0.03	0.13	0.05	0.23	0.13	0.03	0.06	0.06
USLE_K2	0.24	0.28	0.32	0.37	0.20	0.17	0.49	0.37
SOL_EC2	0.00	0.00	0.00	0.00	0.00	0.00	0.00	0.00
SOL_Z3	1651.00	711.20	482.60	762.00	457.20	1320.80	1651.00	1651.00
SOL_BD3	1.45	1.83	2.50	1.60	2.50	1.55	1.35	1.83
SOL_AWC3	0.06	0.09	0.01	0.14	0.01	0.02	0.16	0.12
SOL_K3	450.00	6.80	600.00	7.90	550.00	400.00	130.00	17.00
SOL_CBN3	0.36	0.29	0.26	0.00	0.10	0.36	0.23	0.23
CLAY3	2.50	11.50	5.00	10.00	5.00	1.50	4.50	6.50
SILT3	17.25	56.14	25.00	57.09	25.00	1.53	41.22	59.31
SAND3	80.25	32.36	70.00	32.91	70.00	96.97	54.28	34.19
ROCK3	30.00	51.86	98.00	19.59	98.00	54.01	0.00	27.81
SOL_ALB3	0.12	0.13	0.14	0.23	0.19	0.12	0.15	0.15
USLE_K3	0.24	0.20	0.00	0.37	0.00	0.17	0.49	0.28
SOL_EC3	0.00	0.00	0.00	0.00	0.00	0.00	0.00	0.00
SOL_Z4	-	736.60	-	787.40	-	-	-	-
SOL_BD4	-	2.50	-	2.50	-	-	-	-

SOL_AWC4	-	0.01	-	0.01	-	-	-	-
SOL_K4	-	500.00	-	140.00	-	-	-	-
SOL_CBN4	-	0.10	-	0.00	-	-	-	-
CLAY4	-	5.00	-	5.00	-	-	-	-
SILT4	-	25.00	-	25.00	-	-	-	-
SAND4	-	70.00	-	70.00	-	-	-	-
ROCK4	-	98.00	-	98.00	-	-	-	-
SOL_ALB4	-	0.19	-	0.23	-	-	-	-

Climate Data definition

A description of the rainfall and temperature data used to force SWAT model for the simulation of the hydrological cycle will be provided here. Moreover this topics will be described afterwards in depth with an accurate analysis of the observed variables both for historical and future climate datasets, focusing also on climate change analysis.

Precipitation data

Precipitation (P) is arguably the most important driver of the hydrological cycle, but also one of the most challenging to estimate (Daly et al., 2008; Michaelides et al., 2009; Kidd and Levizzani, 2011; Tapiador et al., 2012)

Precipitation data can be simulated by SWAT internal weather generator or introduced as daily record in SWAT model. In this study, daily rainfall records from the Sardinian government observational network were used from 1979 to 2008. Due to lack of validated rainfall datasets after 2008, MSWEP dataset (Beck et al., 2017) was used to force SWAT model from 2009 to 2017. SWAT sub-basins are associated to specific rainfall stations based on the distance between the sub-basin centroid and the station, as shown in Figure 12

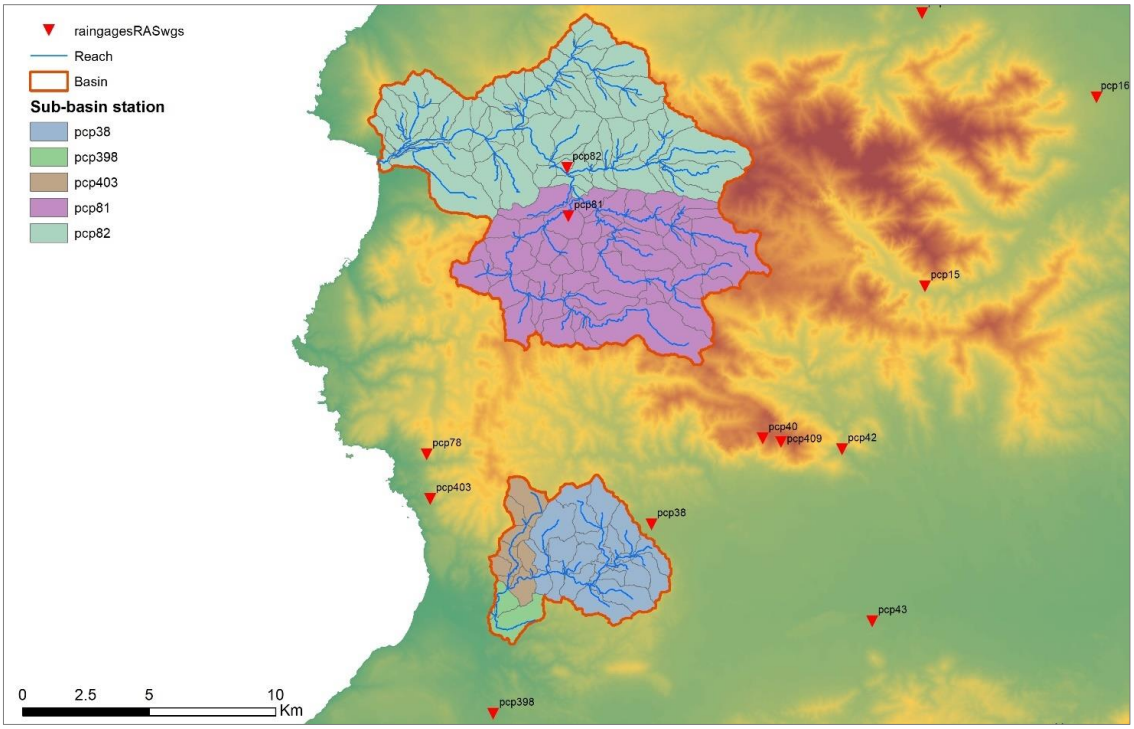

Figure 12 - Precipitation measurement stations (red triangles) and associated sub-basins within the watershed

Monthly mean precipitation values range from 40 mm to 100 mm in winter months and below 10 mm in July (Figure 13), consistently with the strong seasonality typical of the Sardinian semi-arid climate.

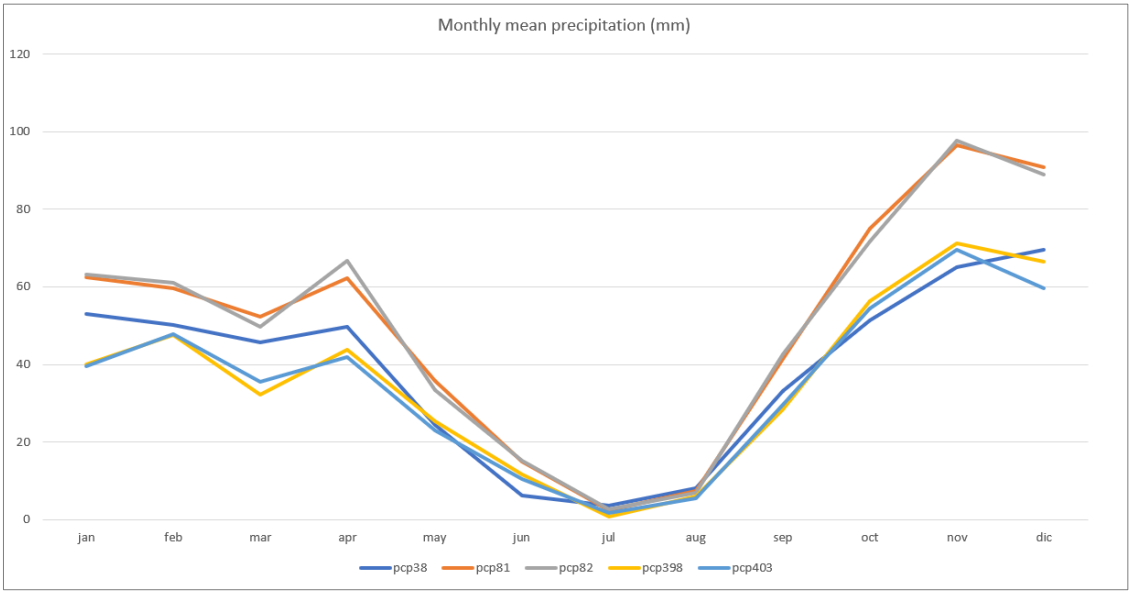

Figure 13 - Mean monthly rainfall in the different stations of the area.

Seasonal cumulated values (Figure 14) better show that most of the precipitations are distributed in the period from september to february.

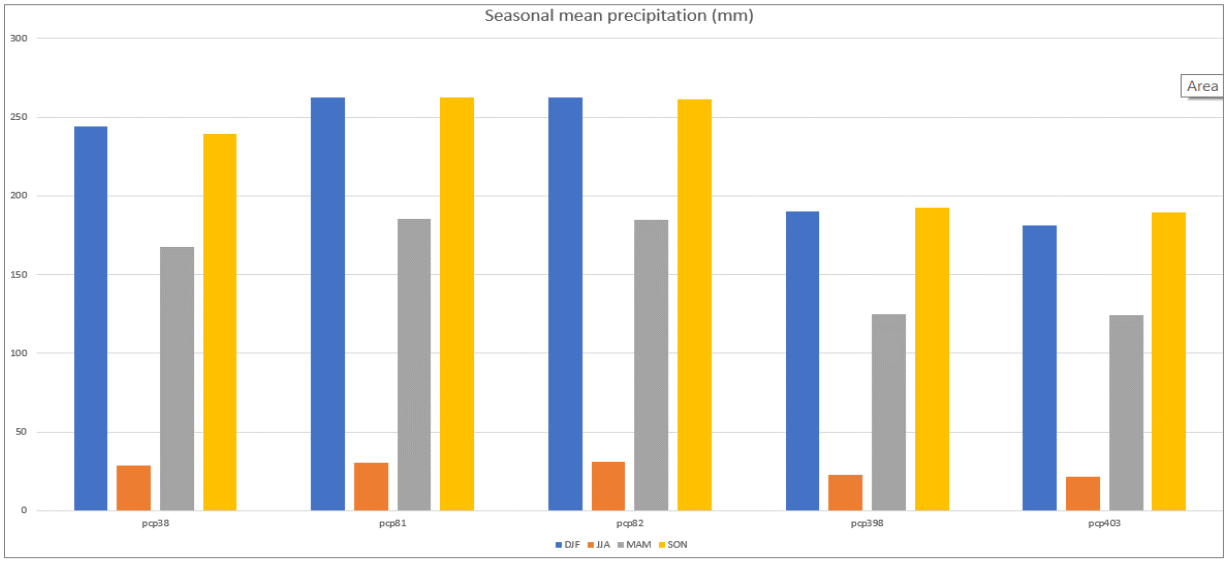

Figure 14 - Seasonal cumulated rainfall for the stations pcp38, pcp81, pcp82, pcp398 and pcp403. DJF stands for winter, MAM for spring, JJA for summer and SON for autumn.

MSWEP stands for Multi-Source Weighted-Ensemble Precipitation and is a new fully global historic precipitation dataset (1979–2017) with a 3-hourly temporal and 0.1° spatial resolution. It is the result of the complementary strengths of gauge, satellite and reanalysis-based data over the entire globe, widely validated with large scale evaluations. Simple interpolation based on distance was made to assign MSWEP precipitations to SWAT sub- basins, as shown in the map (Figure 15)

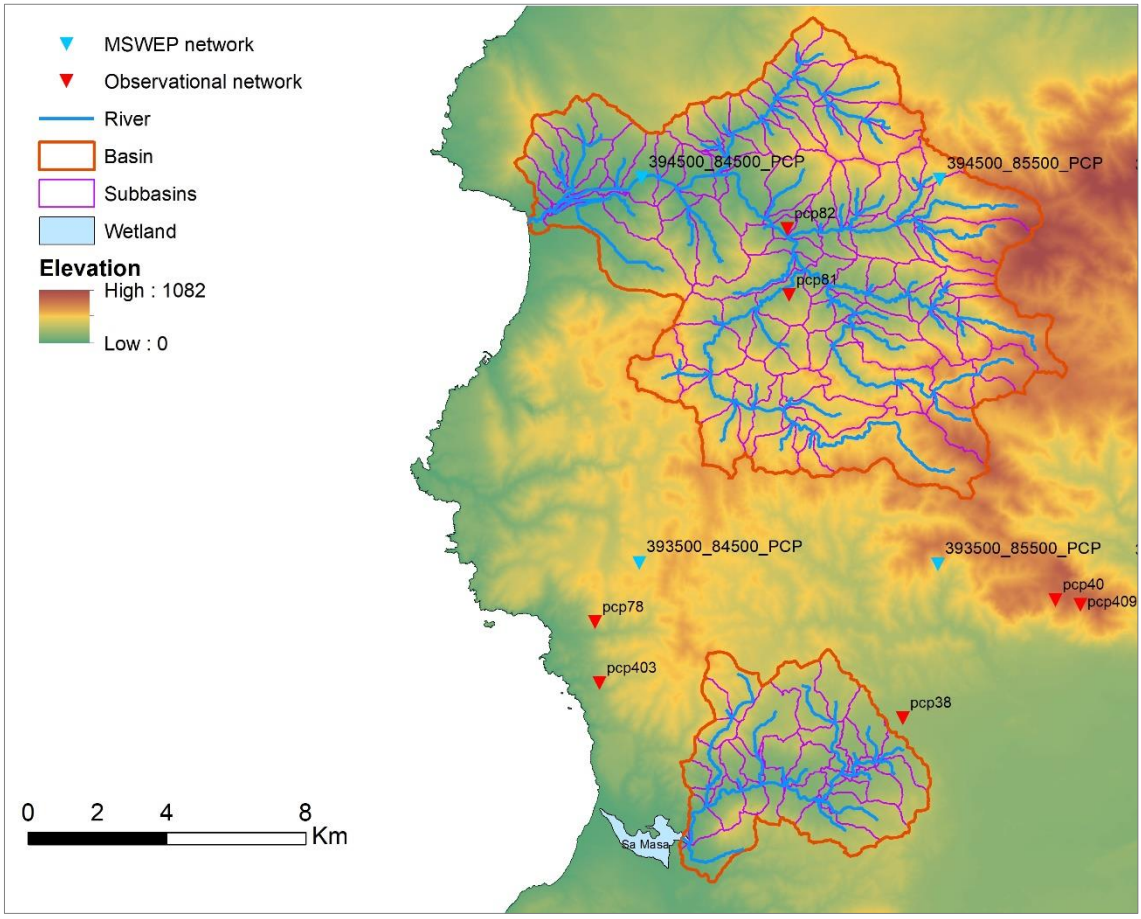

Figure 15 - Observational vs MSWEP dataset rainfall network

Simple statistics were used for the evaluation of the reliability of MSWEP dataset. Chart in Figure 16 shows the monthly mean cumulated rainfall for the station of Iglesias and the corresponding MSWEP dataset virtual station, highlighting a good agreement and a relatively small negative bias (total mean bias -8%) especially in winter months, that has been adjusted increasing precipitation in these months for the period 2009-2017.

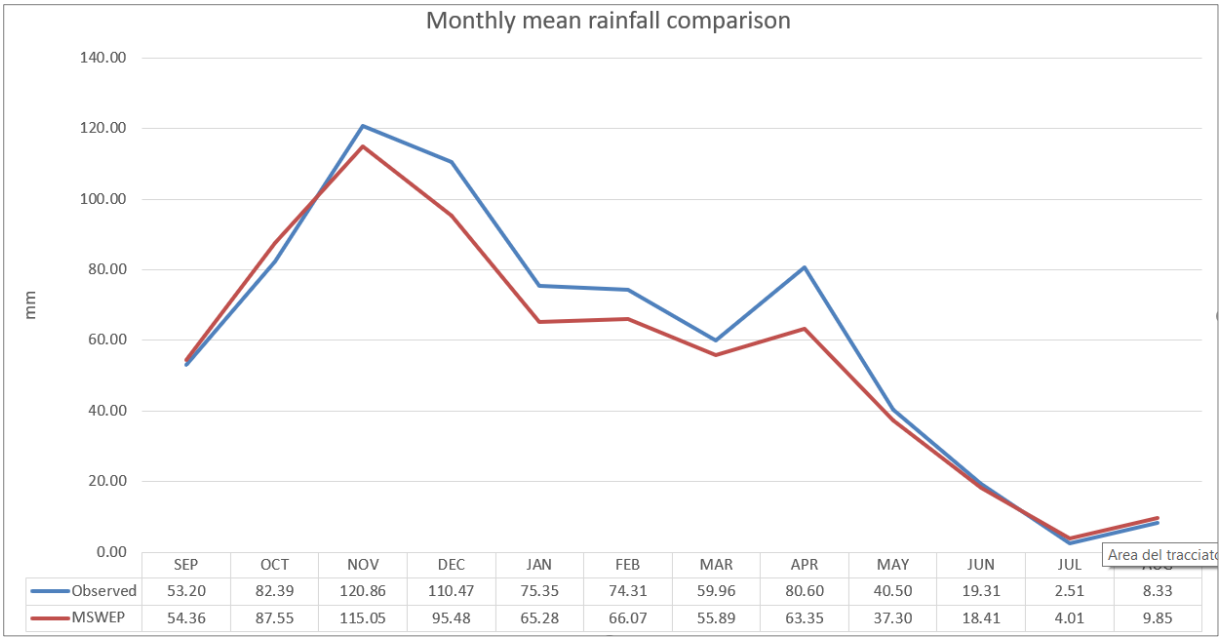

Figure 16 - Comparison of the monthly mean cumulated precipitation between observed data (blue line) and MSWEP dataset (red line)

Mean Absolute Error (MAE) and Root Mean Square Error (RMSE) was also calculated as follows:

$$MAE = \frac{1}{N}\sum_{k=1}^{N}|p_k - o_k|, \qquad RMSE = \sqrt{\frac{1}{N}\sum_{k=1}^{N}(p_k - o_k)^2} \quad ,$$

where N is the number of observed/modeled days and p_k and o_k stand for simulated and observed values. Scores of MAE and RMSE for all the stations of the study area are reported in Table 3, showing a good agreement between observations and MSWEP rainfall data.

Station	MAE	RMSE
pcp38	2.31	6.62
pcp81	2.27	6.27
pcp82	2.27	6.18
pcp398	1.9	5.6
pcp403	2.06	5.88

Table 3 - MAE and RMSE scores for each stations calculated using observations and MSWEP daily rainfall values

Temperature data

Temperature values can be simulated or introduced as daily record in SWAT model. In this study, for the historical period, temperature was simulated by the SWAT internal Weather Generator, starting from simple statistics (Figure 17) coming from 49 stations all over the island. This choice was made due to the lack of daily values and validated datasets. The only weather stations falling in the study area is located nearby Iglesias town and related statistics are shown in Figure 17

STATION	WEA26
WLATITUDE	39.30
WLONGITUDE	8.53
WELEV	193.00

Month	Max	Min	Std Max	Std Min
Jan	14.65	5.27	3.80	2.76
Feb	15.29	5.57	3.70	2.82
Mar	17.67	6.82	3.19	2.68
Apr	20.30	8.42	3.85	2.68
May	24.77	11.57	4.16	2.55
Jun	30.84	15.57	4.64	2.70
Jul	34.73	18.21	4.32	2.70
Aug	34.85	18.51	4.43	2.25
Sep	30.94	16.56	4.13	2.16
Oct	25.07	13.33	3.70	2.79
Nov	19.93	9.64	4.02	2.67
Dec	16.44	6.96	3.52	2.84

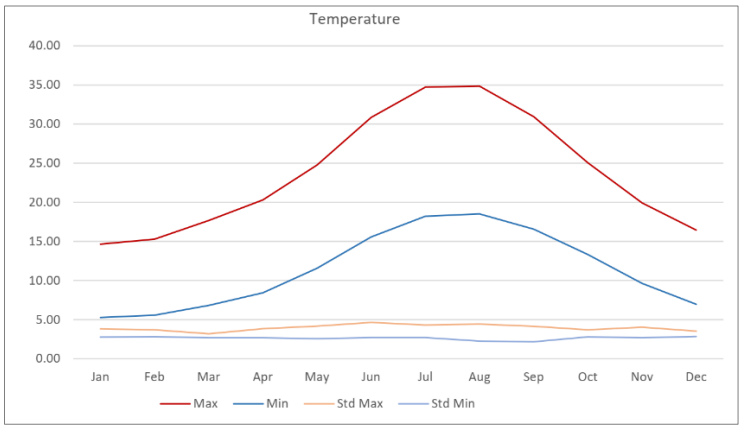

Figure 17 - Statistical data used to generate daily values by the SWAT weather generator

Maximum mean temperatures range from around 15°C in winter to 35°C in summer, while minimum usually exceed 5°C in winter and always fall above 15°C from June to October. The diel temperature excursion between minimum and maximum is usually high, going from 10°C in winter to 15-18°C in summer months, as highlighted in the chart in Figure 17.

Calibration of the SWAT model

Physically based numerical models, such as SWAT, are regulated by a number of parameters with a specific physical meaning and spatial distribution. Most often, available data on study areas are scarce or incomplete, contain errors or do not have the proper spatial scale. Furthermore, a model can be calibrated for different purposes, defining specific limits of use of the model. For instance, a model optimized for the simulation of the streamflow might not well reproduce sediments or nutrients cycle. Abbaspour et al. (2007), probed that multi-objective functions and multi-site calibration significantly improve the goodness of calibration.

Calibration of the model was performed using Sequential Uncertainty Fitting SUFI-2 (Abbaspour et al., 2004; Abbaspour et al., 2007) that takes account of all the input and output sources of uncertainty such as the uncertainty in the input data, parameters and observed data. The simulation uncertainty is expressed by the 95% Percentage of Prediction Uncertainty (95PPU), calculated at the 2.5% and 97.5% levels of the cumulative distribution of an output variable obtained through Latin Hypercube (LH) sampling (Abbaspour et al., 2007). The LH sampling is performed within the range of the hydrological and soil parameters given by the user. Hence, for each simulation, a combination of parameters' values gives a precise output curve, for example, river discharge in time. The

different curves of river discharge, obtained using different parameters' sets for each simulation, can be figured as a band of signals that is the 95PPU band. The uncertainty is then quantified by the R-factor, which is the average thickness of the 95PPU band divided by the standard deviation of the measured data, and by the P-factor that is the percentage of observed data bracketed by the 95PPU. While monitoring the model uncertainty, SUFI2 measures the fitting of the simulation with the observations using Nash-Sutcliffe index (NS) (Nash & Sutcliffe, 1970), reducing the parameters ranges around the values that give the best NS index. NS index is expressed as:

$$NS = 1 - \frac{\Sigma_i (Q_m - Q_s)^2}{\Sigma_i (Q_{m,i} - \overline{Q}_m)^2}$$

where Q is a variable (e.g., discharge), and m and s stand for measured and simulated, respectively, and the bar stands for average. NS variates from 1 (perfect model) to -∞, having a good model reliability with values above 0.5. The best solution is hence a parameter set that is a combination between a relatively low model uncertainty and a good fitting of the model output with the observed variable or variables. An interesting relation between parameters and model output can be summarized by the **FIGURE 18** (Abbaspour,2007) that shows how the range of the parameter's value can affect the uncertainty of the model. In (a), the range of the parameter variability is restricted to a single value (left side) and the model's output is hence a curve. As the parameter's range becomes wider (b) the output of the model increases its variability, producing a "band of curves" that increases its thickness (c) together with the parameter's width. In (d) the red curve is the observed data, while the grey band still represents the variability of the output of the model, meaning that the model is unable to reproduce observations.

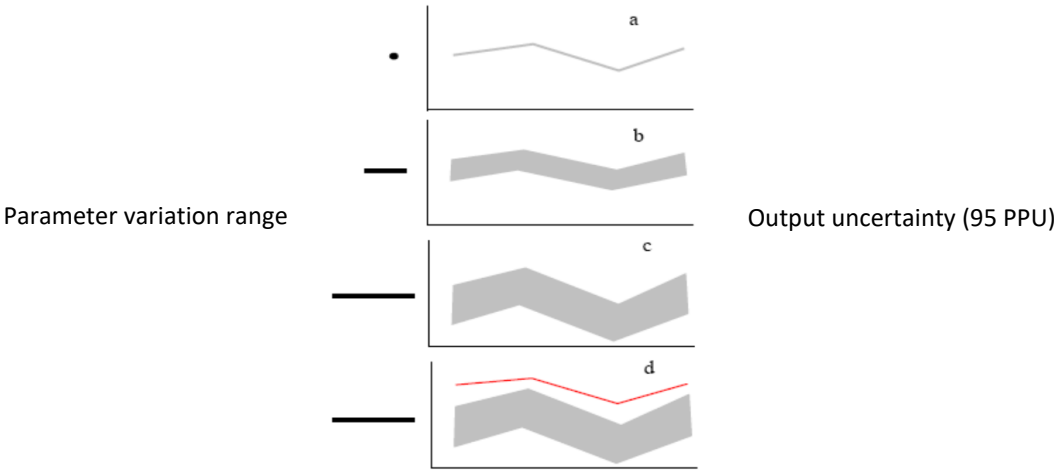

Figure 18 - Relationship between parameter values and model uncertainty

Daily streamflow data from 1985 to 1994 was used for calibration, dividing the time series in calibration period (1985-1992) and validation period (1992-1994). First approach to calibration was the analysis of simulated discharge against measured streamflow at the control point of Rio Mannu di Fluminimaggiore (see Figure 7), comparing different time scales: monthly (Figure 19) and daily (Figure 20).

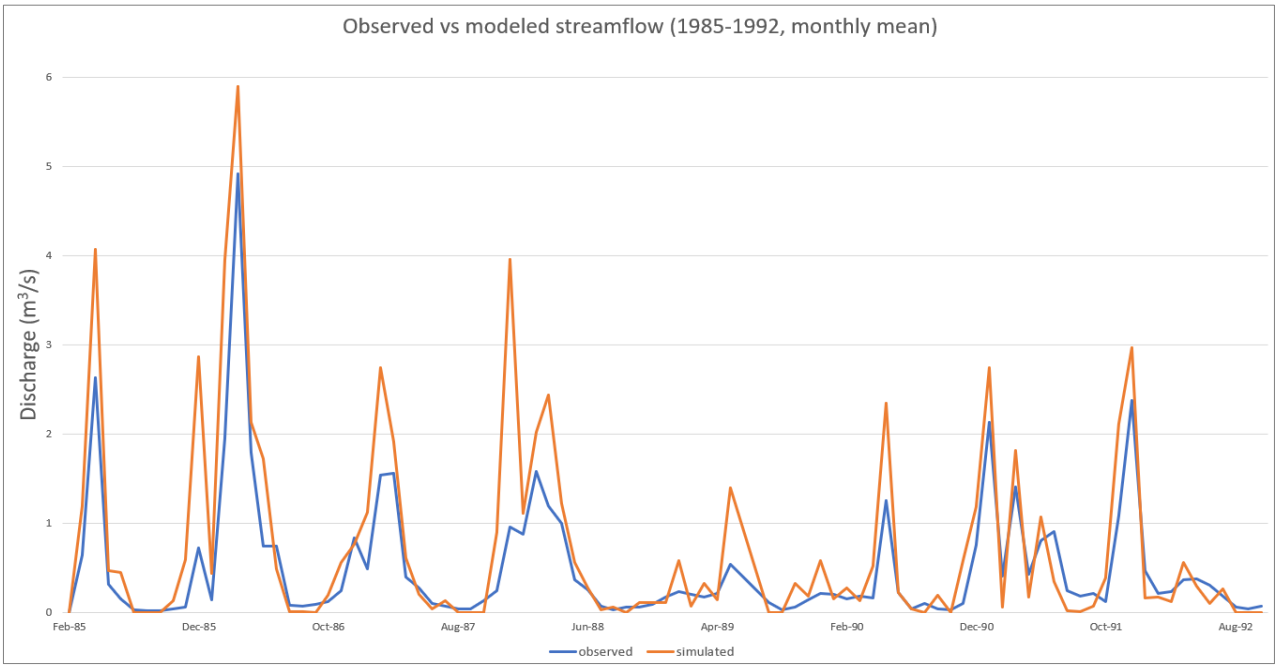

Figure 19 Observed vs modeled discharge before calibration at monthly time-step

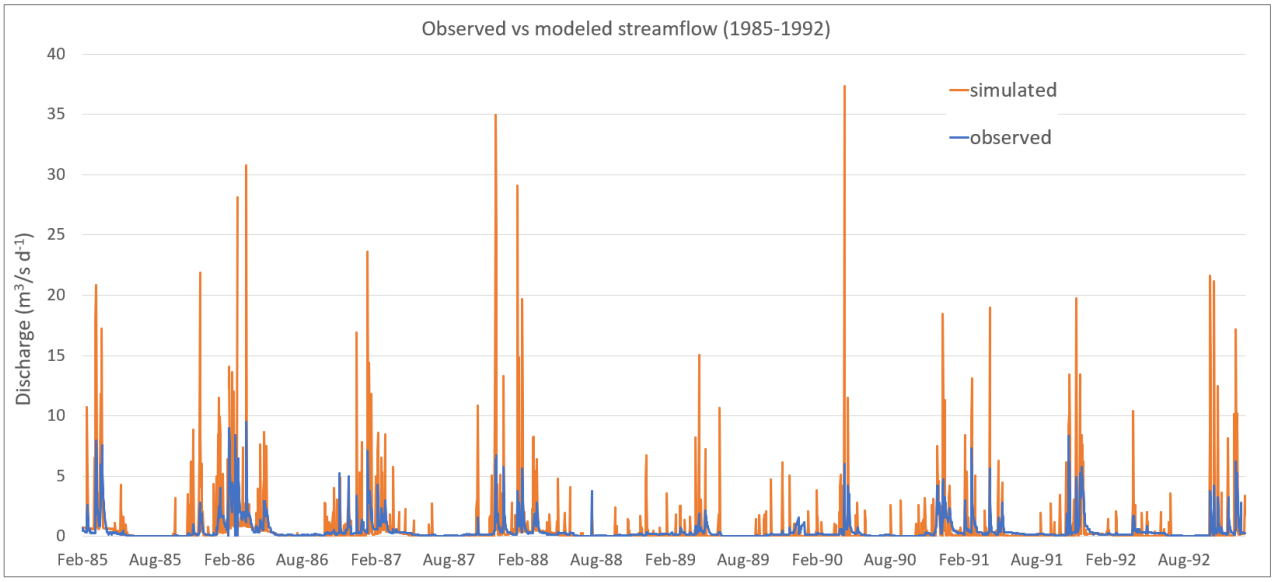

Figure 20 - Observed vs modeled discharge before calibration at daily time-step

Parameters choice was made starting from some considerations on the curves in Figure 19 and Figure 20: assumed a general overestimation of the flow was, mainly caused by a wrong infiltration/runoff rate, with extremely rapid baseflow response and low evapotranspiration rates. In a previous study (Marras et al. 2014) calibration of the SWAT model of the Sardinian was carried out with good results, hence the resulting parameterization was also considered in this setup. Here follows a description of the parameters included in calibration procedure, that was performed with the software SWAT-CUP using SUFI2 method.

Table 4 - Parameters modified during calibration and their natural ranges of variation

Parameter	**Meaning**	**min value**	**max value**
CN2	SCS runoff curve number	35	98
ALPHA_BF	Baseflow alpha factor (days).	0	1
SOL_K	Saturated hydraulic conductivity	0	2000
SOL_AWC	Available water capacity of the soil layer	0	1
CH_K2	Effective hydraulic conductivity in main channel alluvium	0.01	500
CH_N2	Manning's "n" value for the main channel	0.01	0.3
ALPHA_BNK	Baseflow alpha factor for bank storage	0	1
ESCO	Soil evaporation compensation factor	0	1
SLSUBBSN	Average slope length	10	150

A sensitivity analysis (Figure 21) was performed, setting a parameter's wide range of variation, in order to evaluate which parameters were more influent for the ouput variable (discharge). In this

analysis, the larger, in absolute value, the value of t-stat, and the smaller the p-value, the more sensitive the parameter.

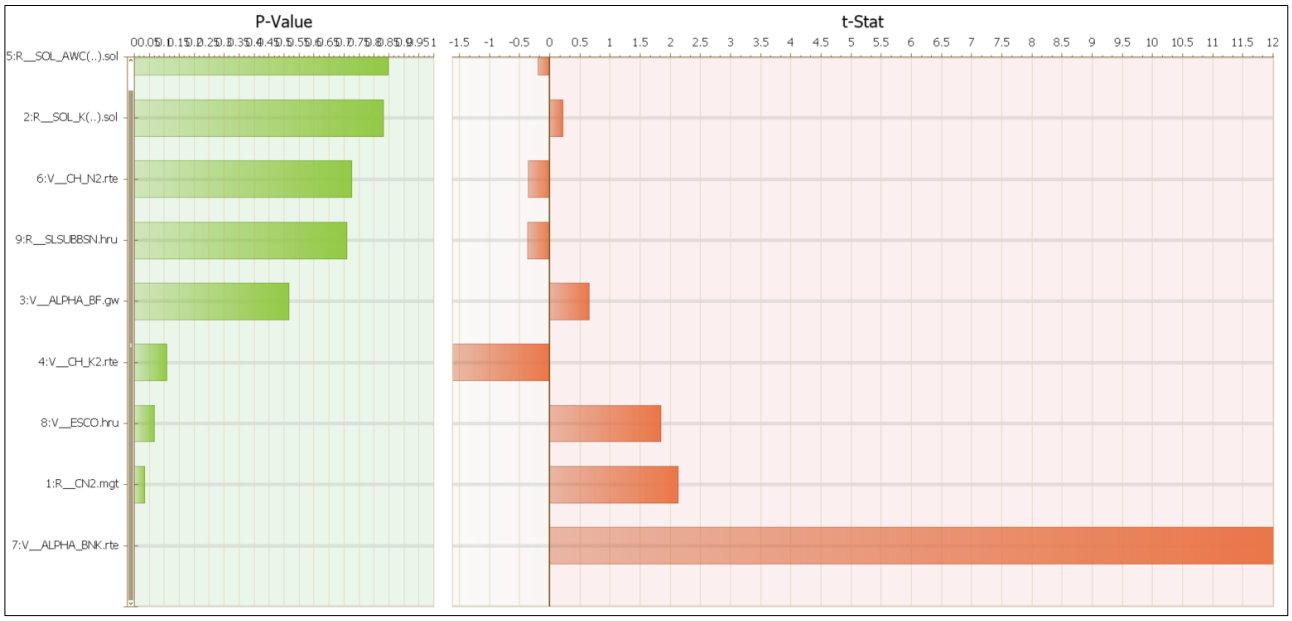

Figure 21 - Sensitivity analysis of the parameters modified during calibration. In this analysis, the larger, in absolute value, the value of t-stat, and the smaller the p-value, the more sensitive the parameter.

Sensitivity analysis results suggested that most sensitive parameters regard baseflow, curve number and soil evaporation, that were hence modified paying more attention in agreement with previous considerations. The final calibration procedure was performed running 480 model iterations, many as suggested in literature in order to restrict parameter's range, hence uncertainty, at each run, around the values that produced the best result. Hence, final result is one of the possible combinations of parameter values that give the best NS index and the lower uncertainty. Final parameter values are shown in Table 5, specifying which values were modified as relative change and which ones were instead setup as absolute values. CN2, SOL_K, SOL_AWC and SLSUBBSN were modified with relative change method, meaning that their absolute value, that is different for each soil, was multiplied by 1 - best value (eg CN2 absolute values, that range from 35 to 98, were multiplied by 1-0.51). Parameters modified with value setting method were set as absolute values.

Table 5 - Parameters final values and calibration method

Parameter	Method	Best value
CN2	Relative change	-0.510417

ALPHA_BF	Value setting	0.771875
SOL_K	Relative change	0.073021
SOL_AWC	Relative change	0.590993
CH_K2	Value setting	97.39765
CH_N2	Value setting	0.088567
ALPHA_BNK	Value setting	0.176042
ESCO	Value setting	0.293421
SLSUBBSN	Relative change	0.109114

The result at daily time-step (FIGURE 22) was quite sactisfactory, with a very good p-factor and r-factor indexes, meaning that almost all the observations can be reproduced by the model with relatively small uncertainty, and a good NS index confirmed also by a good R2 value. However, It is never correct to assume that only one set of parameters can represent a watershed, which was modeled by very uncertain information about soil, landuse, climate, management, measured data used for calibration, etc. (Abbaspour, 2015), meaning that this calibration set is only one of the possible solutions.

```
1 Goal_type= Nash_Sutcliff    No_sims= 480   Best_sim_no= 149
2
3 Variable           p-factor  r-factor  R2    NS     bR2
4 FLOW_OUT_48        0.92      0.99      0.69  0.66   0.5473
5
```

Figure 22 – Statistics of the SWAT calibration results at daily time-step

Also visual analysis of the calibrated streamflow against observed data shows good results, with quite good fitting of the curves and a relatively narrow 95PPU band (Figure 23).

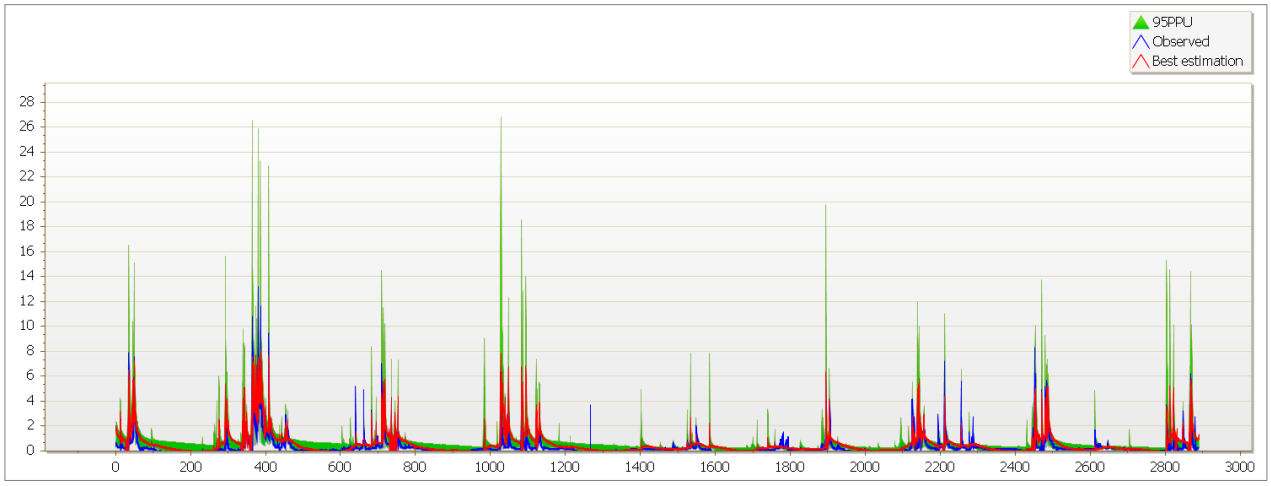

Figure 23 - Calibration of the daily streamflow (1985-1992) at the Flumineddu measurement station

Daily calibration performance was also validated at monthly time-step (FIGURE 24) giving better results, due to the coarser scale of analysis, scoring a NS index of 0.88. Considered that the result of the future projection was expected to be given at the monthly scale and considering that observation data used as model input has not such good quality, no further calibration was retained to be done.

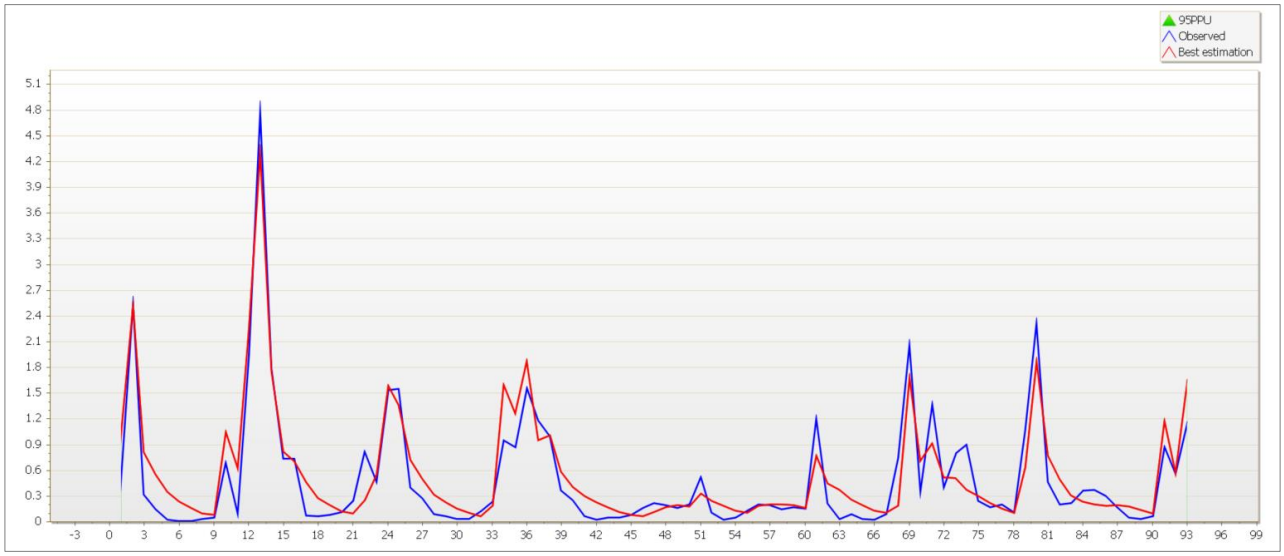

Figure 24 - Simulated against observed streamflow validation at the monthly time step.

SWAT-HM heavy metal model

Heavy metal transport modeling can provide helpful information for pollution prevention and remediation strategies. However, heavy metal models are still simplified and, up to now, most metal budget assessment did not fully address all the primary input and output pathways (Zhou et al. 2019). Relative to the heavy metal input data, measured data for the estimating HM outputs (such as the metal fluxes in surface runoff, eroded soil and leaching flow) are often more scarce or inaccurate, reflecting the difficulties in field sampling and the variability of heavy metal output fluxes both in space and time. (Bengtsson et al., 2006; Gray et al., 2017; Peraza-Castro et al., 2016; Quinton and Catt, 2007; Tao et al., 2003). Hence, uncertainty becomes an important issue in HM accounting, which is, however, not addressed in most studies (Zhou et al., 2019 under review).

Model description

Meng et al. (2018) coupled SWAT with a heavy metal model to simulate the long-term fate and transport of HM at the watershed scale. SWAT-HM is hence a physical and process-based model that simulates the metal transport from the upland to the river outlet. SWAT-HM differs from event-oriented models such as the TREX model (Velleux et al., 2006, 2008), which is operated with high time resolution (hourly and sub-hourly) and hence potentially fulfills the short-term risk identification and analysis (Meng et al., 2018). Three main reactions are considered in the heavy metal transformation model: sorption, complexation and slow reaction, that is important in long-term simulations. The schematic diagram in **FIGURE 25** and **TABLE 6** explain the three upland and channel main reactions in the SWAT-HM model: (a) the adsorption and desorption of free ions (M^{n+}) and labile metal (M_l), the association and dissociation between free ions (M_{n+}) and metal complexes (M_l) in the solution, and the slow reaction between labile metal (M_l) and non-labile metal (M_n) in the solid, where k_{ads}, k_{des}, ka, k_d, k_1 and k_{-1} are the partition coefficients/rate constants; (b) simplified heavy metal transformation model, in which free ions (M_{n+}) and complexes (M_l) are regarded together as dissolved phase metal (M_d). M_l is the fraction of metal that is available for reactions, while the M_n is the fraction of metal that is not reactive.

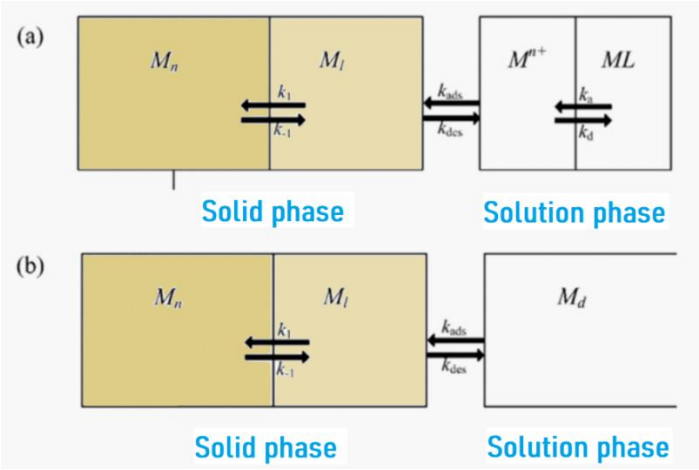

Figure 25 - Graphical representation of the metal transformation model in the soil-water environment. (reproduced from Degryse et al., 2009)

Table 6 - Three major reactions in the soil-water environment and their kinetics equations, equilibrium constants, response times and reaction rates

Reaction	Formula	Kinetics equation, equilibrium constant, response time	Reaction rate	Zn	Pb
Sorption	$M_l \rightleftarrows^{k_{des}}_{k_{ads}} M^{n+}$	$\theta \frac{d[M^{n+}]}{dt} = -k_{ads}\theta[M^{n+}] + k_{des}\rho M_l$ $\rho \frac{dM_l}{dt} = -k_{ads}\theta[M^{n+}] - k_{des}\rho M_l$ $K_d^{lab/free} = \frac{M_l}{[M^{n+}]} = \frac{k_{des}}{k_{ads}\frac{\rho}{\theta}}$ $T_C^1 = \frac{1}{k_{des} + k_{ads}\frac{\rho}{\theta}}$	$k_{ads}(10^3 s^{-1})$ $k_{des}\frac{\rho}{\theta}(10^6 s^{-1})$ $T_C^1(s)$	3.31 25 300	1..2 14 700
Slow reaction	$M_n \rightleftarrows^{k_{-1}}_{k_{1s}} M^{n+}$	$\frac{dM_l}{dt} = -k_1 M_l + k_{-1} M_n$ $\frac{dM_n}{dt} = k_1 M_l - k_{-1} M_n$ $K_s = \frac{M_l}{M_n} = \frac{k_{-1}}{k_1}$ $T_C^3 = \frac{1}{k_{-1} +}$	$k_1(10^4 d^{-1})$ $k_{-1}(10^4 d^{-1})$ $T_C^3(s)$	8.37 12.6 478	7.25 5.25 800

Relations between k_d and pH are expressed by the following equations:

For Zn, hml k_d = 10**(-2.48 +0.69 * pH + 0.67 * LOG10(soc))

For Pb, hml k_d = 10**(1.32 +0.40 * pH + 0.50 * LOG10(soc))

Upland phase

In the upland phase of SWAT-HM, metals are divided in: dissolved metal in soil-aqueous phase, labile metal in soil-solid phase and non-labile metal in soil-solid phase. The model simulates equilibrium-based sorption reaction between Dissolved metal and labile metal, as well slow aging reaction between labile and non-labile metal. Metal moves vertically in soil layers through leaching and capillary flow, induced by evapotranspiration, and horizontally from the upland to the river channel via soil erosion, runoff, infiltration and lateral flow.

Leaching is simulated based on quantitative comparison of the hydrological dispersion rate and metal species transformation rate, like adsorption and desorption, it is justified to assume a local equilibrium for Zn and Pb. The key parameter of this process is the K_d coefficient and the change of metal in soil is then function of time, metal concentration and flow rate:

$$M_{flow} = M_0 \cdot \left(1 - \exp\left(\frac{-w_{mobile}}{SAT + K_d \rho d} t\right)\right)$$

where M_{flow} is the amount of heavy metal transported with flow in the soil per hectare (kg ha^{-1}), M_0 is the initial amount of mobile heavy metal in the soil per hectare (the sum of the Md and M_l amounts, kg ha^{-1}), t is the time, w_{mobile} is the amount of mobile water (mm), SAT is the saturated soil moisture (mm), d is the depth of the soil layer (mm), and ρ is the soil bulk density (kg m^{-3}) (Meng Y. et al, 2018).

Upward migration of the metal from the deeper layer to the surface layer of the soil is allowed through the rising soil water that moves within evapotranspiration and contains dissolved metals. The upward migration is simulated using a function that is derived as follow:

$$M_{\mathrm{up}} = M_0 \cdot \frac{w_{\mathrm{evap}}}{wtr + K_{\mathrm{d}} \rho d} t$$

where M_{up} is the amount of heavy metals moving to the surface soil layer per hectare (kg ha^{-1}), w_{evap} is the amount of water moving upward as a result of evaporation (mm), and *wtr* is the water content of the subsurface soil layer (mm).

[M^{n+}] is assumed to remain unchanged in the soil layer within a time step during upward migration. Also plant uptake is modeled, using a simple Plant Uptake Factor (PUF) (Swartjes, 2011). Heavy metal balance is computed at the HRU level and all the contributes from each HRU within the sub-basin are summed to output total metal load from the sub-basin to the river channel. Wastes and dumps contribute to the metal load through weathering, as well atmospheric deposition fertilizers and livestock manures can be inputted to the model.

Heavy Metals in solid phase move with particles when soil erosion occurs. The equation that quantifies the amount of metals transported with soil is

$$M_{ero} = (M_l + M_n) \cdot sed_{ero} \cdot \varepsilon \cdot UF$$

where M_{ero} is the amount of heavy metal transported with eroded soil per hectare (kg ha^{-1}), M_l and M_n are the concentration of labile or non-labile metal in soil (mg kg^{-1}), respectively, sed_{ero} is the amount of sediment transported to the channel per hectare (kg ha^{-1}) (Meng Y. et al.,2017), ε is the enrichment ratio of heavy metal (Quinton and Catt, 2007), defined as an analog of the enrichment ratios for other chemicals (nitrogen, phosphorus and pesticide) in SWAT (Knisel, 1980; Neitsch et al., 2011), and UF is a unit conversion factor that has a value of 10^{-6}.

Channel phase

The channel phase consists in the simulation of the transport of the heavy metals in the stream or other water bodies. River channel is simplified with the assumption of a water column overlying sediments with a certain number of layers, and processes are simulated separately for streambed and water. In the water column metal can be present as dissolved metal in the aqueous phase and particulate metal with a labile and a non-labile metal fraction. In stream sediments as well, metal can be present as dissolved phase in the pore water, labile and non-labile fractions in the solid phase. River channels receive the contribution of the non-point and point sources of the corresponding sub-basin. During the transfer to the basin outlet, depending on the conditions and dynamics, additional processes such as diffusion, burial, settling and re-suspension can be simulated. Diffusion of dissolved metal between the water column and riverbed pore water is controlled by the concentration gradient (Lick, 2008). The burial process is the downward movement of the particulate metal to the deeper sediment layers. Conventionally, top layer of the stream sediments is modeled as “active layer” (Figure 26) and its thickness can be changed in the simulations. Metals can be buried below active layer in the deep layer.

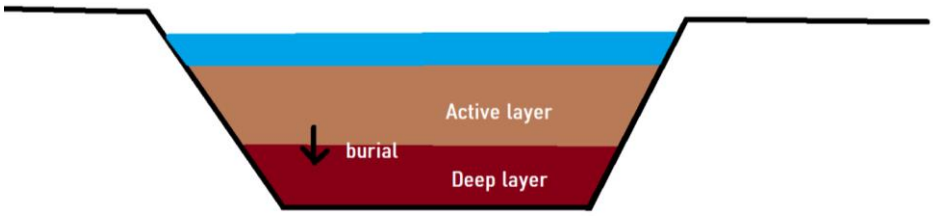

Figure 26 - Scheme of the stream sediment modelization

Settling and resuspension of metals in suspended and bed sediments, are simulated starting from the sediment budget of SWAT model as shown in the following equations:

$$M_{\text{set}} = sed_{\text{set}} \cdot (M_{\text{l,p}} + M_{\text{n,p}}) \cdot UF$$

$$M_{\text{res}} = sed_{\text{res}} \cdot (M_{\text{l,b}} + M_{\text{n,b}}) \cdot UF$$

where M_{set} and M_{res} are the amounts of settled and resuspended heavy metal (kg), respectively; sed_{set} and sed_{res} are the amounts of settled and resuspended sediment (kg), respectively; $M_{l,p}$ and $M_{n,p}$ are the concentrations of the labile and non-labile metal in the suspended sediment (particulate phase, mg kg^{-1}), respectively; $M_{l,b}$ and $M_{n,b}$ are the concentrations of the labile and non-labile metal in the bed sediment (mg kg^{-1}), respectively; and UF is a unit conversion factor, 10^{-6} (Meng Y. et al., 2017).

Diffusion process is the movement of dissolved metal from the water column to the pore water of the riverbed and vice versa. Diffusion process is controlled by the concentration gradient (Lick, 2009) the metal moves from the higher to the lower concentration medium, following the equation:

$$M_{\text{dif}} = V_{\text{d}} \cdot \left| [M_{\text{d,w}}] - [M_{\text{d,b}}] \right| \cdot UF$$

where M_{dif} is the diffusion flux of heavy metal (kg m^{-2} d^{-1}), V_d is the diffusion velocity (m d^{-1}), [Md,w] and $[M_{d,b}]$ are the concentrations of dissolved metal in the water column and in the pore water of bed sediment (mg L^{-1}), respectively, and UF is a unit conversion factor, 10^{-3} (Meng Y. et al., 2017).

Burial is the downward movement of the metals from the active riverbed layer to the deeper sediment layers. This process is represented by the equation:

$$M_{\text{bur}} = V_{\text{b}} \cdot (M_{\text{l,b}} + M_{\text{n,b}}) \cdot \rho_{\text{b}} \cdot UF$$

where M_{bur} is the burial flux of heavy metal (kg m^{-2} d^{-1}), V_b is the burial velocity (m d^{-1}), ρ_b is the bulk density of bed sediment (kg m^{-3}), $M_{l,b}$ and $M_{n,b}$ are the concentrations of the labile and non-labile metal in the bed sediment (mg kg^{-1}), respectively, and UF is a unit conversion factor, 10^{-6}.

Atmospheric deposition is modeled in SWAT-HM as annual rate of total atmospheric deposition (g ha^{-1} yr^{-1}), setting a fraction of labile metal. Daily deposition amount of labile metal is then the total deposition rate multiplied by the fraction of the labile portion and it is added to the labile metal pool of the first soil layer, while the non-labile fraction is added to the non-labile metal pool of the first soil layer.

SWAT-HM model implementation

Measured concentration of Zn and Pb in soil, water, air and stream-sediment from samples collected by IGEA were used for this study. Samples of different mediums were collected after the mines' definitive closure, in the context of different environmental characterization plans. Here follows a description of each dataset.

Soil samples

A total 144 samples, collected in soils, tailings and dumps, were used to model non-point sources in SWAT-HM. Soil samples, distributed as shown in Figure 27 and 3, were collected from 2004 to 2010 by IGEA and measures of metals concentration (Zn, Pb, As, Cd, Hg, etc.), humidity, pH and density are available for each sample. The soil samples were characterized using standard official Italian analytical methods for soils (GURI, 1999).

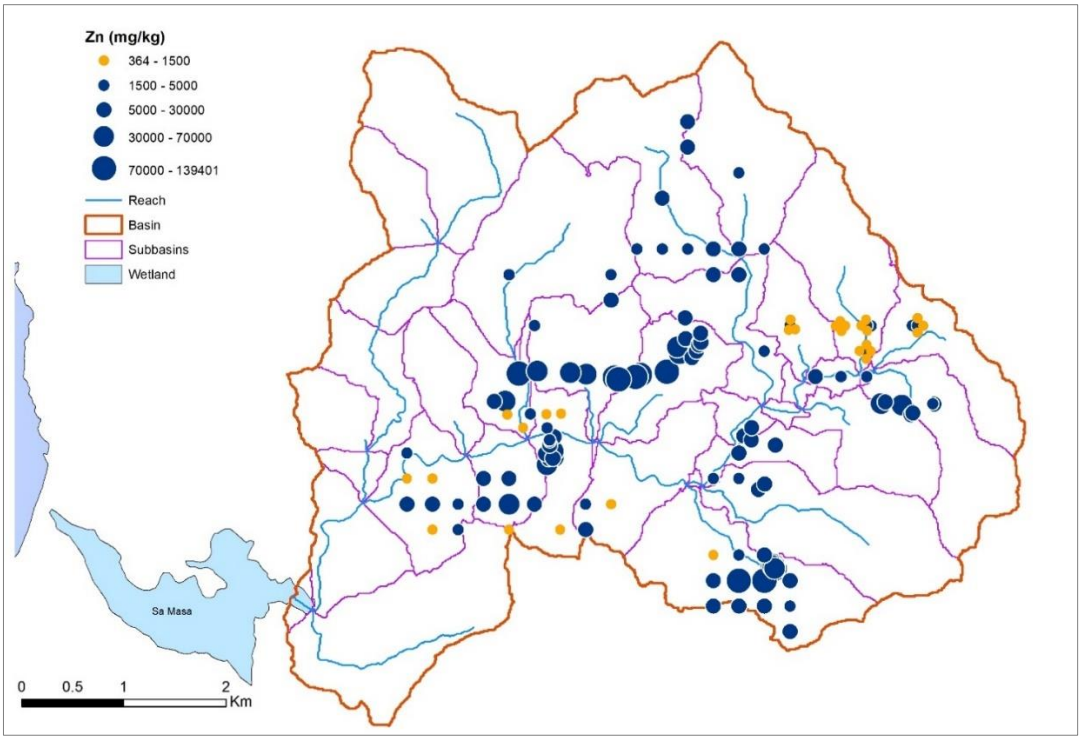

Figure 27 – Map of the soil samples for which total Zn was measured and their distribution over the Rio San Giorgio basin. Green spots are samples with Zn concentration below the law limit, black spots are instead samples over the concentration limit.

FIGURE 27 shows the location of the Zn sampling sites and the concentration range of each sample. No values of Zn concentration below the limit for urban areas (150 mg/kg) were measured, and a significant number of samples have values 1 or more orders of magnitude higher than the limit for industrial areas (1500 mg/kg). FIGURE 27 shows the location of the Pb sampling sites and the concentration of each sample. Most of the samples have values above the concentration limit for industrial areas, with very high values close to 100 times the legal limit around the mining areas.

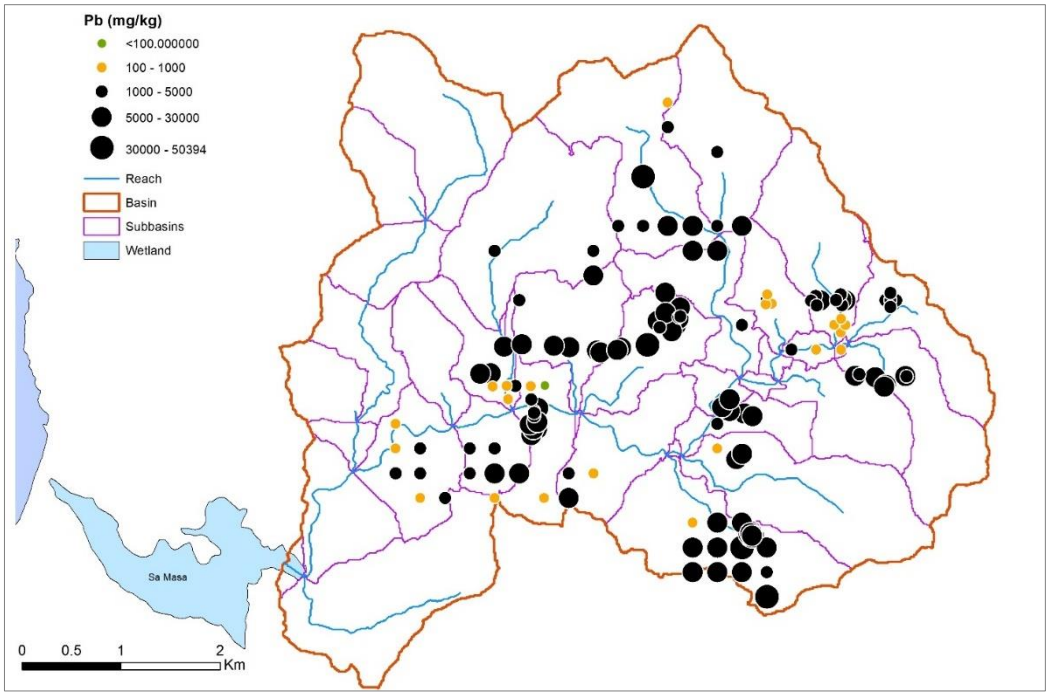

Figure 28 Map of the soil samples for which total Pb was measured and their distribution over the Rio San Giorgio basin. Green spots are samples with Pb concentration below the law limit, yellow spots are above the limit for urban areas but below the limit for industrial areas and black spots are the samples over the concentration limit for industrial areas.

Table 7 - Statistics of Zn and Pb samples in the area

	Zn (mg/kg)	Pb (mg/kg)
Maximum	139401	50394
Minimum	364	97
Average	17606	8223
Std. Dev.	26560	10002
Legal limit (industrial use)	1500	150
Legal Limit (Urban areas)	1000	100

TABLE 7 resumes some statistics the Zn and Pb soil samples: the maximum, the minimum, the simple average of the concentration and the limit concentration imposed by Italian laws for industrial and urban land use. The resulting medium concentration of the Zn is around 11 times the limit allowed by the law (Dlgs. 152/06) for industrial use areas, while the Pb average concentration is around 50 times higher compared to the allowed limit for industrial areas.

Soils samples and respective Zn and Pb concentrations have been overlapped with HRUs map, using GIS-based spatial tools, to obtain the concentration of the two metals in each HRU. The map in **FIGURE 29** shows the spatial distribution of the soil samples within the HRUs, differentiating the

HRUs with measures (beige areas) and HRUs where no collected samples were retrieved (green areas). For areas not covered by samples, background values of metals' concentration reported by IGEA were used, on the basis of the geological features of the HRUs, as shown in Table 8.

Table 8 – background concentration values for Pb and Zn for each main lithology.

Lithology	**Pb (mg/kg)**	**Zn (mg/kg)**
Sandstones	1.493	1.887
Carbonates	4.298	7.559
Schist	1.975	3.745

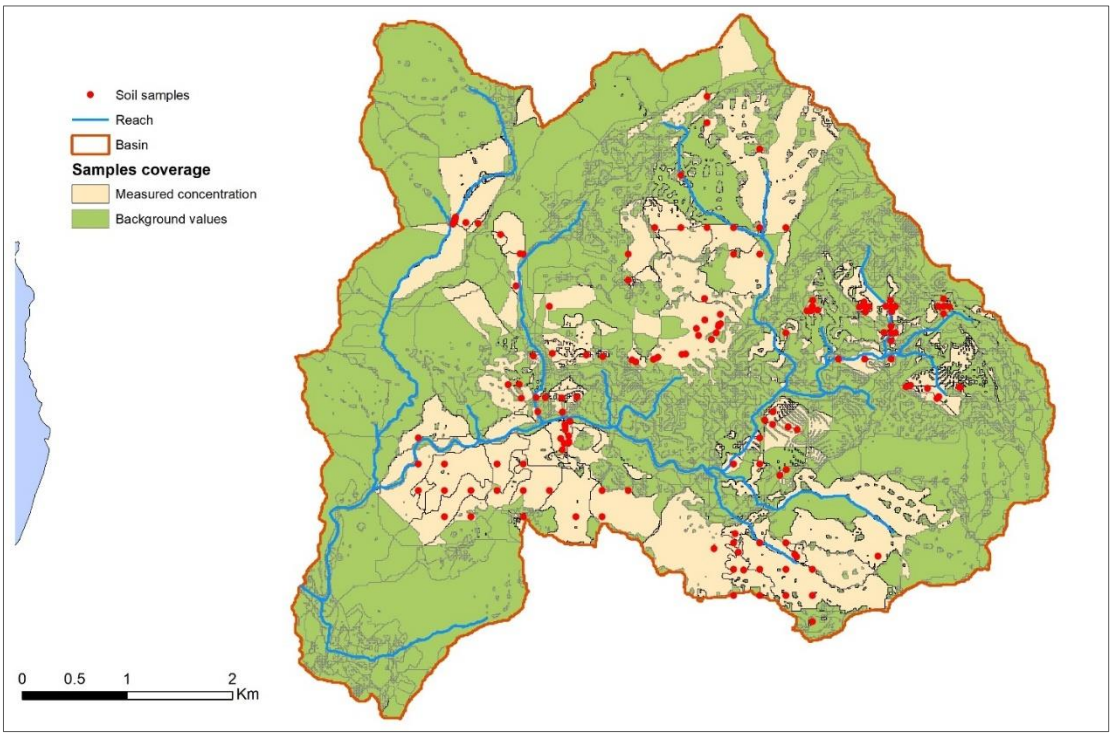

Figure 29 – Distribution of the soil samples related to the HRUs subdivision. Green areas indicate HRUs with no sampled soils, beige areas indicate HRUs in which soil samples (red spots) have been collected.

Values of pH were also measured in collected soil samples (TABLE 9). When soil pH value was not given, the mean value of 7,9 (over all the samples) was used. Lower values of pH measurements between 3 and 5 were found nearby San Giorgio mine and Monte Scorra mine, probably related to mine acid drainage. Neutral to basic values are probably related to the presence of carbonate rocks of the *Gonnesa Group*.

Table 9 - Simple statistics for measured pH in soil samples

Mean	Max	Min	Std. Dev.
7.89	8.75	3.27	0.15

Waste rock dumps

Waste rock dumps are modeled in SWAT-HM as fraction of each HRU. For this purpose, GIS tools helped first to delineate the waste deposits within the watershed, using satellite data and RAS database, and then allowed to determine the waste fraction in each HRU through a simple intersection of the two layers. Hence, concentrations of Zn and Pb in wastes and tailings were averaged for each dump and assigned to the intersecting HRUs. .

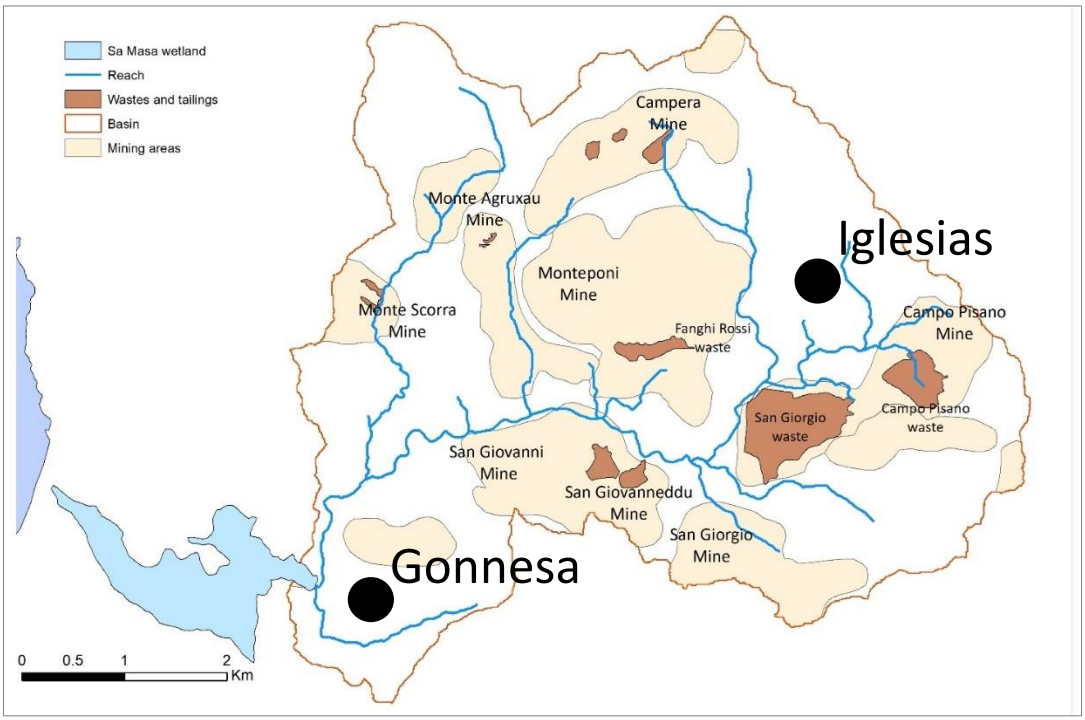

Figure 30 - Distribution of mining areas and main mine wastes in the basin

Stream sediment data

Stream sediments' samples were collected by IGEA in 2006 in 14 sampling sites. In each sampling site Zn and Pb concentrations and pH were measured as reported in FIGURE 31.

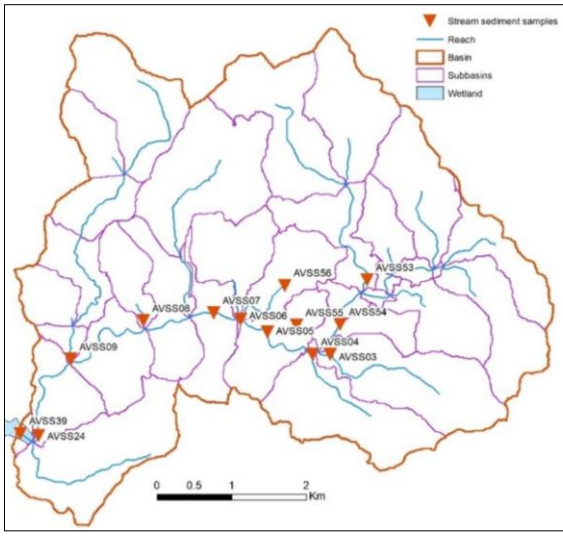

Sample	Zn (mg/kg)	Pb (mg/kg)	pH
AVSS44	8558.00	6347.00	8.65
AVSS56	36155.00	6607.00	9.06
AVSS55	125365.00	24228.00	8.37
AVSS54	17917.00	2524.00	8.07
AVSS53	19947.00	2961.00	8.65
AVSS39	20541.00	10897.00	9.01
AVSS24	37668.00	10739.00	8.50
AVSS09	3041.00	1931.00	8.26
AVSS08	3625.00	1855.00	9.00
AVSS07	70216.00	10088.00	7.58
AVSS06	80679.00	16482.00	8.63
AVSS05	131304.00	40059.00	8.37
AVSS04	5071.00	3838.00	8.28
AVSS03	22775.00	7622.00	8.53

Figure 31 - Stream sediment samples map and measures of Zn and Pb concentrations. Red values are the highest values, while blue values are the lowest.

Sample AVSS05, collected downstream of Campo Pisano, San Giorgio and San Giovanneddu wastes, shows the highest concentrations of Zn and Pb, while lowest values of both metals were measured more downstream (samples AVSS08 for Pb and AVSS09 for Zn). Despite this, concentration increases again in the most downstream samples, nearby the main river's outlet (AVSS024 and AVSS039). Hydrological tracer studies from De Giudici et al. (2017) show that biogeochemical activity can be active in natural abatement from river waters.

Point sources

Two point-sources release urban wastewater in the Rio San Giorgio. Point sources have been modeled, inputting, as mentioned above, a constant daily of water amount obtained by simple division of the annual discharge. No data about concentration of metals in wastewaters was retrieved.

Atmospheric deposition

Atmospheric deposition was measured by IGEA in 3 stations (FIGURE 32) and synthetized as an annual constant rate (g ha^{-1} yr^{-1}) starting from daily rates (TABLE 10), assuming these values to be constant during the simulation's time range. The monitoring of the deposition was conducted from June 2007 to January 2008.

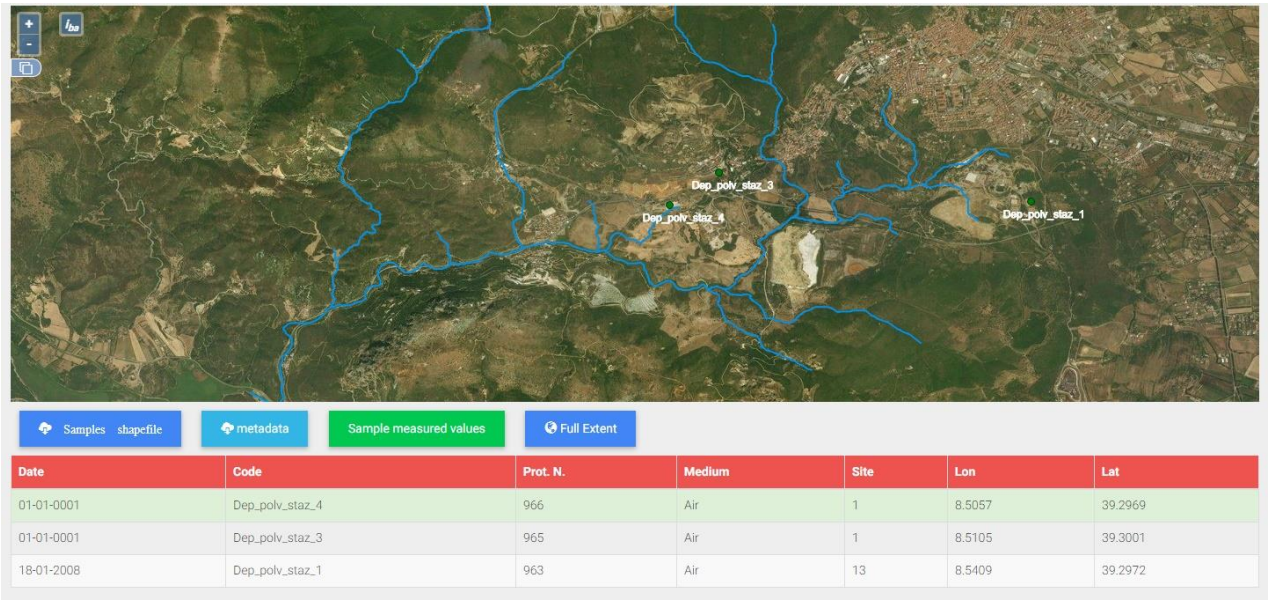

Date	Code	Prot. N.	Medium	Site	Lon	Lat
01-01-0001	Dep_polv_staz_4	966	Air	1	8.5057	39.2969
01-01-0001	Dep_polv_staz_3	965	Air	1	8.5105	39.3001
18-01-2008	Dep_polv_staz_1	963	Air	13	8.5409	39.2972

Figure 32 - Location of the atmospheric deposition measurement stations in the study area

	Dep_polv_staz_1			Dep_polv_staz_3			Dep_polv_staz_4		
Date	Tot ($gr/m^2 \times day^{-1}$)	Pb (mg/kg)	Zn (mg/kg)	Tot ($gr/m^2 \times day^{-1}$)	Pb (mg/kg)	Zn (mg/kg)	Tot ($gr/m^2 \times day^{-1}$)	Pb (mg/kg)	Zn (mg/kg)
01-Jun-07	61.7	756	3952	121,4	8874	23117	61,3	9168	14254
26-Jul-07	40.7	2923	8823	560,9	4030	18472	57,3	13847	65820
26-Sep-07	61.8	3508	12820	173,9	6889	53580	121,6	7681	52249
15-Nov-07	45.1	821	3184	190,1	2066	7255	60,1	10135	15906
18-Jan-08	27.8	680,2	4050,5	54,8	1981	7021	25,2	12134	18560

Table 10 - Total deposition rates and concentration of metals in dust

Model validation

The model accuracy depends on the input data quality and on the observations used for calibration. Lack of high-density sampling in water quality continuous monitoring (e.g. monthly or daily water sampling) and the absence of a streamflow measurement gauge in the Rio San Giorgio, poses some limitations in calibration and, then, in the use of semiautomatic procedures, such as the SUFI-2 algorithm. For this reason, we used a deterministic approach. Metal parameters could only be determined from the information available in the related research papers (Meng et al., 2018; Allison & Allison, 2005; Buekers et al., 2008), varying the values within the suggested ranges and evaluating the effects on model performances, thus causing uncertainty in their estimation. Model performances were evaluated with a simple correlation between observations and model's simulated concentration (**FIGURE 34** and **FIGURE 35**).

SWAT-HM parameters can be divided in two groups: parameters provided by the SWAT model and parameters that specifically pertain the heavy metals characteristics. Coupling the metal model with SWAT allows to use several hydrological output parameters, such as w_{mobile}, w_{evap}, sed_{ero}, sed_{set}, and sed_{res}, to simulate metal behavior. The parameterization and calibration of the hydrological model is hence crucial for the heavy metal transport simulation, and its accuracy is discussed in the **SWAT MODEL** section. Specific metal parameters are the slow reaction kinetic rates (k_{-1}, k_1), the diffusion velocity V_d, the burial velocity V_b, the weathering rate r_w, the partition coefficient for soil (K_d1), for channel sediment (K_d2), and for bed sediment (K_d3), and user can define different values for each HRU or set global values depending on information's availability. Partition coefficients are related with K_{ads} and K_{des} with the equation:

$$K_d^{lab/free} = \frac{M_l}{[M^{n+}]} = \frac{k_{des}}{k_{ads}\frac{\rho}{\theta}}$$

Table 11 - Summary of the soil-liquid partition coefficient K_d (L kg^{-1}) and slow reaction rates k_{-1} (d^{-1}) and k1 (d^{-1}) based on the literature. Values with * are minimum, maximum and average

Parameter	Zn	Pb	Reference
LogK_d1 (in soil)	-1.0-5.0 (3.1) *	0.0 - 4.9 (2.7) *	Allison and Allison (2005)
LogK_d2 (in channel)	3.5-6.9 (5.1) *	3.4 - 6.5 (5.6) *	Allison and Allison (2005)
LogK_d3 (in bed sediment)	1.5-6.2 (4.8) *	2.0 - 7.0 (5.1) *	Allison and Allison (2005)
k_{-1}	$k_{-1} = 3.35\cdot10^{-3} - 4.18\cdot10^{-4}\cdot pH$	$k_{-1} = 1.55\cdot10^{-3} - 1.38\cdot10^{-4}\cdot pH$	Meng et al. (2018) Buekers et al. (2008)
k_1	$k_1\cdot10^{-3} - 4.18\cdot10^{-4}\cdot pH$	$k_{-1} = -3.0\cdot10^{-4} - 1.38\cdot10^{-4}\cdot pH$	Buekers et al. (2008)

SWAT Heavy Metal model output was compared with Zn and Pb measured concentration in stream water. We assumed that measurements represent the daily mean value. However, many studies have shown that metal concentrations can vary notably within a day (Aubert et al., 2014; Kirchner and Neal, 2013; De Giudici et al., 2017). Despite many measures were retrieved, as mentioned above, no continuous time series exist on the same sampling point, representing a primary issue in calibration procedure. Moreover, in the first test of the model (Meng et al., 2018), dissolved metal loads were used instead of concentration values and, due to the availability of continuous time series, SUFI-2 procedure (Abbaspour et al., 2004,2007) was implemented leading to a stronger calibration and uncertainty assessment. Table 12 shows the final values of the parameters obtained after running the model with different combinations of values within their range. Parameters that start with R are relative values, namely multiplicative factors that increase or decrease the absolute values, while parameters starting with V are absolute values. V^bd is the diffusion velocity of the metal from the sediment to the water body and Vb is the velocity of the metal burial in the sediments of the riverbed to the inactive layer. The weathering rate is a factor that adjusts the weathering during rainfall events.

Table 12 – Fitted ranges of parameters in the heavy metal module

Parameter	**Description**	**Metal**	**Values**	**Reference Source**
R__*Kd*1	Multiplicative factor for solid-solution partition coefficient in soil (L kg^{-1})	Zn Pb	0.674 0.470	Allison and Allison (2005) and Degryse et al. (2009)
V__*Kd*2	solid-solution partition coefficient in channel water (L kg^{-1})	Zn Pb	13962 1000	Allison and Allison (2005)
V__*Kd*3	solid-solution partition coefficient in bed sediment (L kg^{-1})	Zn Pb	200 100	Allison and Allison (2005)
R__*k*1	Multiplicative factor for kinetics rate of forward slow reaction (d^{-1})	Zn Pb	-0.62 – 0.51 -0.30 – 0.50	Buekers et al. (2008)
R__*k*-1	Multiplicative factor for kinetics rate of backward slow reaction (d^{-1})	Zn Pb	-0.62 – 0.51 -0.30 – 0.50	Buekers et al. (2008)
V__V^bd	diffusion velocity in water body (m d^{-1})	Zn Pb	$6.33 \cdot 10^{-2}$ $4.20 \cdot 10^{-1}$	Frogner-Kockum et al. (2016)
V__*Vb*	burial velocity in bed sediments (m d^{-1})	Zn Pb	$2.3 \cdot 10^{-3}$ $5.0 \cdot 10^{-3}$	Arnold et al. (2011) Gualtieri (1999)
V__*rw*	weathering rate (--)	Zn Pb	$1.13 \cdot 10^{-4}$ $1.13 \cdot 10^{-4}$	Bennett et al. (2000) Malmström et al. (2000)

Samples from 19 sampling stations, collected between December 2006 and April 2007 by IGEA S.p.A., were used. Samples consist in 57 measures of Zn and 56 of Pb concentration (almost 3 measures in 3 different days for both metals for each sample) collected in the Rio San Giorgio from the headwaters to the outlet along the main flow path. Moreover, data from the study of De Giudici et al (2017) were used. Here follows the map (FIGURE 33) of the water sampling sites that have been used in this study.

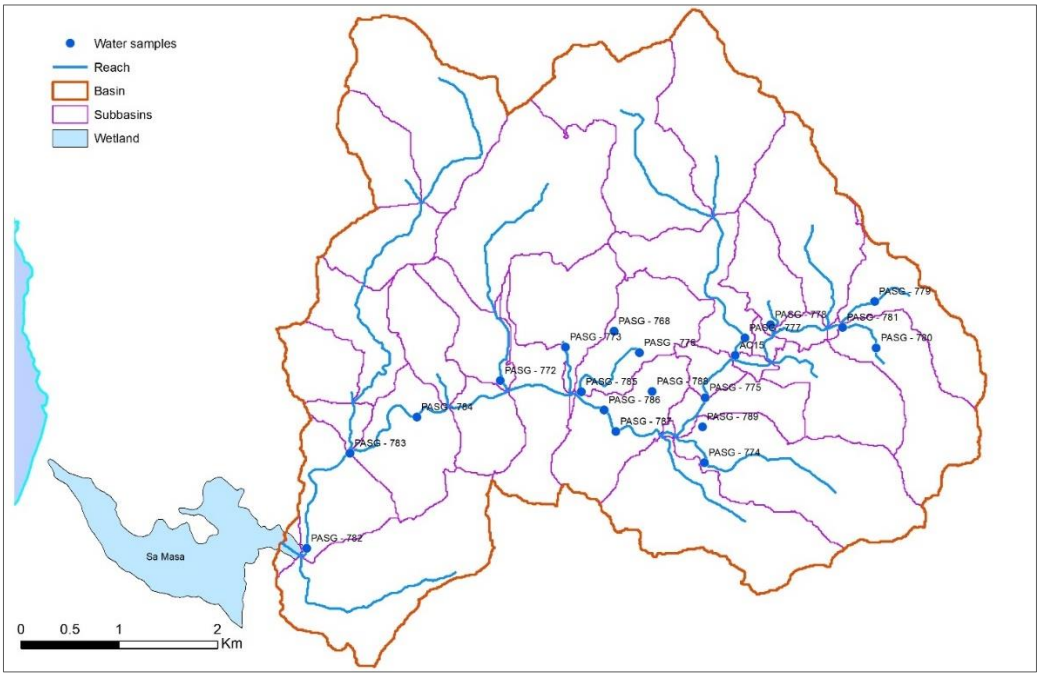

Figure 33 - Distribution of the water sampling sites in the basin. For each point Zn and Pb concentrations were measured in 3 different days between december 2006 and april 2007

Chart in Figure 34, that represents the correlation in bi-logarithmic scale between observed and modeled Zn concentration in different sub-basins (identified by the numbers), shows a good agreement at the main outlet (159), in correspondence of Fanghi Rossi waste (142) and nearby San Giorgio Mine (156). Red line represents excellent agreement among measured and calculated values. The area delimited by green and purple lines represent the limit within 1 order of difference in concentration. Values outside this range are considered to have a significant mismatch with observations, mostly notable for some of the upstream sub-basins (132, 134 and 136). Analysis of model simulation indicates that, based on the available dataset, calculated concentration is underestimated, particularly for lower concentration.

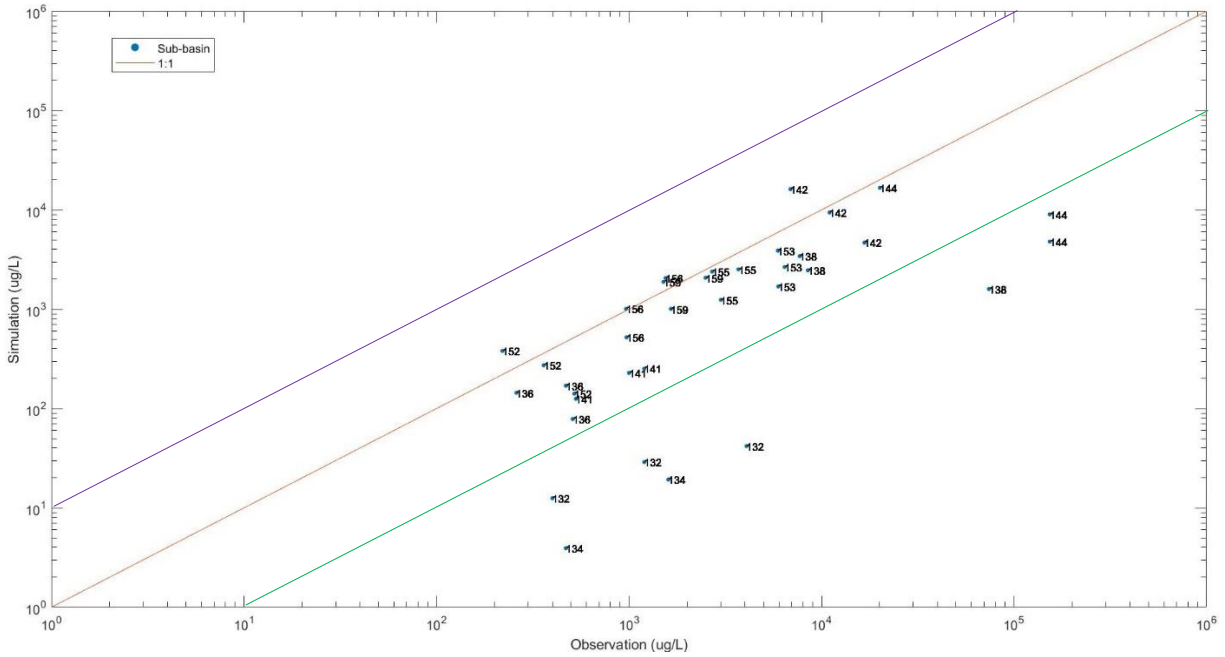

Figure 34 - Modeled vs observed Zn concentration in different sub-basins (numbers indicate the sub-basin ID) and in different times. Green and purple line represent of 1 order of difference between observed and modeled concentration.

Pb simulation was less accurate than Zn, showing (FIGURE 35) generally bad results for most of the sub-basins. Nevertheless, there is good agreement between measured and simulated concentrations at the main outlet (sub-basin 159), nearby San Giorgio tailings' dam (sub-basin 146), at the bottom of San Giovanni wastes (sub-basin 153) and for the sub-basin 155, last one before confluence with the tributary that drains Monte Scorra mining area.

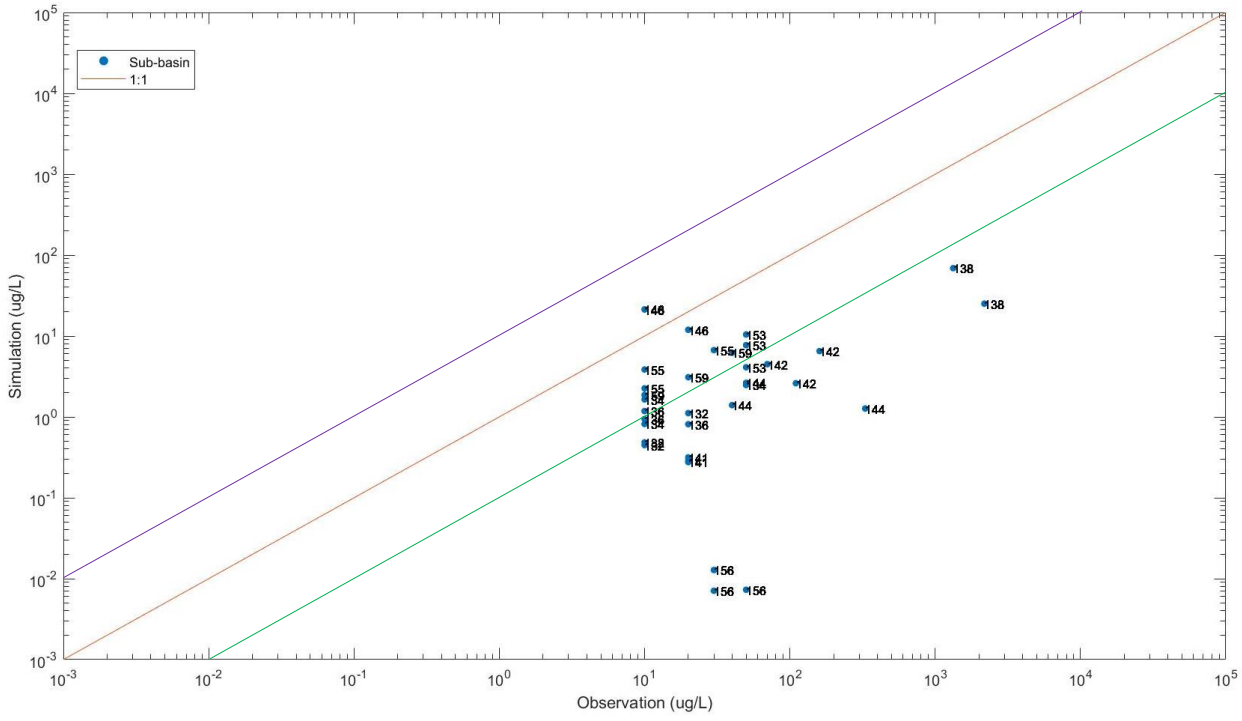

Figure 35 Modeled vs observed Pb concentration in different sub-basins (numbers indicate the sub-basin ID) and in different times.

Bibliography

Abbaspour, K.C., Johnson, C., Van Genuchten, M.T., 2004. Estimating uncertain flow and transport parameters using a sequential uncertainty fitting procedure. Vadose Zone J. 3, 1340–1352.

Abbaspour, K.C., Yang, J., Maximov, I., Siber, R., Bogner, K., Mieleitner, J., et al., 2007. Modelling hydrology and water quality in the pre-alpine/alpine Thur watershed using SWAT. J. Hydrol. 333, 413–430

Abbaspour, K., 2015. User Manual for SWAT-CUP, SWAT Calibration and Uncertainty Analysis Programs. Swiss Federal Institute of Aquatic Science and Technology, Eawag, Duebendorf, Switzerland

Allison, J.D., Brown, D.S., Kevin, J., 1991. MINTEQA2/PRODEFA2, a Geochemical Assessment Model eSystems: Version 3.0 User's Manual. Environmental Research Laboratory, Office of Research and Development, US Environmental Protection Agency, Athens.

Allison, J. D. And T. L. Allison. Partition coefficients for metals in surface water, soil, and waste. U.S. Environmental Protection Agency, Washington, DC, 2005.

Arangino A., Aru A., Baldaccini P., Vacca S., 1986. Carta dei suoli delle aree irrigabili della Sardegna. R.A.S. - E.A.F., Cagliari.

Arnold, J.G., Srinivasan, R., Muttiah, R.S., Williams, J.R., 1998. Large Area Hydrologic Modeling and Assessment Part I: Model Development1. Wiley Online Library.

Aru A., Baldaccini P., Vacca A., 1991. Nota illustrativa alla Carta dei suoli della Sardegna in scala 1:250.000

Aubert, A.H. et al., 2014. Fractal Water Quality Fluctuations Spanning the Periodic Table in an Intensively Farmed Watershed. Environmental Science & Technology, 48(2): 930-937. DOI:10.1021/es403723r

Bagnold, R.A., 1977. Bedload transport in natural rivers. Water Resour. Res. 13 (2), 303–312.

Beck H.E., Vergopolan N., Pan M., Levizzani V., Van Dijk A. I. J. M., Weedon G.P., Brocca L. , Pappenberger F. , Huffman G. J., and Wood E. F., 2017. Global-scale evaluation of 22 precipitation datasets using gauge observations and hydrological modeling

Beck, H. E.: MSWEP Version 2 documentation, Tech. rep., Princeton University, www.gloh2o.org, last access: August 2017.

Bengtsson, H., Alvenäs, G., Nilsson, S.I., Hultman, B., Öborn, I., 2006. Cadmium, copper and zinc leaching and surface run-off losses at the Öjebyn farm in Northern Sweden—Temporal and spatial variation. Agriculture, Ecosystems & Environment, 113(1): 120-138. DOI:https://doi.org/10.1016/j.agee.2005.09.001Degryse et al., 2009

Bennett, J.W., Comarmond, M.J., Jeffery, J.J., February 2000. Comparison of Oxidation Rates of Sulfidic Mine Wastes Measured in the Laboratory and Field.

Buekers, J., Degryse, F., Maes, A., Smolders, E., 2008. Modelling the effects of ageing on Cd, Zn, Ni and cu solubility in soils using an assemblage model. Eur. J. Soil Sci. 59, 1160–1170.

Cadeddu A., Lecca G., 2003. Sistema Informativo dei Suoli della Sardegna da interfacciare al modello idrologico SWAT, Report interno del CRS4 - Centro di Ricerca Sviluppo e Studi Superiori in Sardegna, 2003.

Chow, V.T., Maidment, D.R., Mays, L.W., 1988. Applied Hydrology. McGraw-Hill Inc., New York, 572 pp.

Daly, Chris & Gibson, W. & Taylor, G. & Johnson, G. & Pasteris, Phillip. (2002). A Knowledge-Based Approach to the Statistical Mapping of Climate. Climate Research - CLIMATE RES. 22. 99-113. 10.3354/cr022099.

Degryse, F., Smolders, E., Parker, D., 2009. Partitioning of metals (Cd, Co, Cu, Ni, Pb, Zn) in soils: concepts, methodologies, prediction and applications–a review. Eur. J. Soil Sci. 60, 590–612.

Frogner-Kockuma' P., Goransson P., Aslundc E., Landella M., Stevensc R., Tengberg A., Goransson G., Ohlsson Y., 2016. Metal contaminant fluxes across the sediment water interface. Marine Pollution Bulletin n°07S5.

Gray, C.W., Monaghan, R.M., Orchiston, T., Laurenson, S., Cavanagh, J.-A., 2017. Cadmium losses in overland flow from an agricultural soil. Environmental Science and Pollution Research, 24(30): 24046-24053. DOI:10.1007/s11356-017-0117-9

GURI, 1999. Metodi ufficiali di analisi chimica del suolo, Supplemento ordinario alla Gazzetta Ufficiale n. 48, 21.10.1999 – Serie generale.

Hargreaves, G., Samani, Z.A., 1985. Reference crop evapotranspiration from temperature. Appl. Eng. Agric. 1, 96–99.

Kirchner, J.W., Neal, C., 2013. Universal fractal scaling in stream chemistry and its implications for solute transport and water quality trend detection. Proceedings of the National Academy of Sciences, 110(30): 12213. DOI:10.1073/pnas.1304328110A.S.

Levizzani, Vincenzo & Kidd, Chris. (2011). Status of satellite precipitation retrievals. Hydrology and Earth System Sciences. 15. 1109-1116. 10.5194/hess-15-1109-2011.

Likuku, K. B. Mmolawa, G. K. Gaboutloeloe, 2013. Assessment of Heavy Metal Enrichment and Degree of Contamination Around the Copper-Nickel Mine in the Selebi Phikwe Region, Eastern Botswana. Environment and Ecology Research 1(2): 32-40, DOI: 10.13189/eer.2013.010202

Malmström, M.E., Destouni, G., Banwart, S.A., Strömberg, B.H.E., 2000. Resolving the scaledependence of mineral weathering rates. Environ. Sci. Technol. 34, 1375–1378.

Meng Y., Zhou L., He S., et al., 2018. A heavy metal module coupled with the SWAT model and its preliminary application in a mine-impacted watershed in China. Science of The Total Environment, 613-614:1207-1219.

Michaelides, Silas & Levizzani, Vincenzo & Anagnostou, Emmanouil & Bauer, P. & Kasparis, Takis & Lane, John. (2009). Precipitation: Measurement, remote sensing, climatology and modeling. Atmospheric Research. 94. 512-533. 10.1016/j.atmosres.2009.08.017.

Montanarella L., Jones R. J. A., The European soil bureau, Research Report n. 6, 1999.
Monteith, J.L., 1965. Evaporation and environment. In: Fogg, G.F. (Ed.), The State and Movement of Water in Living Organisms. Cambridge University Press, Cambridge, pp. 205–234

Moriasi, D.N., Gitau, M.W., Pai, N., Daggupati, P., 2015. Hydrologic and Water Quality Models: Performance Measures and Evaluation Criteria. Transactions of the ASABE, 58(6): 1763-1785. DOI:https://doi.org/10.13031/trans.58.10715

Moriasi D.M., Prasanna H. Gowda, Jeffrey G. Arnold, David J. Mulla, Srinivasulu Ale, Jean L. Steiner, and Mark D. Tomer, 2013. Evaluation of the Hooghoudt and Kirkham Tile Drain Equations in the Soil and Water Assessment Tool to Simulate Tile Flow and Nitrate-Nitrogen. Journal of Environmental Quality, Technical Reports.

Nash, J. E.; Sutcliffe, J. V. (1970). "River flow forecasting through conceptual models part I — A discussion of principles". Journal of Hydrology. 10 (3): 282–290. Bibcode:1970JHyd...10..282N. doi:10.1016/0022-1694(70)90255-6.

Peraza-Castro, M., Sauvage, S., Sánchez-Pérez, J.M., Ruiz-Romera, E., 2016. Effect of flood events on transport of suspended sediments, organic matter and particulate metals in a forest watershed in the Basque Country (Northern Spain). Science of The Total Environment, 569-570: 784-797. DOI:https://doi.org/10.1016/j.scitotenv.2016.06.203

Perra, E.; Piras, M.; Deidda, R.; Paniconi, C.; Mascaro, G.; Vivoni, E.R.; Pierluigi, C.; Marras, P.A.; Ludwig, R.; Meyer, R. Multimodel assessment of climate change-induced hydrologic impacts for a Mediterranean catchment. Hydrol. Earth Syst. Sci. 2018, 22, 4125–4143

Priestley, C.H.B., Taylor, R.J., 1972. On the assessment of surface heat flux and evaporation using large-scale parameters. Monthly Weather Rev. 100, 81–92

Quinton, J.N., Catt, J.A., 2007. Enrichment of Heavy Metals in Sediment Resulting from Soil Erosion on Agricultural Fields. Environmental Science & Technology, 41(10): 3495-3500. DOI:10.1021/es062147h

Righini, G., A. C. Costantini e L. Sulli, La banca dati delle regioni pedologiche italiane, Istituto Sperimentale per lo Studio e la Difesa del Suolo, Firenze, 2001.

Schuol J., Abbaspour K. C., 2006. Using monthly weather statistics to generate daily data in a SWAT model application to West Africa

Swartjes, F.A., 2011. Dealing with contaminated sites: from theory towards practical application. Springer Science & Business Media.

Tao, L. et al., 2003. Transportation processes and rates of heavy metals in an artificial rainstorm runoff under different land use types. Chinese Journal of Applied Ecology, 14(10): 1756.

Tapiador, Francisco & Turk, F.J. & Petersen, Walt & Hou, Arthur & García-Ortega, Eduardo & Machado, Luiz & Angelis, C. & Salio, Paola & Kidd, Chris & Huffman, George & Castro, Manuel. (2012). Global precipitation measurement: Methods, datasets and applications. Atmos. Res.. 104--105. 70-97. 10.1016/j.atmosres.2011.10.021.

Yaobin Meng, Lingfeng Zhou, Saeid Vaghefid, Pier A. Marras, Chunming Sui, Chao Lu, Karim Abbaspour, 2019. Uncertainty-based metal budget assessment at the watershed scale: Implications for environmental management practices. Under review. Journal: Journal of Hydrology

Williams, J.R., Berndt, H.D., 1977. Sediment yield prediction based on watershed hydrology. Trans. ASAE 20 (6), 1100–1104.

Williams, J.R., 1980. SPNM, a model for predicting sediment, phosphorous, and nitrogen from agricultural basins. Water Resour. Bull. 16 (5), 843–848

Chapter 3: CESApp web application

Introduction

In this appendix the development of a web application will be described. In the context of this study, that required the use of numerical models with complex data formats, thousands of input/output file and hundreds of environmental samples, the application was developed to ease the use of this data. Furthermore, was retained important to share the data in a common web environment to enable other researchers and stakeholders of the research project to perform data entry and data report/download.

CESApp Framework

Water quality monitoring systems have been widely studied and developed around the globe (Saparudin et al., 2018). With the development of recent technologies, such as Sensor Web Enablement (SWE), Wireless Sensor Network (WSN) and Internet of Things (IoT), web-based systems are increasingly used for real time monitoring and data collection. Monitoring of water quality by using IoT integrated Big Data Analytics will immensely help people to become conscious against using contaminated water as well as to stop polluting the water (Chowdury et al., 2019). Most of the times, end users of multidisciplinary studies, such as the assessment of the level of pollution, do not have the proper skills to analyze and use research results. For this purpose, web applications are often developed to ease the utilization of these results, by researchers and decision makers.
CESApp is a web-based application, developed with the aim to create a monitoring system and share the results of this study. CESApp is accessible from a simple web browser under authentication. It is based on the server-client paradigm, relies on a Postgres database (https://www.postgresql.org/) with PostGIS spatial extension (), available through a Graphic User Interface (GUI) developed with the Alto Framework (www.altoframework.ithttp:///). The structure is modular, developed to be further improved with new features and possibly connected to real-time monitoring networks. Diagram in **Figure 36** represents the structure of CESApp application: the PostGIS database is the core of the whole system and it directly communicates with the web application in both directions, meaning data can be inserted from the interface to the database or retrieved from the database through the interface.

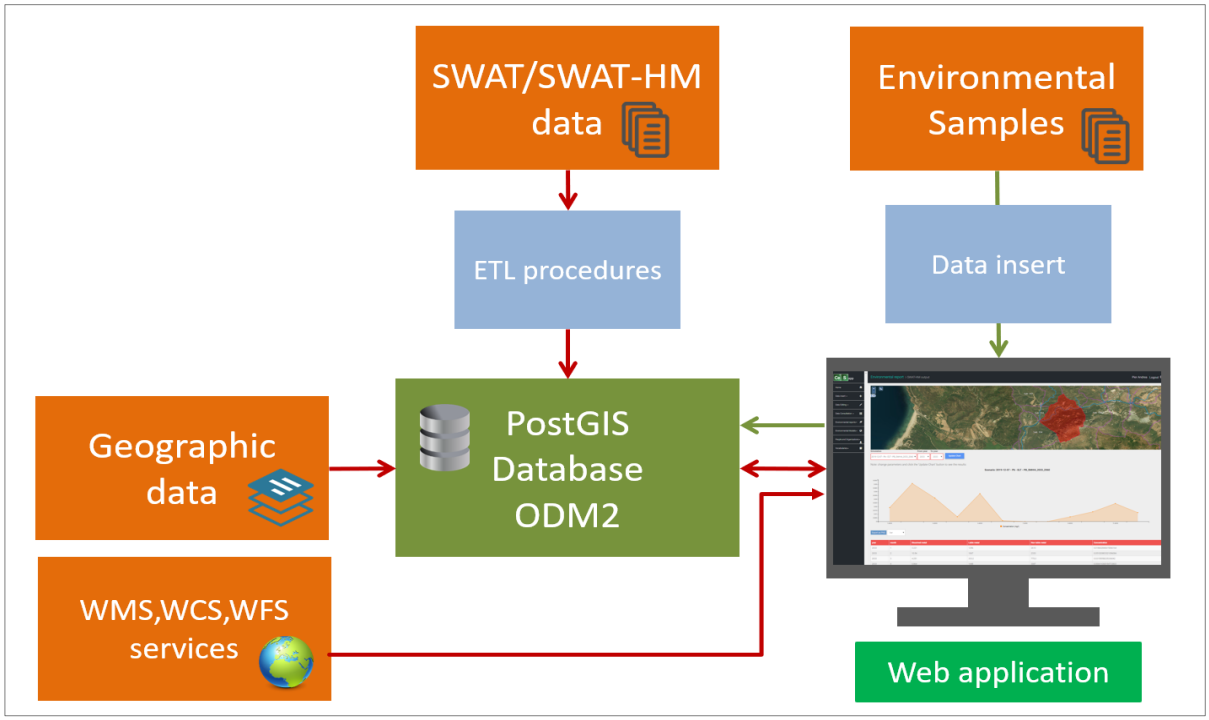

Figure 36 - Diagram of the CESApp application structure

Data from environmental monitoring (Environmental samples) was stored in the Postgres/PostGIS database by manual data entry through the web interface, while model data (SWAT/SWAT-HM data) was directly stored into the database using Extract-Transform-Load (ETL) procedures. ETL procedures make use of algorithms to convert the model's output files into Postgres database standard, Structured Query Language (SQL), making it possible to automate the entry of thousands of records (e.g. daily values of river discharge for 30 years). In this study a Python program was developed to implement the ETL procedure.

Geographic data is stored in the database and rendered in CESApp using Openlayers services (https://openlayers.org/), that can be implemented through Alto Framework. Among geographic data closely linked to this study, some external geographic features were introduced into CESApp. Satellite background map, Sardinia's geological map or mining areas delimitation, were included using Web Map Service (WMS) technology (https://www.opengeospatial.org/standards/wms). This allows to request and render geographic data stored in remote public databases, like the Sardinia's government database (http://webgis.regione.sardegna.it/geoserverraster/ows?service=WMS).

Data model

The CESApp database is based on the Observations & Measurements Standard (OM) (Cox, 2010), recognized by the Open Geospatial Consortium (https://www.opengeospatial.org/), that provides Observations Data Model (ODM2). ODM2 is used as a common basis for domain specific profiles of information exchange (Horsburgh et al., 2016). This standard has been used in successfully projects, such as CUAHSI HIS (http://his.cuahsi.org/), developed by the Consortium of Universities for the Advancement of Hydrologic Science, as well as for the EarthChem project (http://www.earthchem.org/). The interoperability this standard enables, allows the system to easily exchange data with other systems and to be easily connected with measurement sensors. ODM2 has a modular structure, based on a core schema (**FIGURE 37**), which contains entities, attributes, and common relationships for all observations, regardless of their type (Horsburgh et al., 2016). Extension schemas area used to enhance the functionality of the data model depending on the needs and on the complexity of the system. The entities of the core schema used in this study are:

- Actions - Actions are performed by people and may have a result.
- FeatureActions - Which provide flexible linkage between Actions and the Sampling Features on which or at which they were performed.
- Methods - The procedure used to perform an action.
- Organizations - A group of people.
- People - Individuals that perform actions.
- Results - The result of an action.
- Sampling Features - Where or on what an action was performed.
- Units - Units of measure.
- Variables - What was observed.

In ODM2, an observation is the result of 3 elements: it starts from an 'Action' that is performed on or through a 'Sampling Feature' that produces a 'Result'. For instance, the measure of Pb concentration in stream water is defined by: a water collection (Action) that produces a sample (Sampling Feature) on which the concentration of Pb is measured (Result).

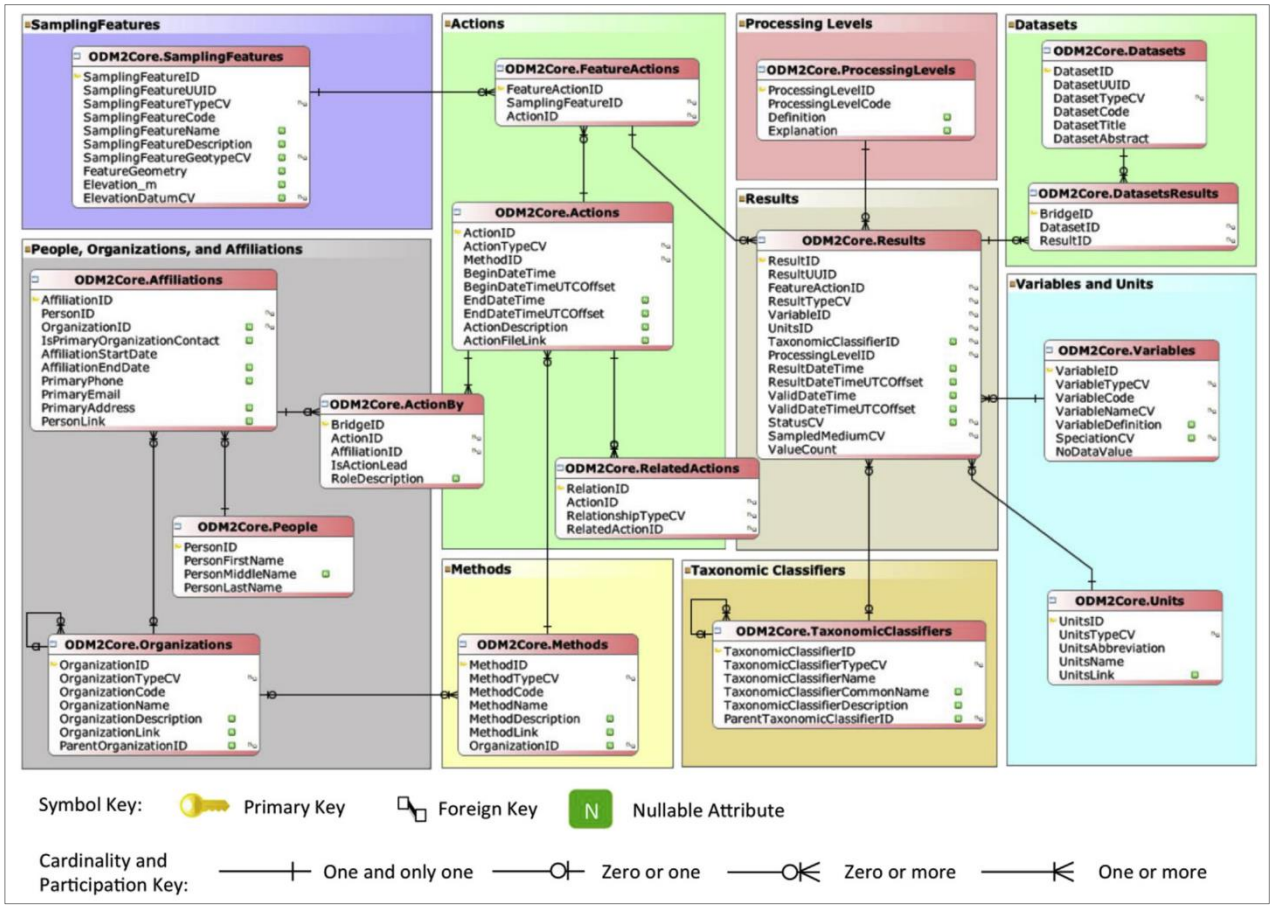

Figure 37 - Entity-relationship diagram of the Core schema

The separation of Actions and their Results may allow/can allow/allows a single Action to produce many Results (e.g., a “Specimen analysis” Action may result in concentration values for many different Variables) (Horsburgh et al., 2016). An action is always performed by some ‘People’, members of a specific ‘Organization’, using a specific ‘Method’. Sampling Features have always a precise spatial reference that defines their position. In this study the field ‘FeatureGeometry’ was used to store samples’ spatial information and render them the different web-GIS based sections of CESApp. Date and time are associated to each Action, Sampling Feature and Result, allowing to define different timing between them (e.g. a sample collection that produces a Result can be performed several months before the analysis of the sample). Moreover, Actions and Results can be carried out by different People, to fit cases in which, for example, samples are collected by some People, but analyzed by external laboratories.

A results extension was also implemented to store the measurement values, using the ‘MeasurementResults’ module. This ‘MeasurementResults’ module allows separating Results

information from the value, giving the possibility to show information about the result but not the value in itself. The ODM2 data model was implemented as a Postgres SQL database, using a predefined build function that automatically sets the database schema, available at the GitHub project page (https://github.com/ODM2/ODM2/tree/master/src/build_schemas/ddl). For more detailed information about ODM2 data model, please consult Horsburgh et al., (2016) and official website at http://www.odm2.org/.

CESApp web interface

The CESApp web application is accessible to CESA project's investigators only, due to sensitive data stored in the system. It has been developed using HTML5, Javascript, jQuery languages, asynchronous JavaScript and XML (Ajax) technology (https://www.w3schools.com/jquery/jquery_ajax_intro.asp). The user interface is divided into eight sections (**FIGURE 38**):

- Data insert
- Data editing
- Data consultation
- Environmental reports
- Environmental models
- People and organizations
- Vocabularies

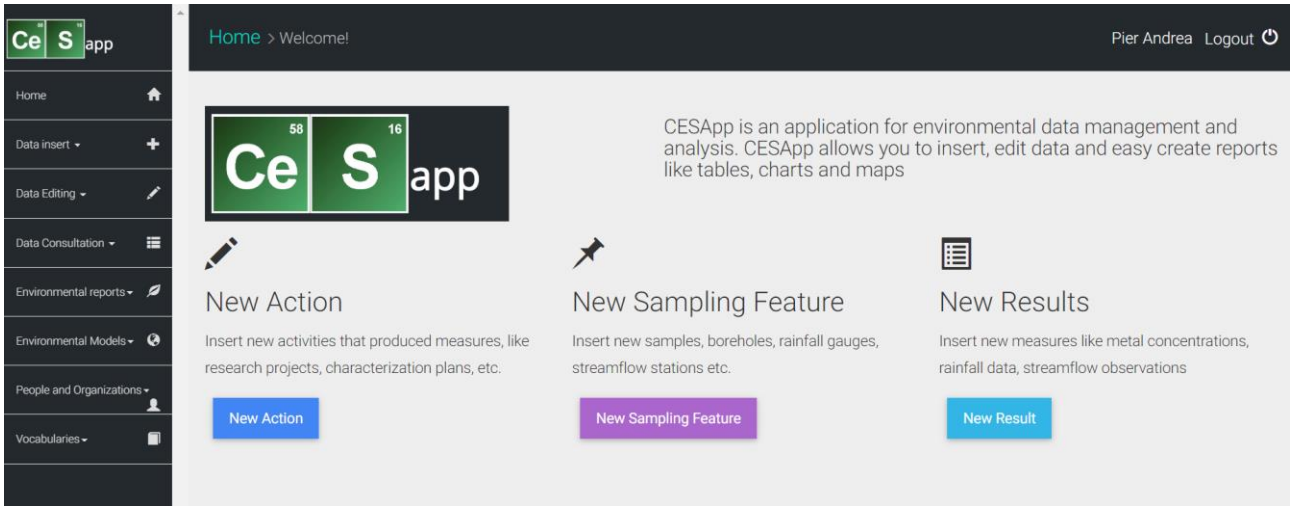

Figure 38 - CESApp web application home page. In the left menù users can find all the main sections.

The data insert section allows users to input Actions, Sampling Features and Results. Each dedicated sub-section consists in an input form, consisting of input text boxes, calendars, maps and dropdowns which facilitate the data insert, avoiding errors and typing mistakes (FIGURE 39). To define an Action, users must specify a Method, either by choosing an existing one or by defining a new one. After specifying a method, the other required parameters are the action type, a description, begin and end time of the Action and, optionally, a related link. Furthermore, for each section, a table containing the last inserted records helps to avoid repetitions of data insert.

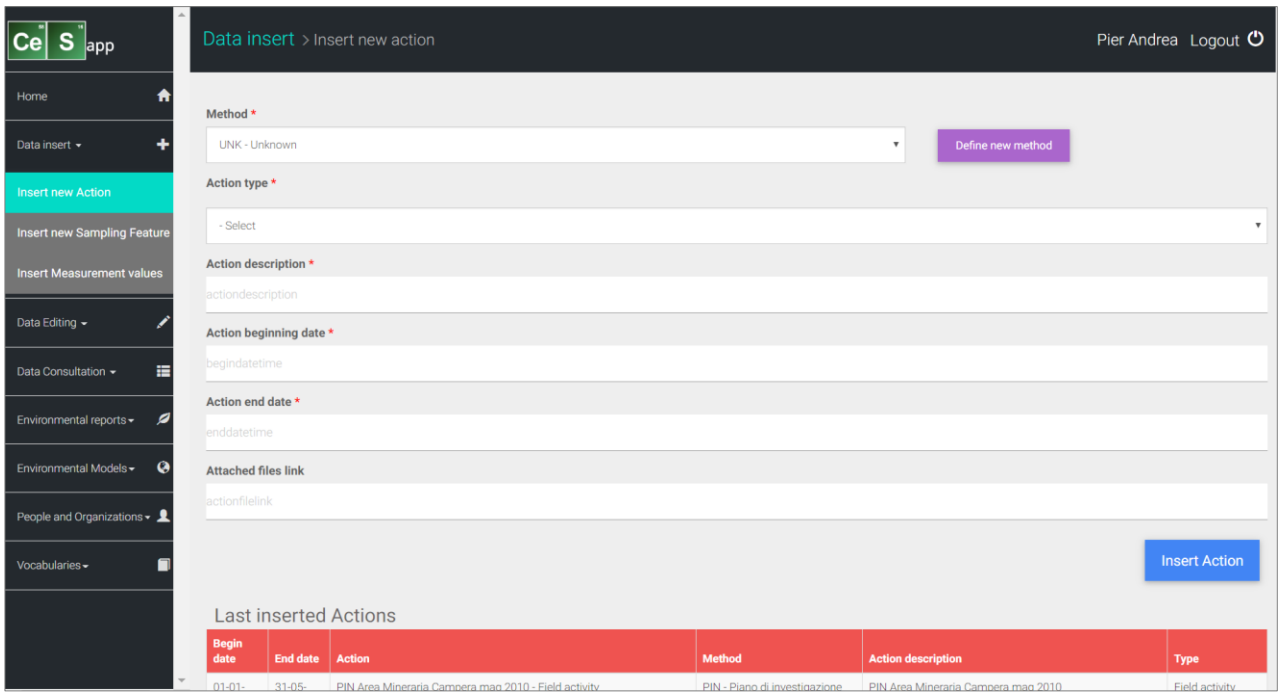

Figure 39 - CESApp application interface. With this form users can input actions.

The sampling Features form requires the following information to define a sample: a sample code, a sample type, that is chosen from a pre-defined list, related Action, mining area or site (a customization for this study), sampled medium and sampling feature's spatial information such as elevation, latitude, longitude and projection that is automatically converted to WGS84 (srid 4326). In addition to the form, a map (FIGURE 40) will also be available. The map allows to manually define the position of the sampling features and gives the possibility to directly record samples in situ through a portable device.

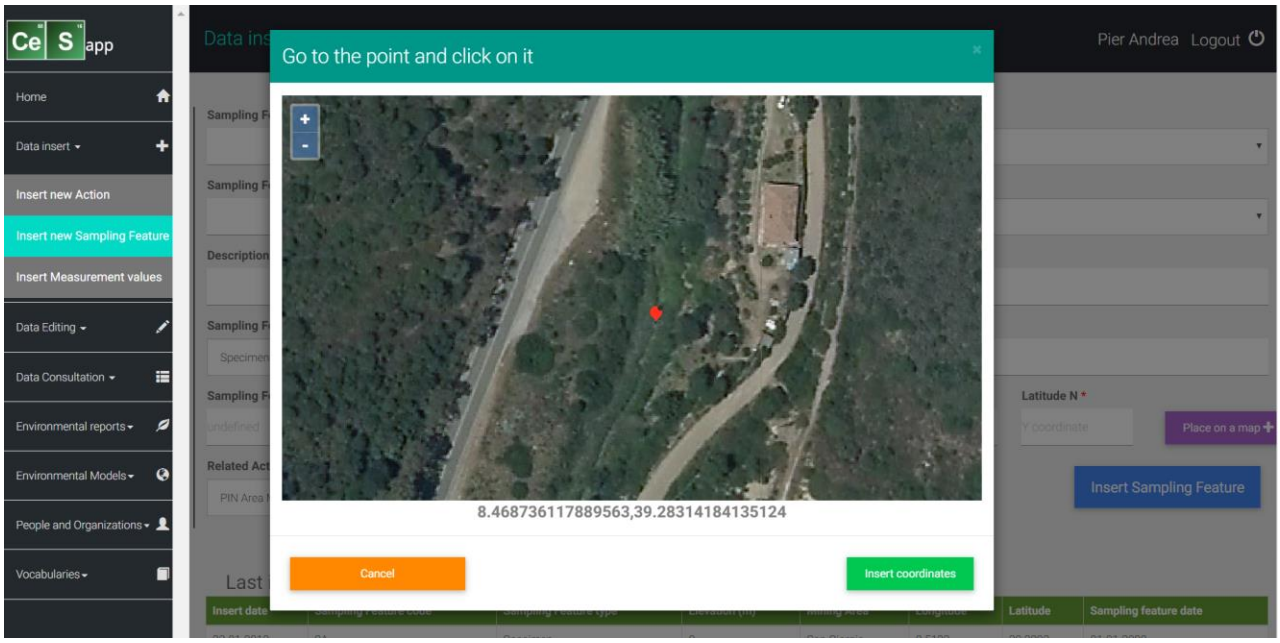

Figure 40 - Sampling Features insert: users can define sample's position by manually clicking the map

The “Insert Measurement Result” section is dedicated to the insertion of effective measurement values., For the research project´s purposes and needs, a simplification was made: result’s information and result’s values are stored with a single insert action but keeping the ODM2 structure in separate entities. A Measurement Result is defined by the following features (**FIGURE** 41):

- related Sampling Feature
- analyst that measured the value in the sample (from a pre-defined list)
- date and (if needed) time
- measured value
- measured variable and
- measure units (pre-defined autocomplete field)
- (optional) protocol number
- (optional) time aggregation interval
- (optional) time aggregation measure units
- (optional) quality code

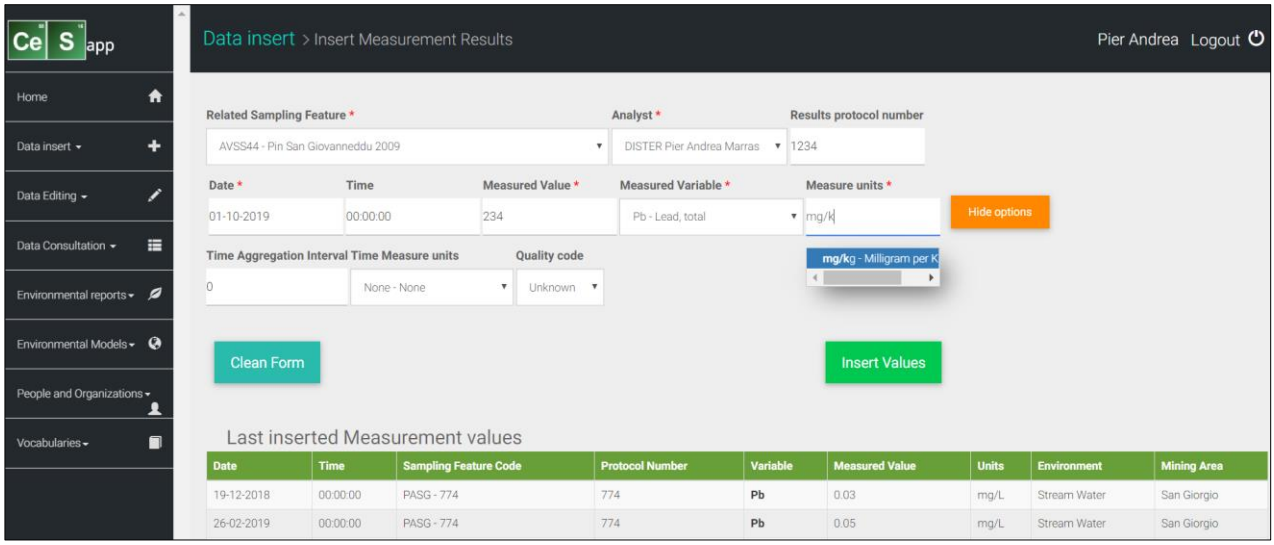

Figure 41 - Insert Measurement Results form, used to store the values.

Inserted data can be edited in the Data Editing section of CESApp. Editing sections, for Actions, Sampling Features and Measurement Results, are structured with a table with search filter that allows users to efficiently search for data to be modified (FIGURE 42).

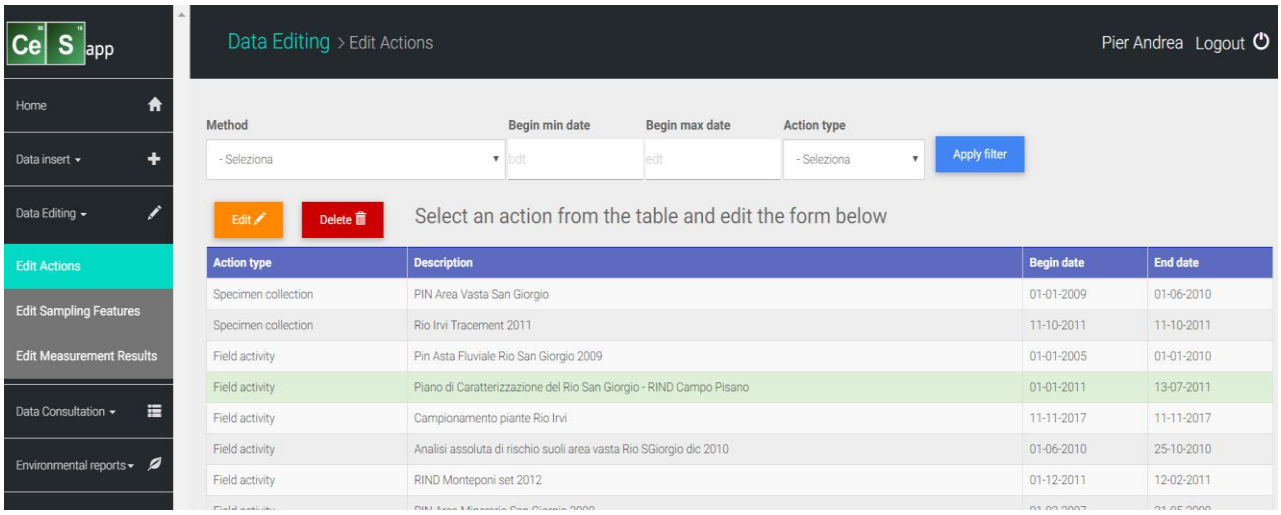

Figure 42 - - Data Editing typical structure: data filters to easily find records, a table of records and buttons for edit/delete options

When the desired record is found, the user can select its correspondent row in the table and two options are shown: edit or delete data. By clicking on “edit data” a form is displayed, and each attribute of the record can be modified and saved (FIGURE 43).

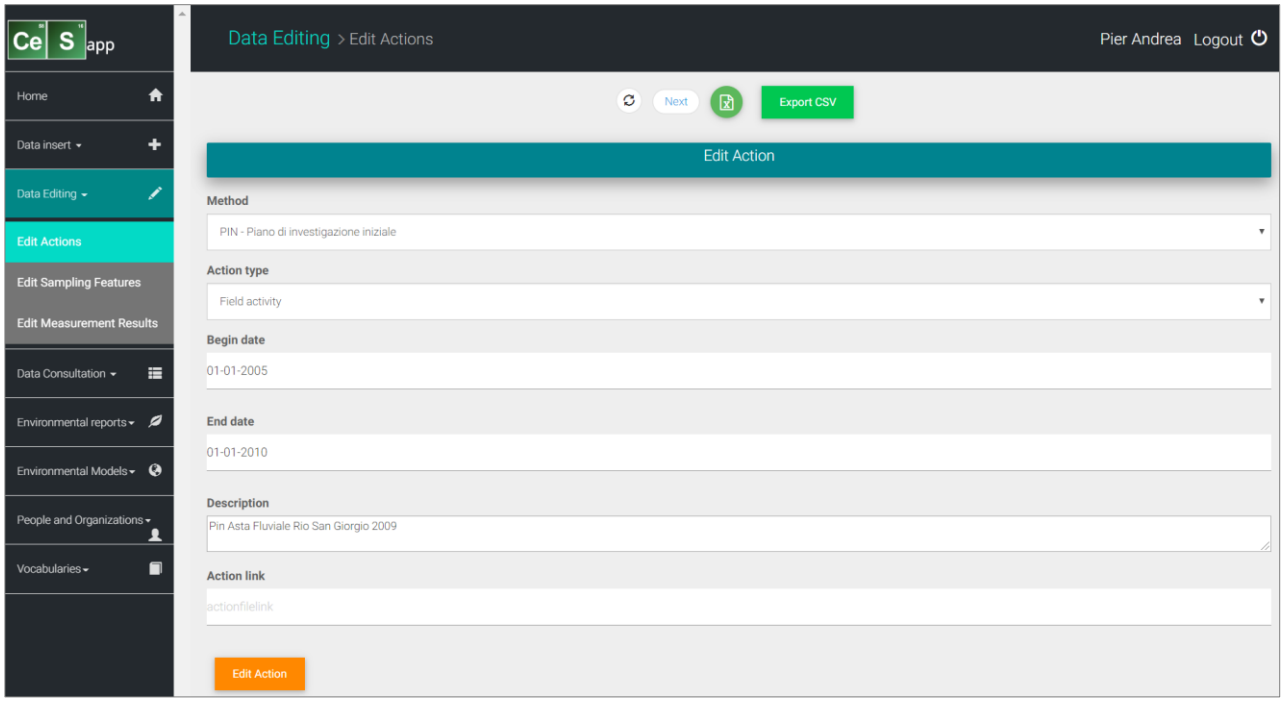

Figure 43 - Typical structure of an edit form

In the "Data Consultation" section, records are simply listed in tables that can be filtered and exported to csv or Excel as shown in **FIGURE 44**.

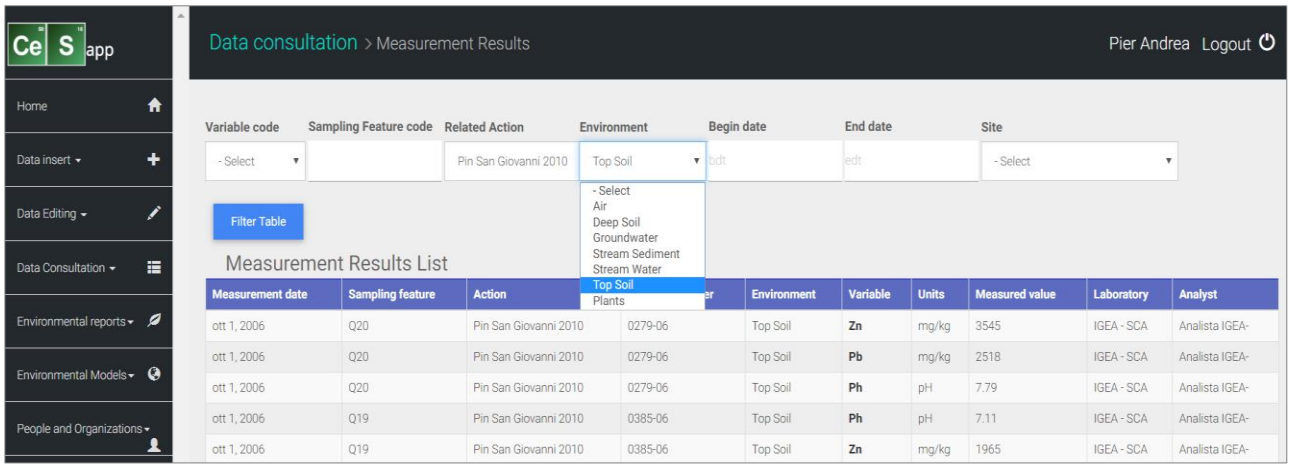

Figure 44 - Data consultation interface, with a simple table and relative filters to retrieve data.

Section Environmental Reports allows to easily create reports on the state of metal pollution, such as charts, maps, tables, and analyze the spatial distribution of the measured variables. Two main sub-sections are available: "Sampling features map" and "Compare samples".

In the Sampling Features map section (**FIGURE 45**), users can find samples through the use of filters (upper form) and see their position in a user-friendly map with a satellite map (Bing Map

https://www.bing.com/maps/aerial) as default background. Other layers, such as geology map, land use map, rivers map, can be overlayed to the map to analyze spatial relationships between samples and other features (e.g. samples and lithology, or samples and land crops and use).

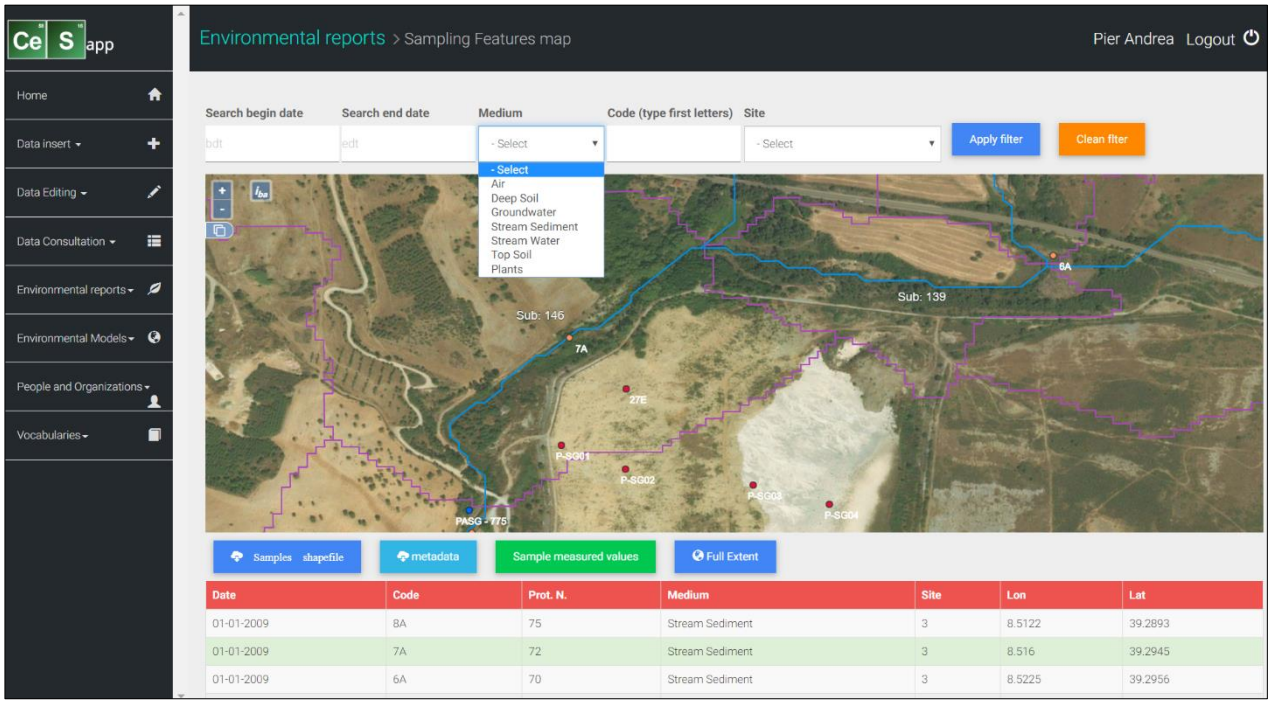

Figure 45 - Samplling features map section

Selecting the desired sample's row, the map is centered on it, allowing to immediately see its position; the related measures (**FIGURE 46**) can be listed by clicking the "Sample measured values" button. A Table containing the related measures can be downloaded in a common format (csv, xls) and samples layer can be converted to shapefile, through the button "Samples shapefile", to be used in desktop applications such as QGIS or other GIS applications.

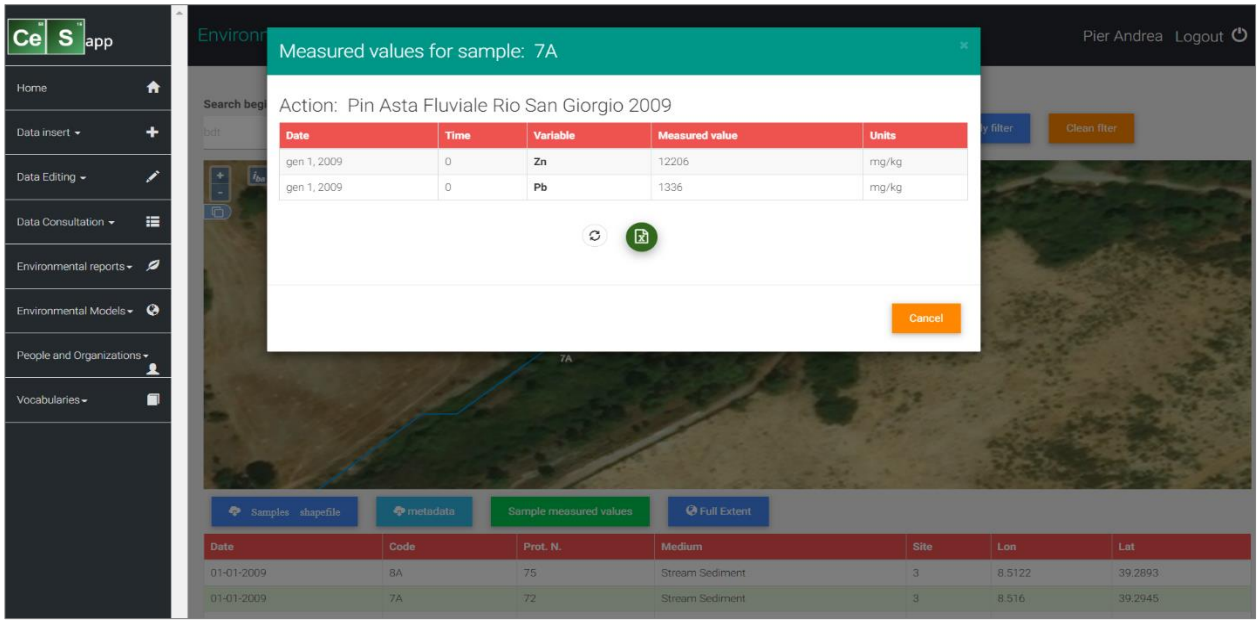

Figure 46 - By selecting the sample in Sampling Features Map section users can quickly retrieve related measures

The "Compare samples" section allows to build a chart composed by the samples filtered by Environment (or medium), by measured variable, by zone (Mining area) and within a certain date range (FIGURE 47). Based on the chosen variable, law limit concentration is automatically shown in the graphic, which can also be zoomed in and out for a more detailed view. This enables to immediately report the state of pollution given by the selected metal (or other elements if recorded) in the analyzed area, constituting a powerful tool of environmental monitoring.

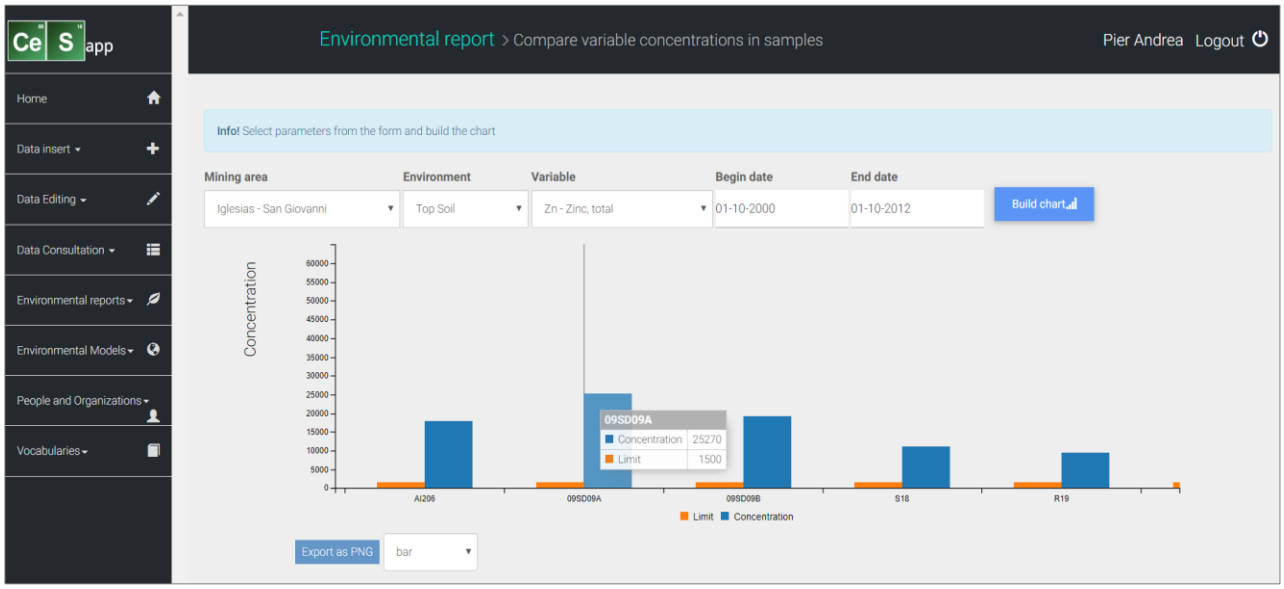

Figure 47 - Compare Samples section, samples, based on the parameters of the filter, can be compared in a chart

An entire section of CESApp, named Environmental Models, is dedicated to the numerical models implemented in this study. The interface in FIGURE 48, that exposes SWAT hydrological model results, consists of a map which includes geographical features of the numerical model (sub-basins, rivers, land-use map, soil map) to help users to associate model results to their spatial distribution. The map allows to select the sub-basin, based on which the model results are reported. Dropdown filters allow to select between the different simulations and the date range. On the right side of the map, a resume of the selected sub-basin's characteristics is given. Results are shown through charts and tables, as depicted in FIGURE 48; the figure shows (for the selected sub-basin, simulation and time range) (a) water balance dynamic graphic, (b) water flow dynamic graphic, (c) water balance dynamic table.

a)

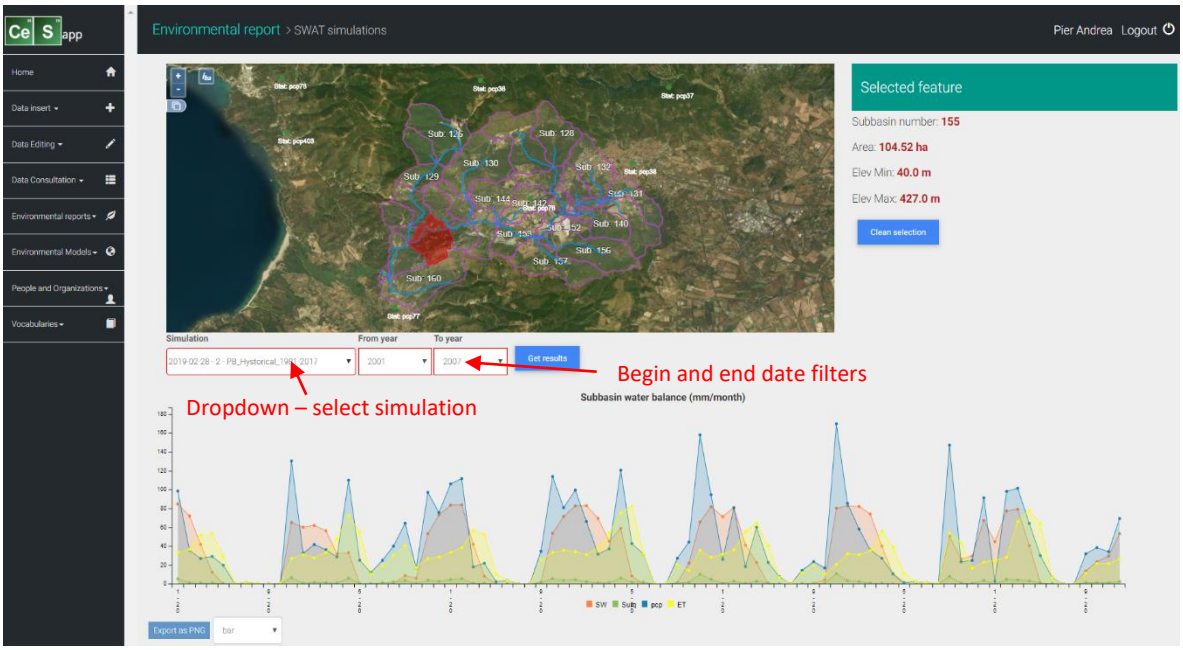

b)

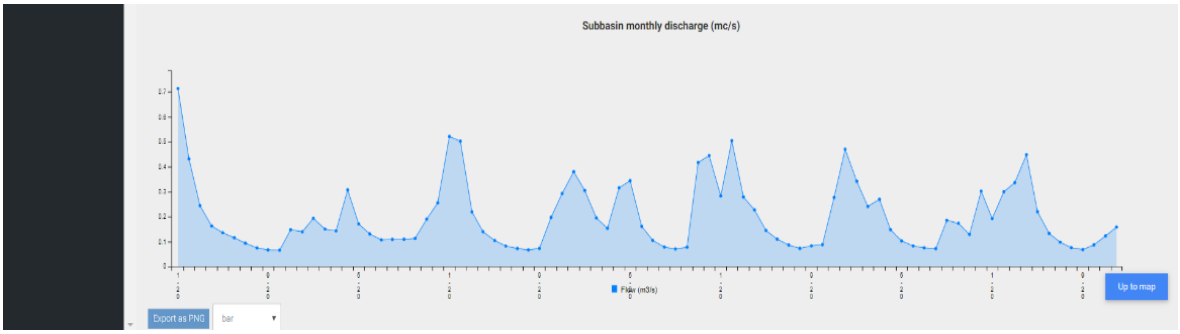

c)

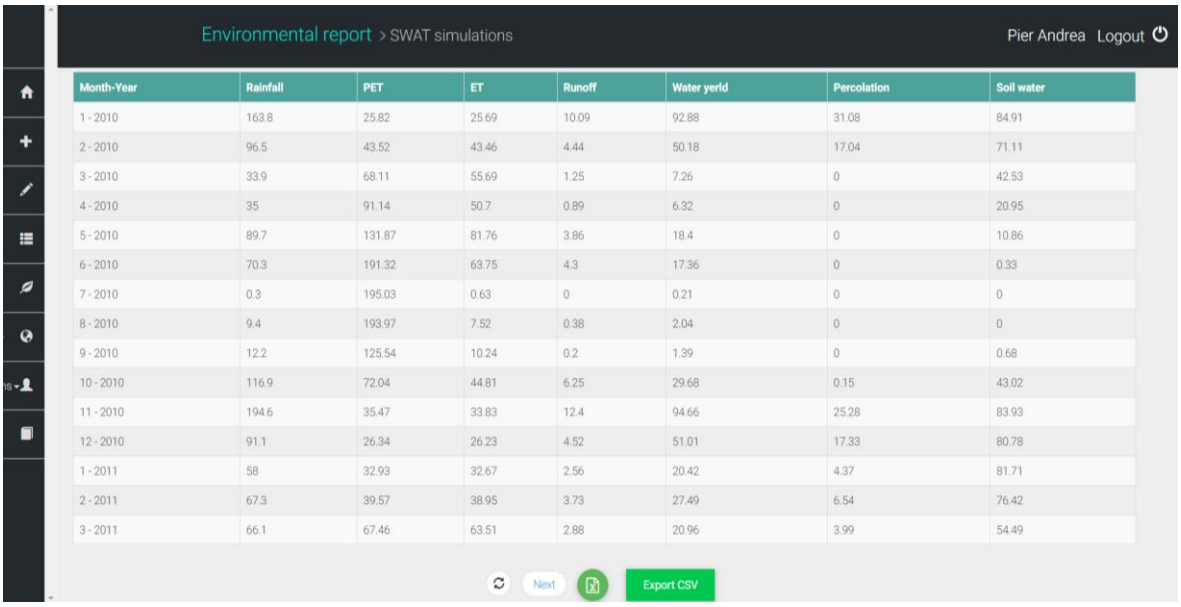

Month-Year	Rainfall	PET	ET	Runoff	Water yeld	Percolation	Soil water
1 - 2010	163.8	25.82	25.69	10.09	92.88	31.08	84.91
2 - 2010	96.5	43.52	43.46	4.44	50.18	17.04	71.11
3 - 2010	33.9	68.11	55.69	1.25	7.26	0	42.53
4 - 2010	35	91.14	50.7	0.89	6.32	0	20.95
5 - 2010	89.7	131.87	81.76	3.86	18.4	0	10.86
6 - 2010	70.3	191.32	63.75	4.3	17.36	0	0.33
7 - 2010	0.3	195.03	0.63	0	0.21	0	0
8 - 2010	9.4	193.97	7.52	0.38	2.04	0	0
9 - 2010	12.2	125.54	10.24	0.2	1.39	0	0.68
10 - 2010	116.9	72.04	44.81	6.25	29.68	0.15	43.02
11 - 2010	194.6	35.47	33.83	12.4	94.66	25.28	83.93
12 - 2010	91.1	26.34	26.23	4.52	51.01	17.33	80.78
1 - 2011	58	32.93	32.67	2.56	20.42	4.37	81.71
2 - 2011	67.3	39.57	38.95	3.73	27.49	6.54	76.42
3 - 2011	66.1	67.46	63.51	2.88	20.96	3.99	54.49

Figure 48 - Dynamic charts of the SWAT water balance section representing water budget terms in mm (a) and streamflow curve in m3(b); Terms of the water balance in exportable table (c). Charts are updatable based on the date filters and on the sub-basin selected

Sub-section “SWAT-Heavy Metals simulations” is dedicated to the heavy metal (HM) transport model’s results. The interface is similar to the previously described SWAT sub-section, as shown in (FIGURE 49). The results of the HM model are displayed based on the area (sub-basin) selected in the top map, on the simulations and desired date range.

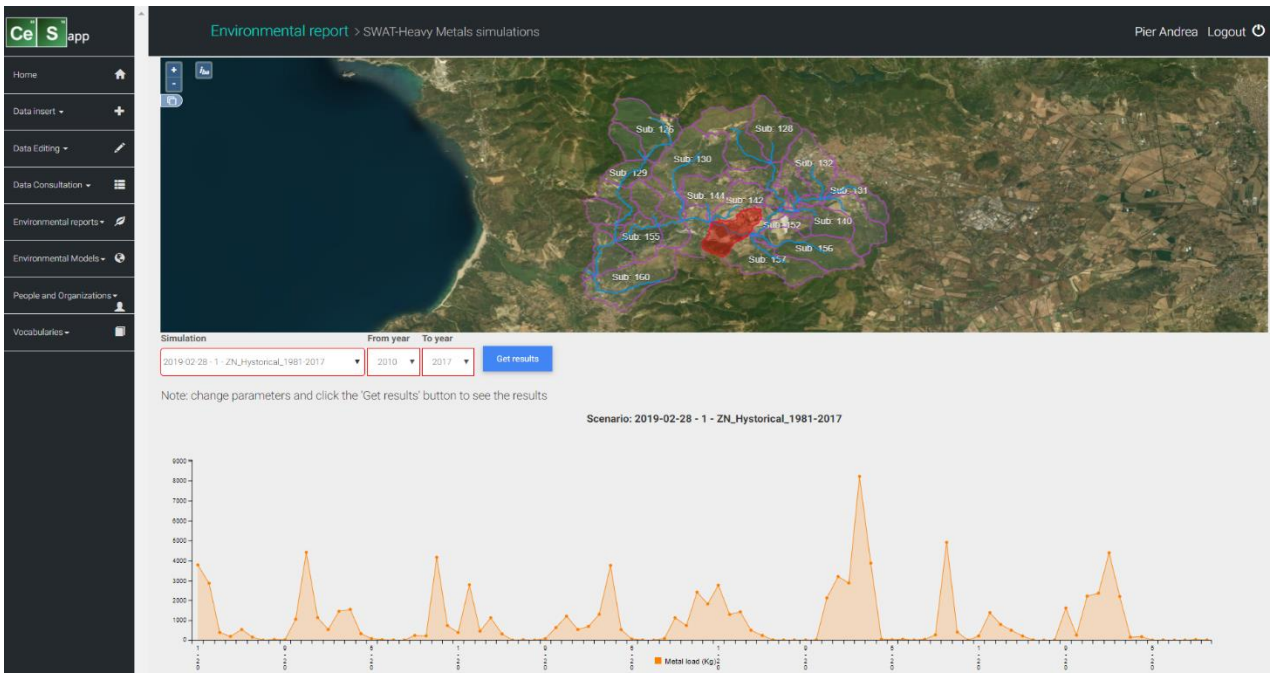

Figure 49 - Example of SWAT-HM output within CESApp: the chart represents the Zn load for the selected scenario (ZN_Hystorical_1981-2017), between 2010 and 2017 in the highlighted sub-basin.

Results are displayed in a chart and in a table (**FIGURE 50**), which can be exported in common formats for desktop use. The chart represents the metal load in kg/month for the selected river sub-basin resulting from the model simulation; the table contains the metal loads divided in dissolved, labile and non-labile metal daily concentration in stream water. This makes the model´s data easy to be understood and used, which is something that normally requires skills and expertise. With this interface, users can extract results of complex models by simply using a web browser that drastically reducing efforts.

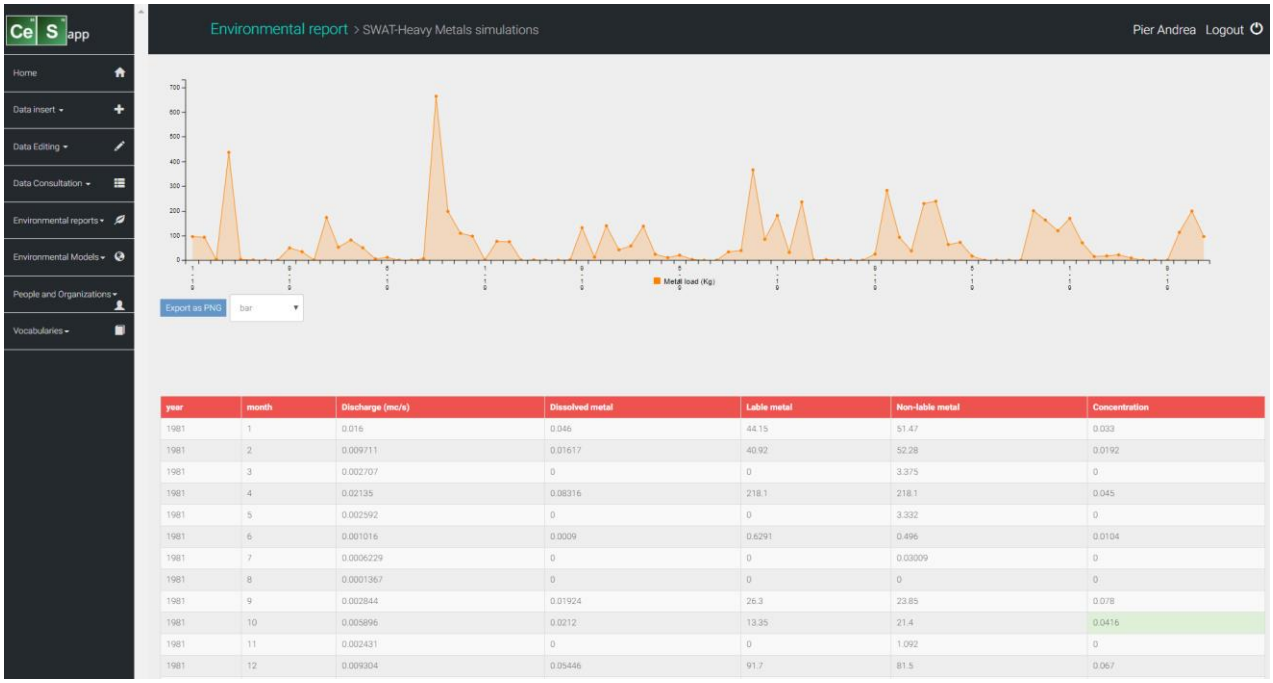

Figure 50 - Results of the SWAT-HM model are returned with a graphic and a table with the detailed values of metal load in the river for the selected period an for the selected simulation.

Bibliography

M. S. U. Chowdury, T. B. Emran, S. Ghosh, A. Pathak, Mohd. M. Alam, N. Absar, K. Andersson, M. S. Hossain. IoT Based Real-time River Water Quality Monitoring System. Procedia Computer Science 155 (2019) 161–168

Cox, S., 2010. Geographic Information: Observations and Measurements OGC Abstract Specification Topic 20, v2.0.0. OGC 10-004r3. Open Geospatial Consortium, Inc, p. 49. http://portal.opengeospatial.org/files/?artifact_id¼41579

Jeffery S. Horsburgh a, *, Anthony K. Aufdenkampe b, Emilio Mayorga c, Kerstin A. Lehnert d, Leslie Hsu d, Lulin Song d, Amber Spackman Jones e, Sara G. Damiano b, David G. Tarboton e, David Valentine f, Ilya Zaslavsky f, Tom Whitenack, 2016. Observations Data Model 2: A community information model for spatially discrete Earth observations.

F. A. Saparudin, T. C. Chee, A. S. Ab Ghafar, H. A. Majid, N. Katiran, 2018. Wireless water quality monitoring system for high density aquaculture application. Indonesian Journal of Electrical Engineering and Computer Science. Vol. 13, No. 2, February 2019, pp. 507~513

Chapter 4: Future precipitation in Sardinia and streamflow changes for a small basin using EURO-CORDEX regional climate simulations and the SWAT model

P.A. Marras, D.C.A. Lima, P.M.M. Soares, G. De Giudici, R.M. Cardoso

Abstract

This work aims at assessing the use of Regional Climate Models (RCMs') long term simulations in order to provide the future climate forcing for the SWAT hydrological model. 14 simulations from the European Coordinated Regional Downscaling Experiment initiative (EURO-CORDEX) at 0.11° resolution were analyzed to assess their reliability on reproducing the historical precipitation properties in Sardinia Island. RCMs simulations were hence compared with measured rainfall of the observational network, with the use of different statistical metrics, from 1979 to 2008 and a weighted climate multi-model ensemble was built. The EURO-CORDEX models can reproduce local precipitation properties, such as spatial patterns and orographic variations, but their performances are still a bit limited in some way. The future simulations concerning Sardinia predict a decrease of mean precipitation values and an increase of extreme events in summer and autumn, especially in the east and south parts of the island. SWAT model was forced with the RCMs to simulate the hydrological cycle in a small watershed in the southwest area of Sardinia. Its ability to reproduce the observed streamflow in historical period was hence assessed, revealing some uncertainties when coupled with some of the RCMs. Future hydrological projections were simulated based on the different SWAT-RCMs combinations. Future projections highlight a decrease in streamflow discharge, that is not very significant due to the presence of continuous wastewater inflows from urban areas, and a more pronounced reduction of surface runoff, reflecting the decrease of precipitation predicted by the climate models.

Introduction

Numerical modeling is nowadays a powerful and wide used tool for the assessment of environmental issues and supporting decision makers for a better plan of land management and water resources. The future basin management should rely on future climate projections at high resolution, in particular, including precipitation.

Moreover, the future evolution of precipitation cumulatively with increased temperatures, in a global warming context, may further exacerbate droughts, heat waves and water shortages as well as more frequent floods and may be critical for many human activities (Soares et al. 2017). For well-planned adaptation measures, which can include the use of impact models driven by Regional Climate Models, decision makers demand more precise projections of how the future might look like (Von Trentini et al., 2019).

A state-of-the-art ensemble of regional climate models for Europe was developed within the CORDEX consortium (EURO-CORDEX European Coordinated Regional Downscaling Experiment). This ensemble was used for projecting the European future climate (Jacob et al. 2014), was extensively evaluated (e.g. Katragkou et al. 2015; Kotlarski et al. 2014) and enabled more detailed studies on the consequences of climate change in specific regions, in particular related to precipitation, temperature and wind (Soares et al. 2017; Cardoso et al. 2018; Nogueira et al. 2019, etc).

Sardinia is a Mediterranean island especially vulnerable to climate change. General Circulation Models (GCM) and Regional Climate Models (RCM) simulations, for future global warming scenarios in the southern Europe domain, project a decrease in mean precipitation with an intensification of extreme values (Sillmann et al. 2013b; Casanueva et al. 2015; Alpert et al. 2002; Sánchez et al. 2004; Gao et al. 2006; Rajczak et al. 2013; Soares et al. 2015). Previous Euro-CORDEX evaluations have been carried out focused Sardinia but only considering historical simulations (Mascaro et al. 2018), or at a larger scale and resolution (Aristeidis G. et al, 2018).

SWAT (Soil and Water Assessment Tool) is a hydrological model functioning on a daily or monthly time step. In addition, it was used for evaluating the impact of climate change and anthropogenic factors on stream flow, agricultural chemical and sediment yields in large river basins (Arnold et al., 1998) SWAT is commonly used in couple with climate models to assess climate change impacts on future water resources and watershed management (Nerantzaki et al., 2016; Perra et al., 2018; Carvalho-Santos et al., 2017). In recent studies (Perra et al., 2018; Piras et al., 2015) conducted in Sardinia, SWAT was combined with ENSEMBLES climate models, providing future climate forcing for water resources assessment and drought risk evaluation. Findings of these researches project a future decrease of mean precipitations and, among them, the streamflow discharge, with an increase of the extreme events

This study aimed at building a Climate Model Ensemble for the Sardinia island (west Mediterranean Sea) in order to characterize the future changes of precipitation and provide future climate forcing to the SWAT hydrological model, using the Euro-Cordex simulations. A module for the assessment

of the heavy metal transport will be then chained to the setup to simulate metals fate and transport for future periods.

Data and Methods

Area of study

The study area is the Sardinia island (Figure 51), which has a surface of around 24,000 km^2 and is located in the west Mediterranean Sea between Italy and Spain. Sardinia has a complex topography mainly characterized by mountains, interrupted by some plain valleys due to tectonic structures (horst-graben).

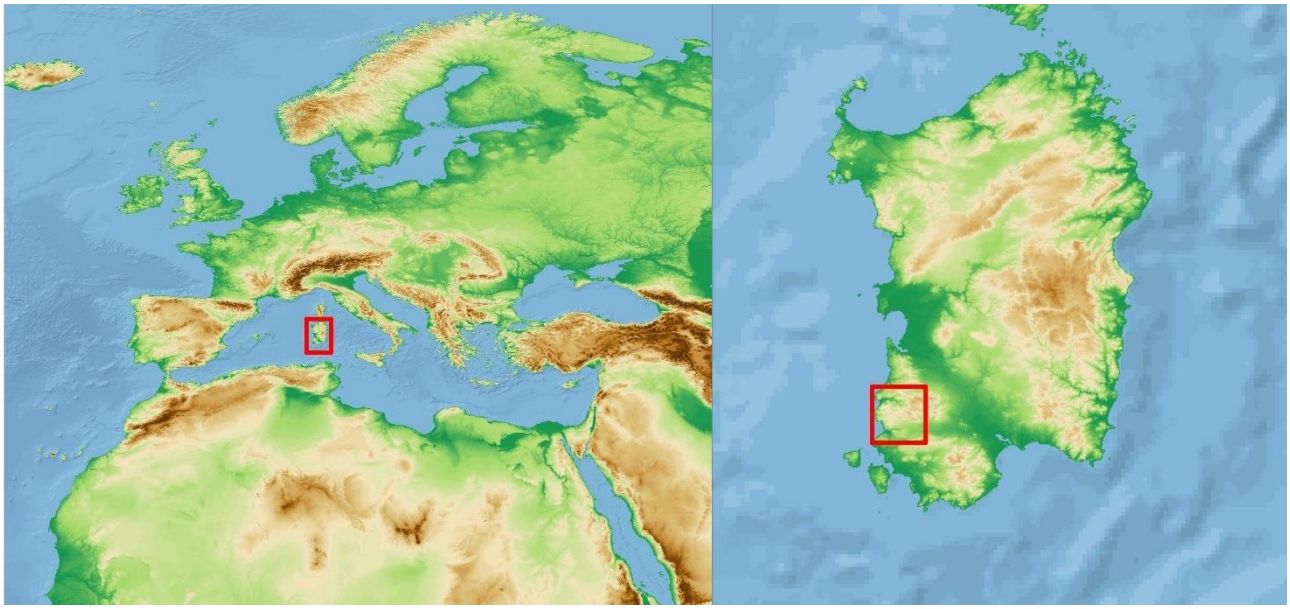

Figure 51 - Study area: domain of the climate change analysis (left) and domain of the SWAT modelization (right)

The highest elevation is given by the Gennargentu mountains (1834 m a.s.l.), located in the center-east of the island, that influences the local circulation and precipitation distribution. Climate in Sardinia is Mediterranean, with the occurrence of a wet period from September to May and very dry summers from June to August (Mascaro et al. 2018).

Observed data

Observed data used in this study includes daily precipitation measured by 242 of the 441 rain gauges of the Sardinian Hydrological Survey for the period 1979-2008. As shown in FIGURE 52, the stations

(red spots) are distributed quite uniformly throughout the island (at least one gauge per 100 km^2) covering a wide range of elevations up to 1467 m a.s.l.

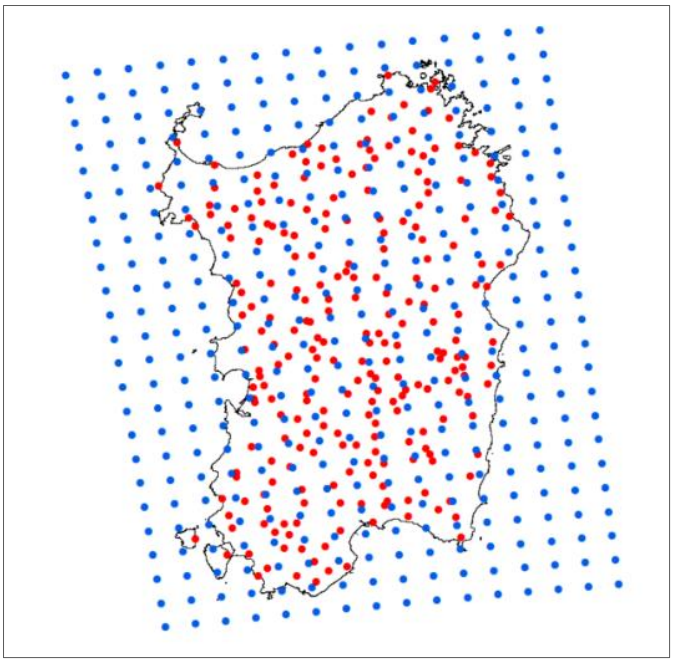

Figure 52 – Euro-CORDEX precipitation regular grid (blue spots) and real stations network (red spots)

The comparation between the observational network and RCMs grid network was carried out through a simple interpolation based on nearest neighbor technique.

Euro-CORDEX Simulations

The Coordinated Regional Climate Downscaling experiment (CORDEX) project (Giorgi et al. 2009) provides a set of Regional Climate Models (RCM) simulations driven by different Global Climate Models (GCM) over Europe, as part of the EURO-CORDEX initiative (Kotlarski et al. 2014; Katragkou et al. 2015). The EURO-CORDEX simulations used in this study cover the period 1976–2005 for the historical climate and 2071–2100 for the future projections, using the RCP8.5 scenario (Riahi et al. 2011). The daily precipitation at 0.11° resolution were retrieved from ESGF portal (Earth System Grid Federation). As shown in Table 1, 13 different model datasets at 0.11° resolution were available in the portal and were analyzed in this study. The model acronyms will be kept in this text to simplify figures, charts and tables (see last column of Table 1).

Table 13. EURO-CORDEX regional climate models considered in the present study, along with the responsible institution, the forcing global climate model, the acronym for each model combination (RCM-GCM).

Institution	Reference	Model	Forcing Model	Acronym
Climate Limited-area Modelling Community	Rockel et al. (2008)	CCLM4-8-17	ICHEC-EC-EARTH	CLM1
			MOHC-HadGEM2-ES	CLM2
			CNRM-CERFACS-CNRM-CM5	CLM3
			MPI-M-MPI-ESM-LR	CLM4
Danish Meteorological Institute	Christensen et al. (2006)	HIRHAM5	ICHEC-EC-EARTH	DMI
Koninklijk Nederlands Meteorologisch Instituut	van Meijgaard et al. (2008)	RACMO22E	ICHEC-EC-EARTH	KNMI1
			MOHC-HadGEM2-ES	KNMI2
Helmholtz-Zentrum Geesthacht, Climate Service Center, Max Planck Institute for Meteorology	Jacob et al. (2001)	REMO2009	MPI-M-MPI-ESM-LR	MPI
Swedish Meteorological and Hydrological Institute	Samuelsson et al. (2011)	RCA4	ICHEC-EC-EARTH	SMHI1
			MOHC-HadGEM2-ES	SMHI2
			CNRM-CERFACS-CNRM-CM5	SMHI3
			MPI-M-MPI-ESM-LR	SMHI4
			IPSL-IPSL-CM5A-MR	SMHI5

Models evaluation

For this study similar metrics to Soares et al. (2017) were used to evaluate the precipitation model's results. The assessment of each model is based on the comparison with Sardinia's 242 station observations. With this purpose, standard statistical errors are computed, for the monthly, seasonal and yearly scales. The following statistics are calculated by pooling together time and space: bias (1), percentual bias (2), mean absolute error (3), mean absolute percentage error (4), root mean square error (5), normalized standard deviation (6), spatial correlation (7) and Willmott-D score (8) (Willmott et al. 2012). The grid points of the EURO-CORDEX RCMs correspond to the nearest neighbors to the Sardinia's station.

$$Bias = \frac{1}{N}\sum_{k=1}^{N}(p_k - o_k), \quad (1)$$

$$Bias\% = \frac{\sum_{k=1}^{N}(p_k - o_k),}{\sum_{k=1}^{N} o_k} \times 100, \quad (2)$$

$$MAE = \frac{1}{N}\sum_{k=1}^{N}|p_k - o_k|, \quad (3)$$

$$MAPE = \frac{\sum_{k=1}^{N}|p_k - o_k|}{\sum_{k=1}^{N} o_k} \times 100, \quad (4)$$

$$RMSE = \sqrt{\frac{1}{N}\sum_{k=1}^{N}(p_k - o_k)^2}, \quad (5)$$

$$\sigma_n = \frac{\sigma_p}{\sigma_o} = \frac{\sqrt{\frac{1}{N}\sum_{k=1}^{N}(p_k - \bar{p})^2}}{\sqrt{\frac{1}{N}\sum_{k=1}^{N}(o - \bar{o})^2}}, \quad (6)$$

$$r = \frac{\sum_{k=1}^{N}(o_k - \bar{o}) - (p_k - \bar{p})}{\sqrt{\sum_{k=1}^{N}(o_k - \bar{o})^2 \sum_{k=1}^{N}(p_k - \bar{p})^2}}, \quad (7)$$

$$D = \begin{cases} 1 - \frac{\sum_{k=1}^{N}|p_k - o_k|}{2\sum_{k=1}^{N}|o_k - \overline{o}|}, \ if \ \sum_{k=1}^{N}|p_k - o_k| \ \leq \ 2\sum_{k=1}^{N}|o_k - \overline{o}| \\ \frac{2\sum_{k=1}^{N}|o_k - \overline{o}|}{\sum_{k=1}^{N}|p_k - o_k|} - 1, \ if \ 2\sum_{k=1}^{N}|o_k - \overline{o}| \ > \sum_{k=1}^{N}|p_k - o_k| \end{cases}, \quad (8)$$

where N is the number of observed/modelled days, o_k and p_k represents the observed/modelled values and, $\overline{o}$ and $\bar{p}$ the mean of observed/modelled values. For the Willmott-D score, a perfect skill is obtained when $D = 1$ and no skill when $D = -1$. The analysis around the mean are done with the metrics in Eq. 1 to 9, and to measure the differences between distributions, the S (Eq. 10) and Yule-Kendall (Eq. 11) skill scores are used. In agreement with Perkins et al. (2007), the probability density functions (PDF) matching scores are computed, as well as the Yule-Kendall skewness measure (Ferro et al. 2005). The PDFs of each dataset are calculated using the daily data.

$$S = \int \min(E_M, E_O), \quad (10)$$

$$YK = \left[\frac{(P_{95} - P_{50}) - (P_{50} - P_5)}{(P_{95} - P_5)}\right]_{model} - \left[\frac{(P_{95} - P_{50}) - (P_{50} - P_5)}{(P_{95} - P_5)}\right]_{obs}, \quad (11)$$

The P represents the percentiles, E_M and E_O represents the empirical distribution function of the model and observed pooled sample, respectively. The S score measures the overlap between observed and modelled PDFs, whilst the Yule-Kendall measure the difference between the two PDFs skewness.

Ensemble building

To perform a robust evaluation of the precipitation response to global warming, a EURO-CORDEX multi-model ensemble was built taking into account the relative performance of each RCM (Christensen et al. 2010). All above metrics were included in the ranking process, except the bias% and MAPE. Since the optimal result of bias, MAE and RMSE is zero, the inverse of its absolute value

was calculated. For normalised standard deviation, since the best result is 1, this metric was transformed as:

$$\vartheta_n = \begin{cases} \sigma_n \ \ if\ \sigma_n < 1 \\ \frac{1}{\sigma_n} \ \ if\ \sigma_n > 1 \end{cases}.$$

At the same way, the Yule-Kendall score became:

$$YK_{new} = \begin{cases} YK + 1 \ \ if\ YK < 0 \\ \frac{1}{YK+1} \ \ if\ YK > 0 \end{cases}.$$

For each metric, the individual model ranks were obtained by dividing each value by the sum of all model values, resulting in a sum of the ranks equal to 1. The ranks of all the metrics were firstly multiplied and then divided by the sum of the weights, resulting in a weight for each model. The precipitation's multi-model weighted ensemble was obtained by multiplying the respective EURO-CORDEX RCM weight as:

$$\overline{pr} = \frac{\sum_{i=1}^{N} pr_i w_i}{\sum_{i=1}^{N} w_i}.$$

SWAT model

SWAT is a physically based semi-distributed model with daily and monthly calculations of hydrological balance parameters in a watershed (Arnold et al. 1998; Neitsch et al. 2011). It is based on physical parameters that the user can modify to better represent the features of the modeled watershed. In the current study, firstly, the SWAT model was run using real precipitation time series as input and calibrated with observed streamflow data. Secondly, the SWAT, model was forced with the Euro-CORDEX climate model results from the historical and future runs. This allowed to quantify the projected changes on the streamflow.

The SWAT model domain, in this study, is a sub-domain of the Sardinia island and is located in the south west region as shown in **FIGURE 53.** Two main watersheds have been identified, a southern one that is the area of interest, and a northern one that contains the only streamflow control gauge of this region, that was used for calibration.

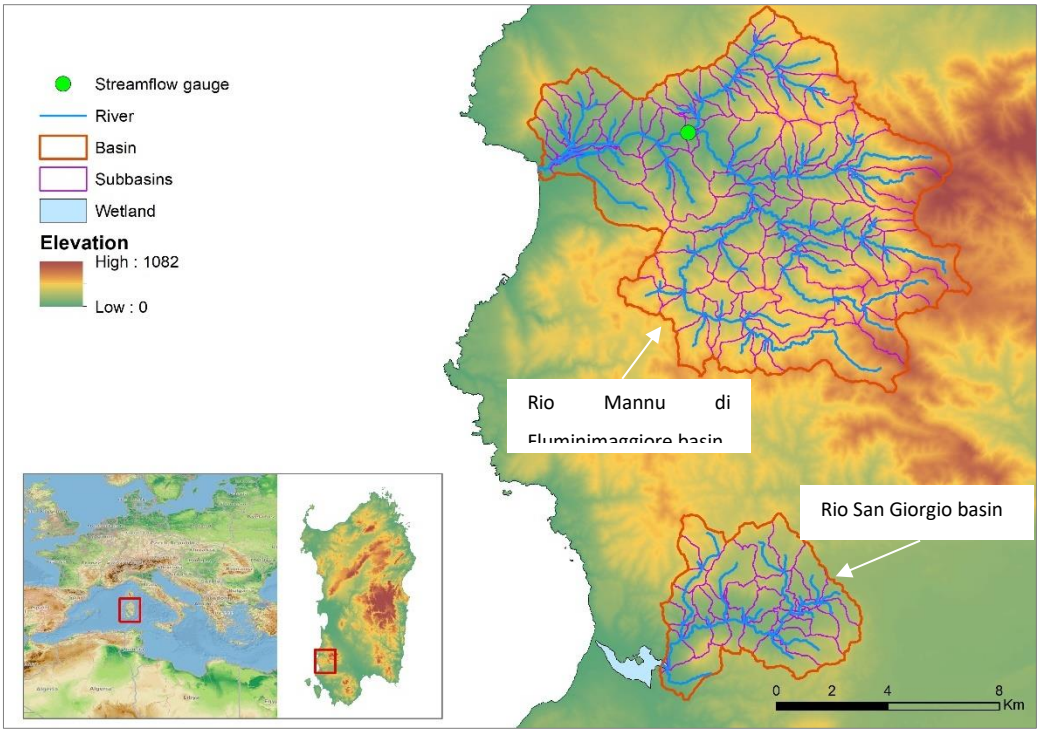

Figure 53 - SWAT model sub-domain within the island of Sardinia. Rio San Giorgio basin (southern basin) is the area of interest, while Rio Mannu di Fluminimaggiore (northern basin) was modeled due to the presence of a streamflow measurement gauge used for model calibration.

Input data for the model setup was retrieved from local government offices and is listed in Table 14. SWAT divides the watershed in sub-basins and calculates the water balance based on the Hydrologic Response Units, namely unique combinations of Land Use, Soil (FIGURE 54) and Slope class. 160 sub-basins and 2773 HRUs were delineated. Slope was split into 3 classes: 0–5%; 5–10%; > 10% to reproduce the spatial variability of this feature in the watershed. Constant daily flow from 2 point-sources of urban wastewater were modeled, with an annual discharge of 900000 m^3/year and 110000 m^3/year. All the input data used to build-up the model is summarized in TABLE 14.

Table 14 - Input data for the implementation of the SWAT model

Input data	Resolution	Source
Digital Elevation Model	10m	Regione Autonoma della Sardegna
Stream Network	-	Regione Autonoma della Sardegna
Soil map and custom database	02:40.0	CRS4 Research Center
Land use map	01:25.0	Regione Autonoma della Sardegna
Point Sources discharge	Annual amount	IGEA s.p.a.
Observed precipitation and measurement network	Daily	Regione Autonoma della Sardegna
Temperature statistics	Monthly	Regione Autonoma della Sardegna

Observed streamflow (for calibration)	Monthly/daily	Regione Autonoma della Sardegna

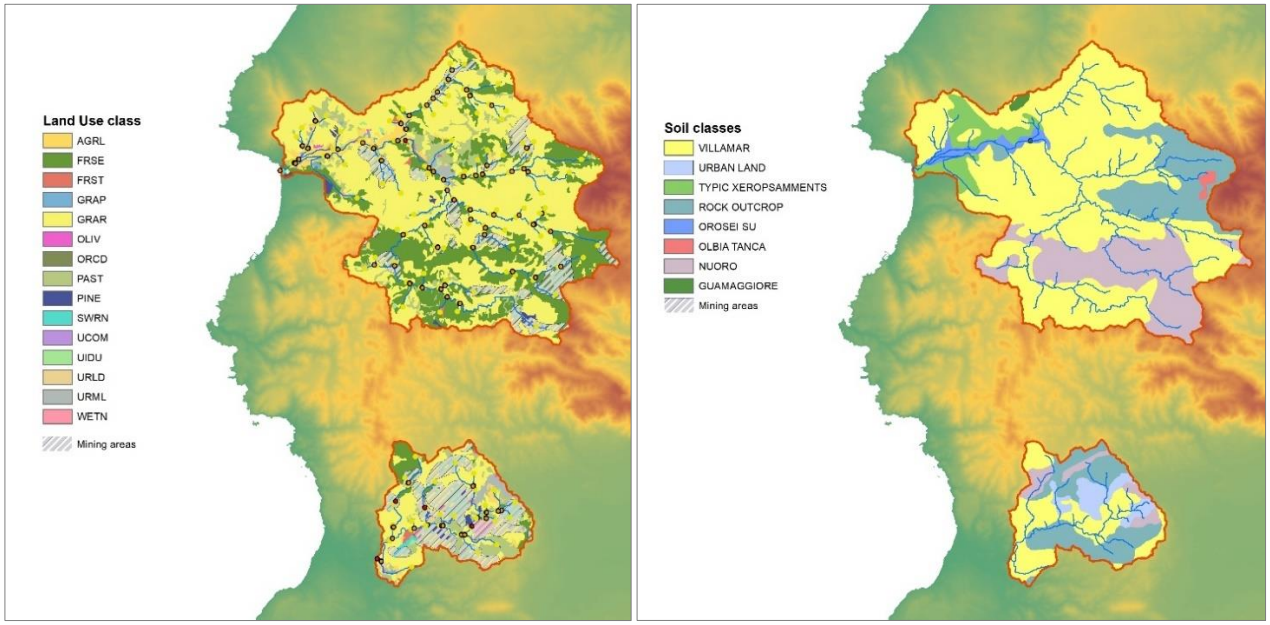

Figure 54 - Land use (left) and soil (right) maps used as input for SWAT model

The model was calibrated and validated against daily streamflow observations (1985-1994), split in two independent series, 1985-1992 for calibration (FIGURE 55) and 1992-1994 (FIGURE 56) for validation, using SUFI-2 procedure (Abbaspour et al., 2007). In SUFI-2 the goodness of the model is evaluated accounting and measuring uncertainty, while the fitting of modeled and observed discharge is measured with Nash-Sutcliffe index that is calculated as follows:

$$NS = 1 - \frac{\sum_i (Q_m - Q_s)_i^2}{\sum_i (Q_{m,i} - \overline{Q}_m)^2}$$

where Q is a variable (e.g., discharge), and m and s stand for measured and simulated, respectively, and the bar stands for average. A perfect model would have a NS index of 1, while a NS below 0 corresponds to an unreliable model. Suggested values of NS are > 0.5. Daily calibration scored a NS index of 0.66 and 0.60 for validation period.

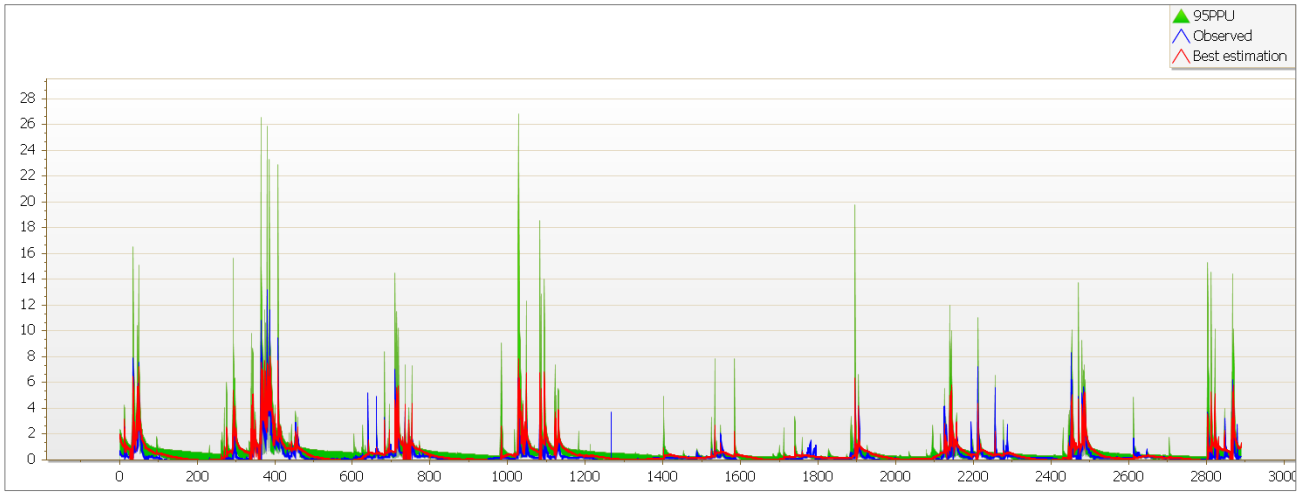

Figure 55 - Calibration of the daily streamflow (m^3/s February 1985- December 1992) at the Flumineddu measurement station scoring a (NS) index of 0.66.

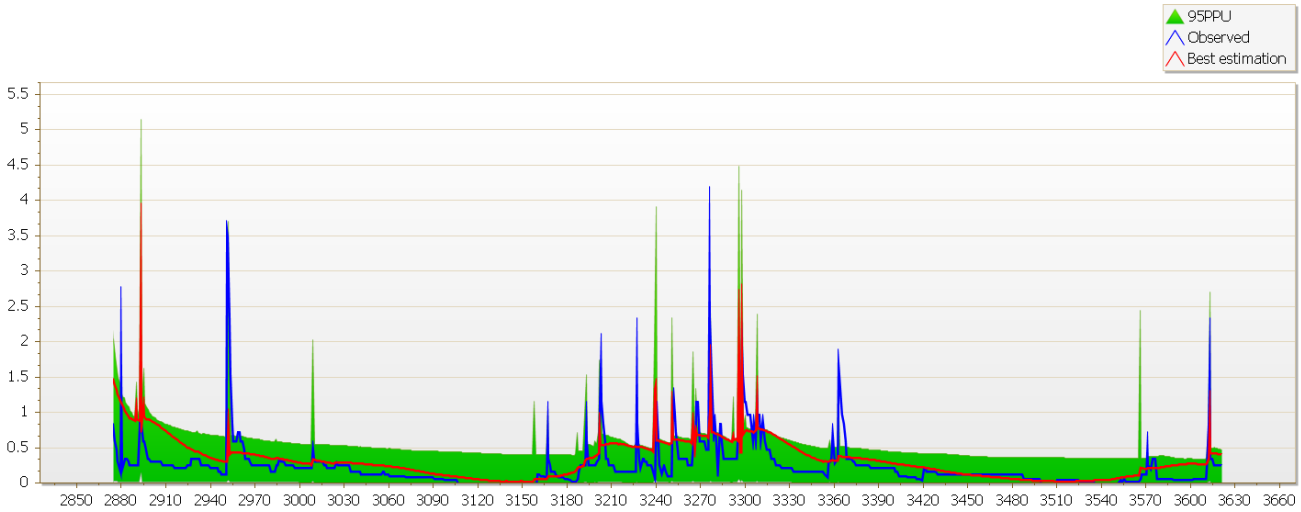

Figure 56 - Validation of the daily streamflow (m^3/s January 1992- December 1994) at the Flumineddu measurement station

Validation at monthly time step (FIGURE 57) was also performed for the period 1985-1992, obtaining a NS of 0.88. The model seems to better reproduce the monthly mean rainfall, in agreement with the chosen scale for long-term future simulations

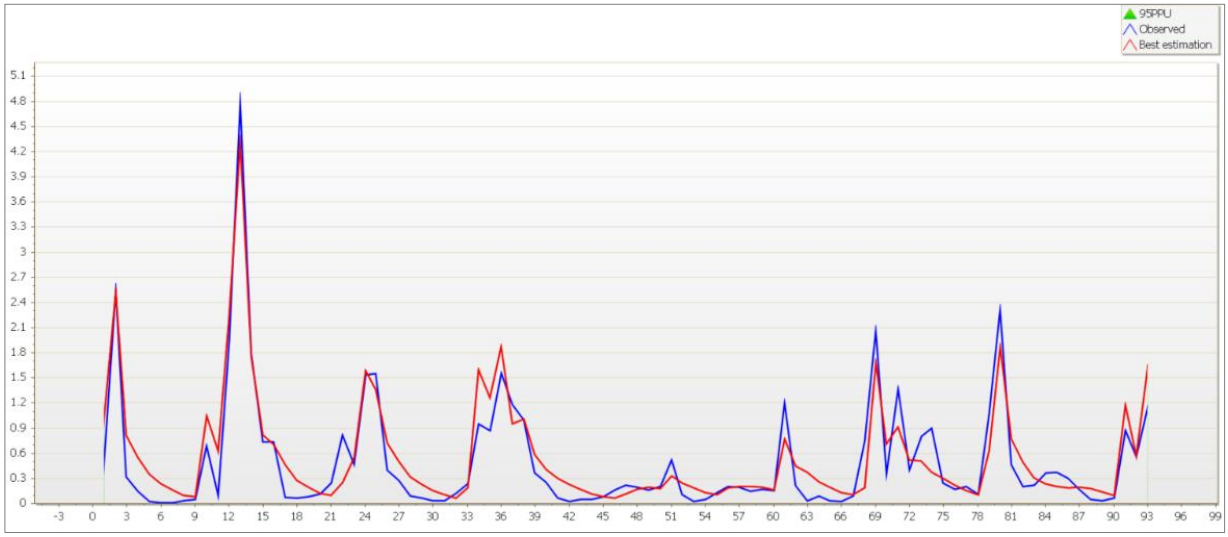

Figure 57 - Monthly streamflow validation ((m^3/s) February 1985- December 1992) at the Flumineddu measurement station

Results and discussion

3.1 Evaluation of observed precipitation

The mean yearly observed precipitation for historical period (1979-2005) is 645 mm, considerably lower than the 710 mm reported by Mascaro (2018) for the period 1950-2005, with lowest value of 365 mm and a maximum of 1040 mm in the Gennargentu mountainous area. Seasonal mean precipitations are distributed as follows:

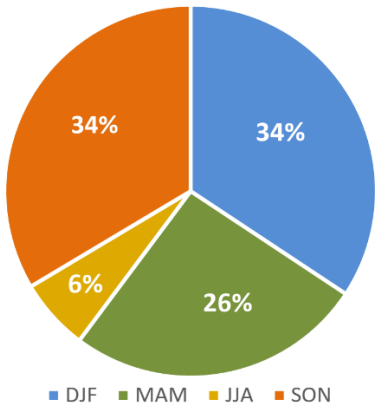

DJF	MAM	JJA	SON
221.09	166.93	40.21	216.26

Figure 58 – Seasonal distribution of the precipitations

Almost the 70% of the total rainfall is distributed between September and February, around 25% in the spring months and only the 6% of the precipitation falls in summer months, revealing a strong seasonality. The spatial variability of the precipitations is very high, especially in winter due to the orographic precipitation. Different seasonal spatial patterns can be seen mainly in spring and summer, with a decreasing rainfall from north-east to south-west, and in winter with a clear precipitation gradient from west to east, with the exception of the mountain range of the south-west area that shows higher precipitation values.

Evaluation of Euro-CORDEX simulations

The assessment of the models for the historical reference period is crucial to evaluate their reliability and determine their weight within the multi-model ensemble for the climate change assessment.

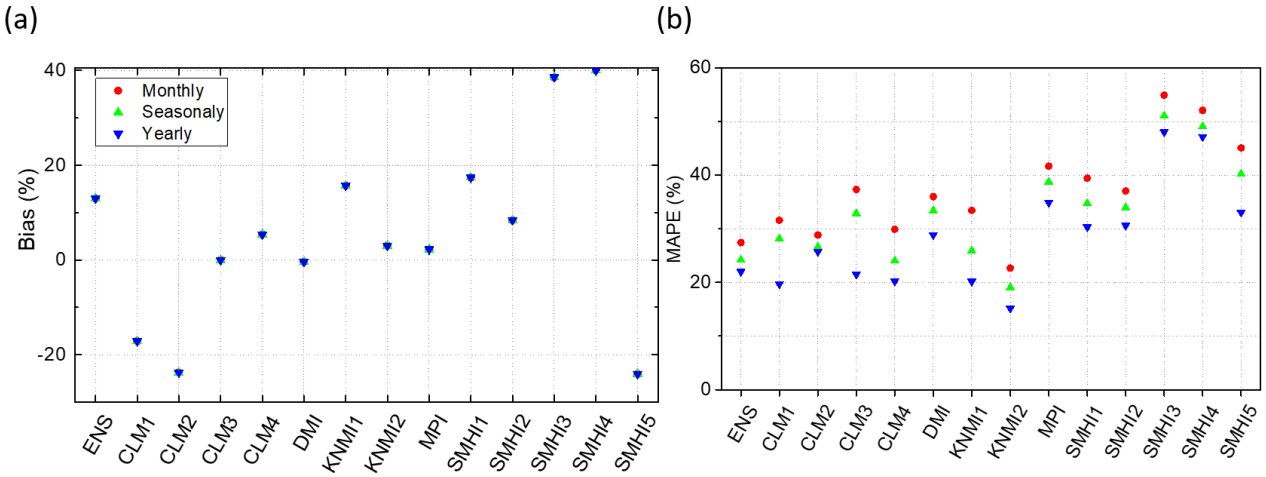

Figure 59 shows the bias and the mean average percentage error of the models and the weighted multi-model ensemble (ENS) against the observed precipitation. CLM3, DMI, KNMI2 and MPI have a good bias for the yearly precipitation, but only KNMI2 shows a good response at the seasonal and monthly scale, while CLM3, DMI and MPI are not reliable at these time scales. KNMI2 shows the lowest MAPE, followed by the KNMI1 and CLM4 models. CLM3 and CLM1 show again good performance at yearly scale, with a big detachment at monthly and seasonal scales.

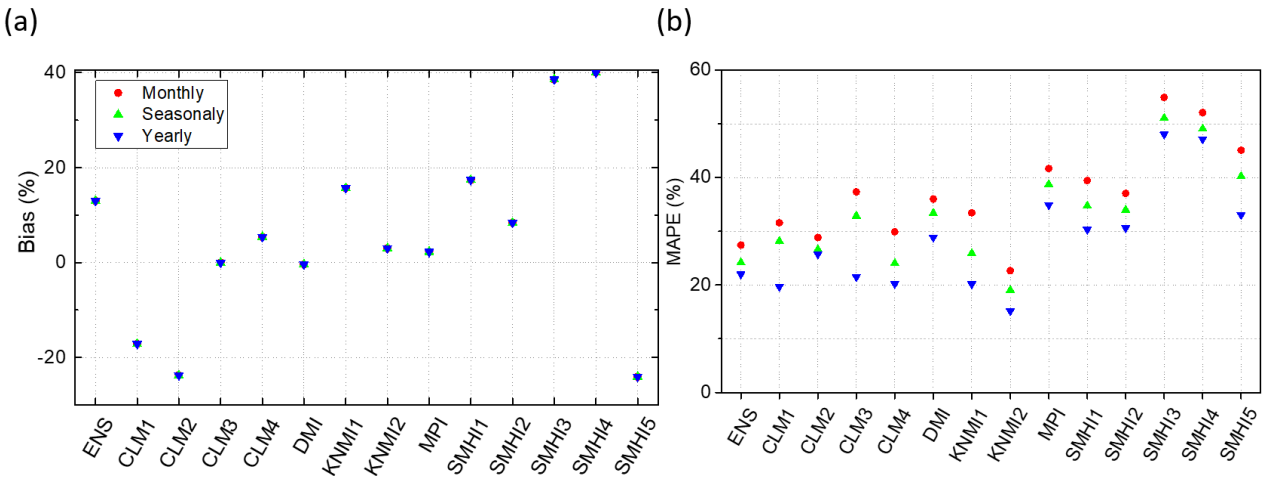

Figure 59. Error measures of EURO-CORDEX RCMs and ENS precipitation against the observational stations data for the Sardinia mainland: (a) percentual bias and (b) mean absolute percentage error. The errors are computed for monthly (red), seasonally (green) and yearly (blue) accumulation periods of precipitation pooling all data together.

Statistical errors and skill scores resumed in TABLE 15, calculated for each model and for the model ensemble, represent different metrics of evaluation that not always reflect the same best performing models. Based on these scores, weighted model ensemble was built, with the weights reported in the mentioned table.

Table 15 - Statistical errors and skill scores for EURO-CORDEX RCMs and ENS against observational stations data. The errors are the seasonal percentual bias, MAPE, normalized standard deviation and Willmott-D score, the yearly spatial correlation

RCMs	Bias%	MAPE	Normalized Standard Deviation	Wilmott-D	Spatial Correlation	S	Yule-Kendall	Weight
CLM1	-17.12	28.16	0.68	0.67	0.56	85.88	0.036	8.53%
CLM2	-23.75	26.62	0.77	0.69	0.45	85.37	0.04	8.52%
CLM3	-0.005	32.87	0.69	0.61	0.34	84.62	0.009	3.96%
CLM4	5.39	24.04	0.98	0.72	0.39	88.78	0.019	12.27%
DMI	-0.4	33.39	1.27	0.61	0.5	90.4	0.072	5.24%
KNMI1	15.68	25.91	0.95	0.7	0.61	82.34	0.027	15.80%
KNMI2	3	19.05	1.01	0.78	0.59	83.13	0.06	27.43%

MPI	2.26	38.75	1.2	0.54	-0.12	88.01	0.074	0.96%
SMHI1	17.42	34.73	1.39	0.59	0.51	88.16	0.04	4.51%
SMHI2	8.39	33.98	1.26	0.6	0.5	86.86	0.043	5.19%
SMHI3	38.59	51.06	1.42	0.4	0.46	89.67	0.025	1.87%
SMHI4	40.03	49.09	1.63	0.42	0.45	91.32	0.032	1.69%
SMHI5	-24.06	40.23	0.93	0.53	0.44	81.61	0.036	4.04%
ENS	12.99	24.18	1.12	0.72	0.57	87.48	0.041	

The FIGURE 60A shows the yearly mean accumulated precipitation for each model and for the weighted multi-model ensemble. KNMI1, KNMI2 and CLM4 reproduce well the spatial patterns, also confirmed by FIGURE 60B that shows the relative differences between the observed annual precipitation and simulated by RCM's. SMHI5 underestimates precipitation in in the east coast and in the southern Campidano area, while SMHI3 and SMHI4 overestimate values in the western stations. MPI and DMI models do not reproduce the spatial distribution of the annual precipitation, particularly the MPI model overestimates rainfall in most of the western stations and underestimates it in all the eastern area.

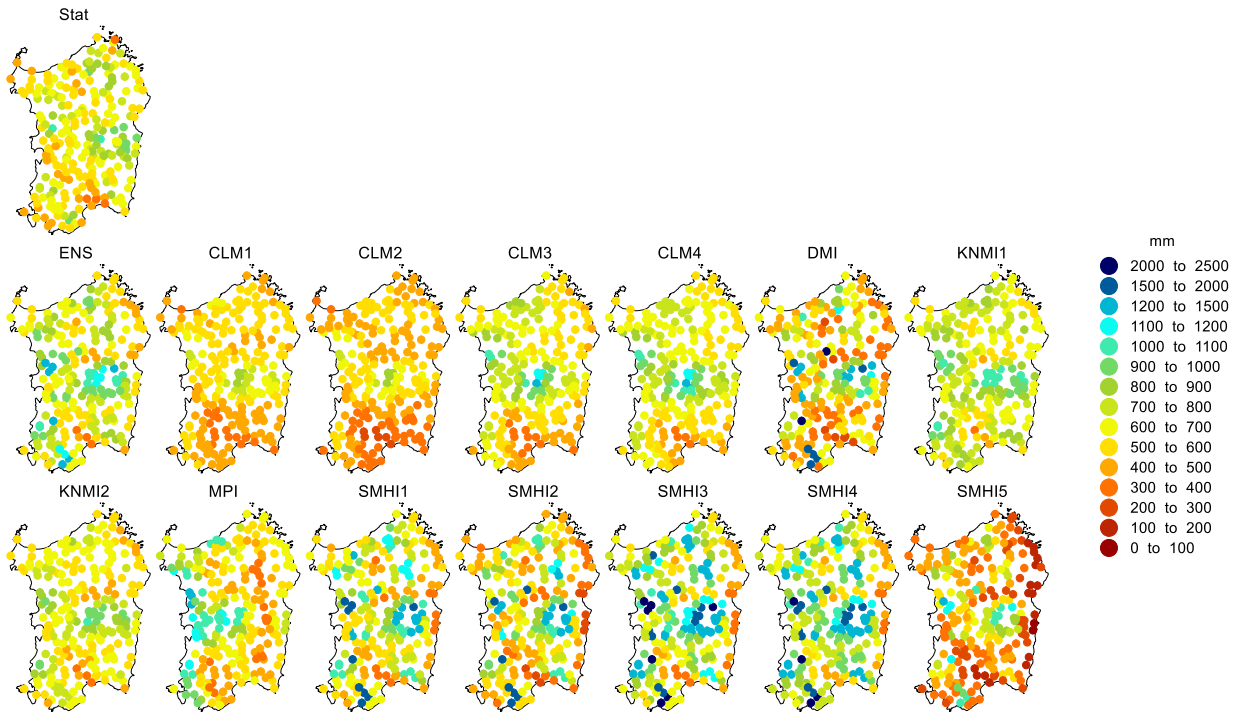

(a)

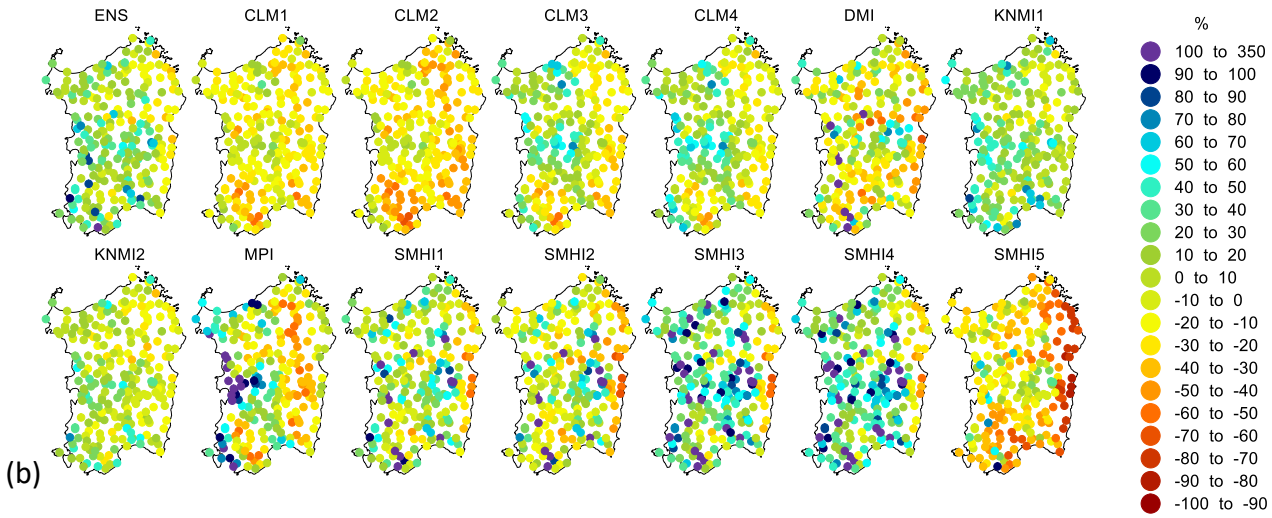

Figure 60. (a) Yearly mean precipitation from observations (1979-2008), from 13 EURO-CORDEX RCMs and from EURO-CORDEX weighted multi-model ensemble (1976-2005); and (b) relative differences between historical EURO-CORDEX individual RCMs runs and the weighted multi-model ensemble against the observations.

The seasonal maps (FIGURE 61), highlight how the complex orography influences the spatial distribution of the precipitations, ranging from values always above 200 mm seasonally in the Gennargentu mountains to values below 100 mm in the southern area around the city of Cagliari, that is the driest zone, even in the winter months.

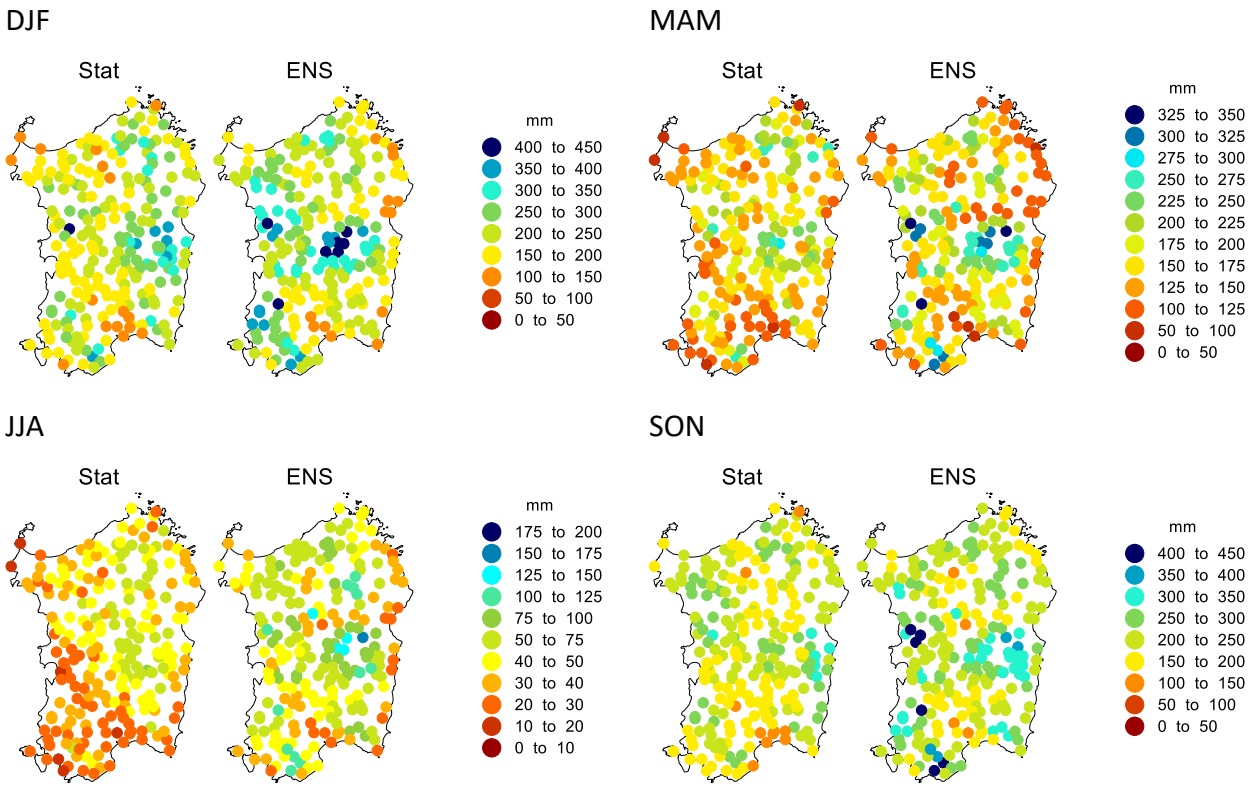

Figure 61. Seasonal mean precipitation from observations (1979-2008) and from the weighted multi-model ensemble (ENS) (1976-2005).

Despite a general overestimation of the precipitations, Model Ensemble reproduces quite well the spatial patterns of seasonal cumulates (FIGURE 61), except in summer months (JJA) were there is a notable spatial and quantitative disagreement. Precipitation in south west area is overestimated in all the seasons, while there is a good reproduction of the patterns in the south Campidano region that is, as mentioned above, one the driest areas. Generally, precipitations in the mountain ranges all over the island are overestimated by ENS, suggesting that EURO-CORDEX RCMs still not capture well the local conditions at small scales of observation.

Precipitation future projections

The projections of precipitation in the future were analyzed using the RCP 8.5 severe scenario. Relative changes in the future (2071 – 2100), given by the weighted multi-model ensemble when compared with the historical period (FIGURE 62), show a general rainfall decrease at the yearly scale,

which is pronounced in the southwest area (-20 to -25 %) with a negative gradient from northeast no southwest. The projected seasonal relative changes highlight different patterns: DJF is characterized by a general decrease of precipitation, larger in the east and southwest parts of Sardinia, amounting to values between -15% and -25%, while in MAM a more considerable change is seem, especially in the south of the island with precipitation reductions from -25% to -30%. In JJA a positive steep gradient has more or less a south east to north west orientation, going from positive changes above 5% to a significant decrease with peak values of -35% in the north west area (

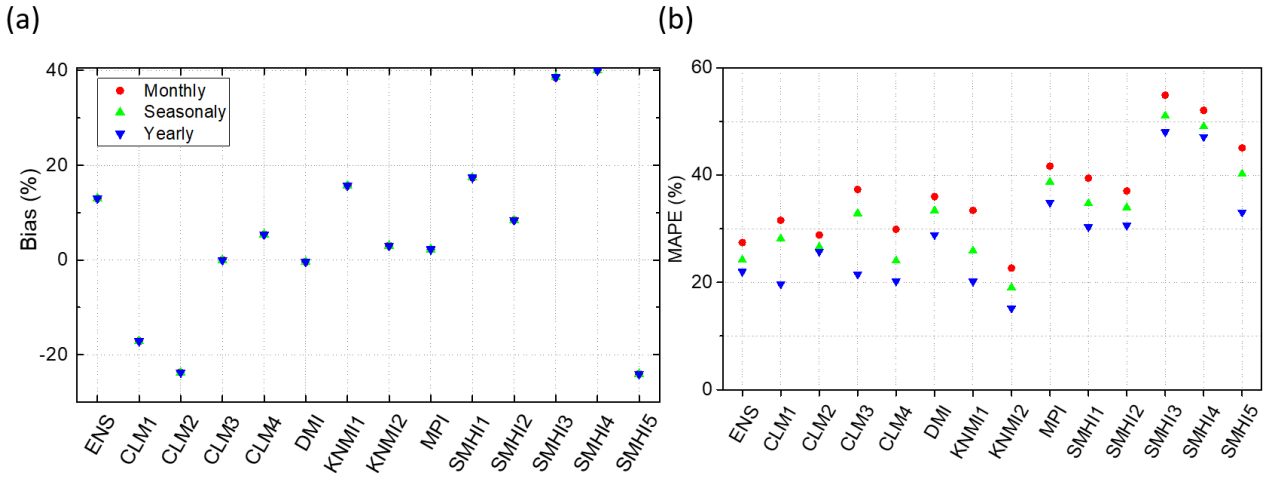

Figure 59). Another gradient of relative change is predicted for SON from north-east to south-west, with positive change up to 5% in the north east, down to -25% in the Sulcis region (south-west cape).

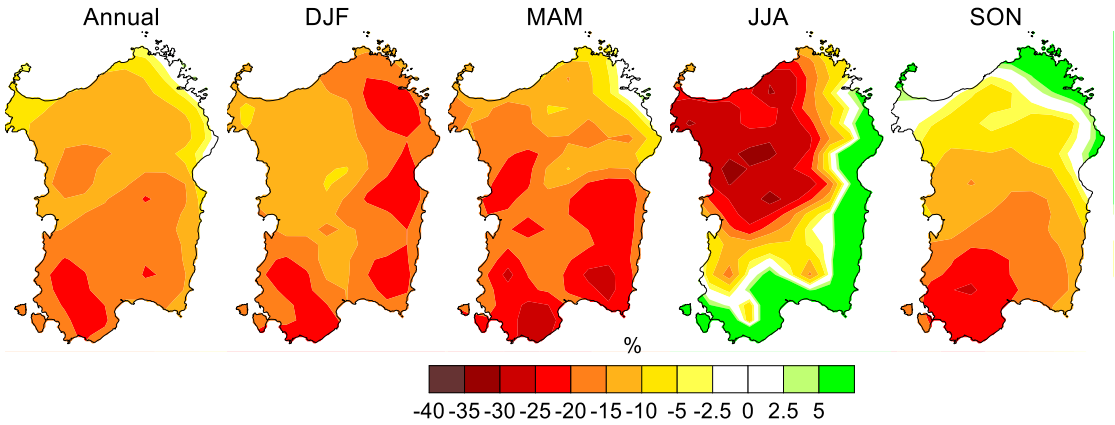

Figure 62. Yearly and seasonal mean precipitation relative changes, (2071-2100 minus 1976-2005)/1976-2005, for the ENS.

The south-west area, except for JJA, is projected to be the most vulnerable area for dryness by the ENS, as highlighted also by the relative change in number of wet days (FIGURE 63) that reaches values around -25% of precipitation events above 1 mm.

Changes in extremes

The decrease in percentage of yearly wet days, predicted by the ENS all over the island (FIGURE 63), has an east by north-east to west by south-west gradient, with larger decreases in the Campidano area (south-west), as mentioned above, in the Gennargentu mountains (center-east) and in the Ottana plain (center-west). These changes are in agreement with others climate change analysis that were performed in the Mediterranean region (Dubrovsky et al., 2013; Ducic et al., 2012;).

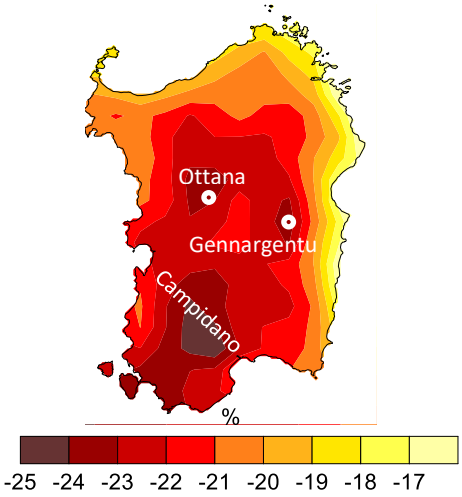

Figure 63. Relative change of the number of yearly wet days (daily precipitation above 1 mm).

The projected relative change in wet days above 10 mm of precipitations shows a different pattern, but adds to a wide-distributed rainfall decrease, with the south-west area that still shows a decrease that could amount up to -25%. The increase of precipitations above 20 mm in some regions, such as Campidano and Sassari's province, may be traced back to the increase of intense rainfall events, as depicted also in FIGURE 65. Rainfall events above 20 mm are instead expected to decrease almost in all the east regions, with higher negative values in the mountainous areas of Gennargentu, and in the south-west range.

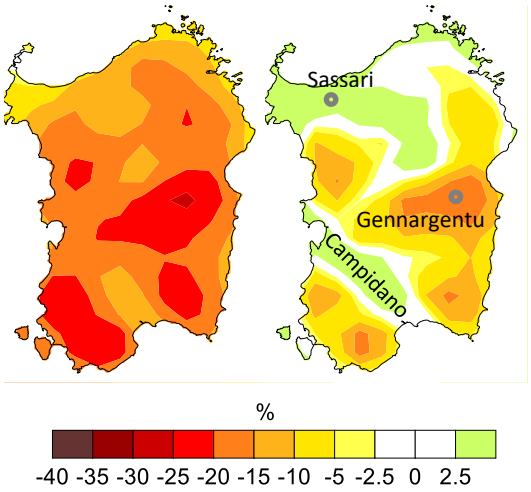

Figure 64. Relative change of number of yearly days when precipitation is above a) 10 mm and b) 20 mm.

Projections for the changes of the higher rank percentiles for future climate (95th and 99.9th percentiles) are depicted in **FIGURE 65**, due also to the use of RCP 8.5 severe scenario, showing an overall increase of both percentiles, with similar spatial patterns. The higher percentages of change are projected for the east side with peaks above +30% in mountainous areas and southern island capes, for 99th percentile. Extremes in the southern and eastern areas are in some way in agreement with the zones historically impacted by extreme rainfalls.

a) b)

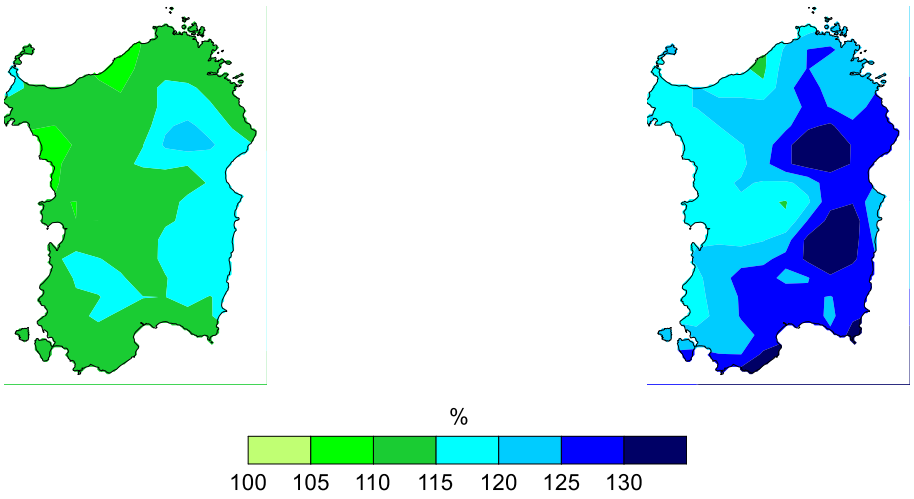

Figure 65 - Relative changes of precipitation 95th and 99th percentiles after adjusting for scale, comparing future (2071–2100) and present (1976–2005)

Hydrological simulations and the impact of Climate Change in a small basin

The SWAT model was firstly forced with EURO-CORDEX historical simulations (1976-2005) in order to compare the model's output with the observed streamflow. All the hydrological simulations were preceded by two years of warm-up, both for historical (1976-1978) and future period (2031-2033). SWAT model's weather generator needs continuous daily rainfall time series, with standard Gregorian calendar. Due to the use of 360 calendar days in the MOHC-HadGEM2-ES GCM simulations, 3 RCMS forced by this GCM have been excluded from the hydrological simulations. Based in the weights assigned to the models to build the ENS, the different SWAT model's outputs have been weighted and an ensemble output was calculated for the period 1985-1992 (FIGURE 66) normalizing the weights to 100% (TABLE 16).

	CLM1	CLM3	CLM4	DMI	KNMI1	MPI	SMHI1	SMHI3	SMHI4
Original ENS weight	8.53%	3.96%	12.27%	5.24%	15.80%	0.96%	4.51%	1.87%	1.69%
Norm. ENS weight	15.56%	7.22%	22.38%	9.56%	28.82%	1.75%	8.23%	3.41%	3.08%

Table 16 - Multi model ensemble (ENS) weights normalized after excluding MOHC-HadGEM2-ES GCM from the hydro-climate simulations

In the following analysis, for practical reasons, each SWAT output resulting from a different forcing model will be mentioned as SWAT-name of the model (e.g. SW-CLM1, SW-MPI), while SWAT weighted output based on multi-model ensemble weights will be named SW-ENS.

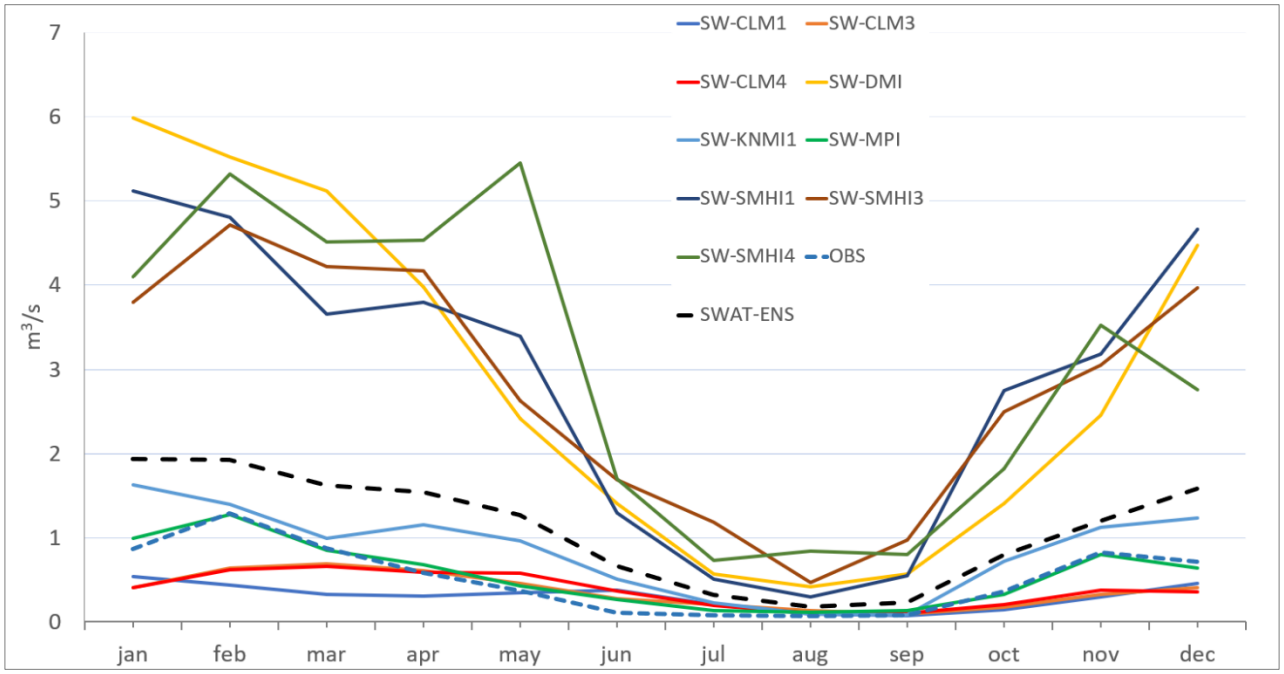

Figure 66 - SWAT monthly mean outflow (1985-1992) under different GCM-RCM forcing. ENS Flow refers to the weighted outflow, calculated using the same weights of the relative forcing climate model.

SWAT Models' outputs show huge biases in some cases (SW-SMHI4, SW-SMHI3, SW-SMHI1 and SW-DMI), while SW-MPI shows the best agreement, followed by SW-CLM1, SW-CLM3, SW-CLM4 and SW-KNM1. As the KNM1 model has the highest weight in the ENS (15.8%, normalized to 28.8%), the SW-ENS outflow has a similar monthly cycle as the SW-KNMI1 outflow, with an overestimation of the discharge that in winter months can reach large values (above 200%). **FIGURE 67** shows the comparison between historical (1978-2005) and future (2033-2060) model's monthly mean outflow at the control point of Rio Mannu di Fluminimaggiore, under different forcing climate models. A general decrease of the monthly mean discharge is expected, as further highlighted by historic/future SW-ENS comparison in **FIGURE 68**.

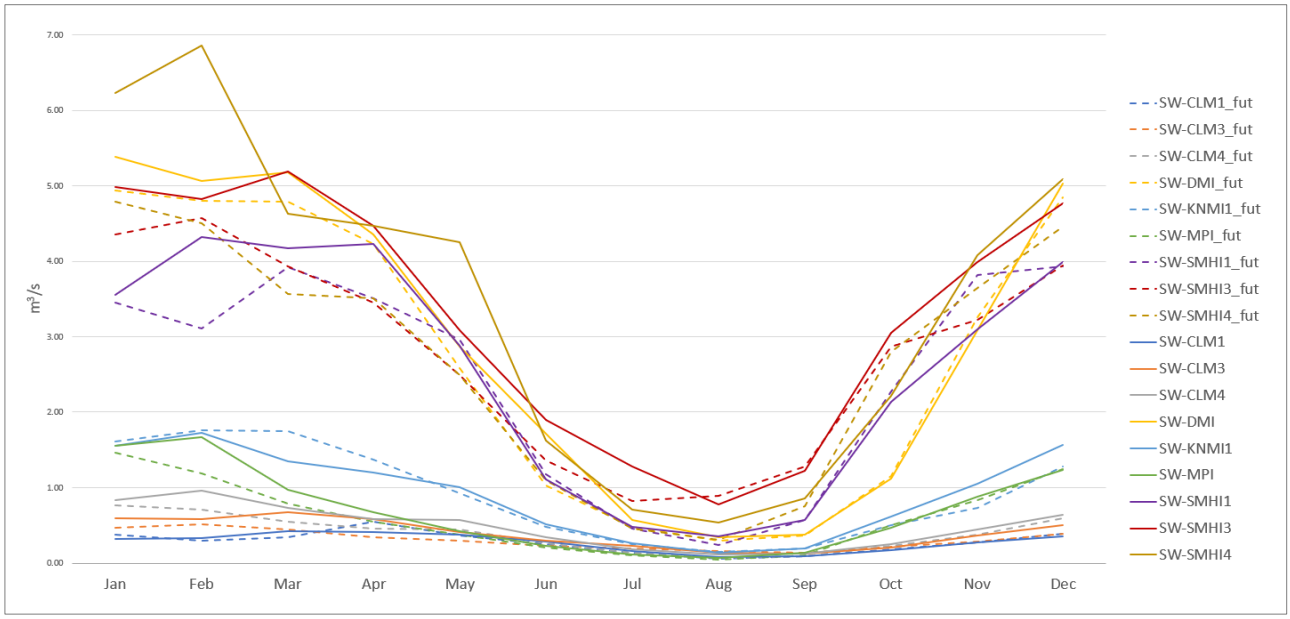

Figure 67 - Monthly mean outflow between SWAT simulations, forced by the different Euro-CORDEX models, comparison between past (1978-2005, continuous lines) and future (2033-2060, dashed lines)

Comparison of historical and future SW-ENS annual cycle (**FIGURE 68**) shows a relative decrease of outflow around -0,15 m^3/s for January, February, May and June, while a small increase of +0.13 m^3/s and +0.9 m^3/s is expected for March and December.

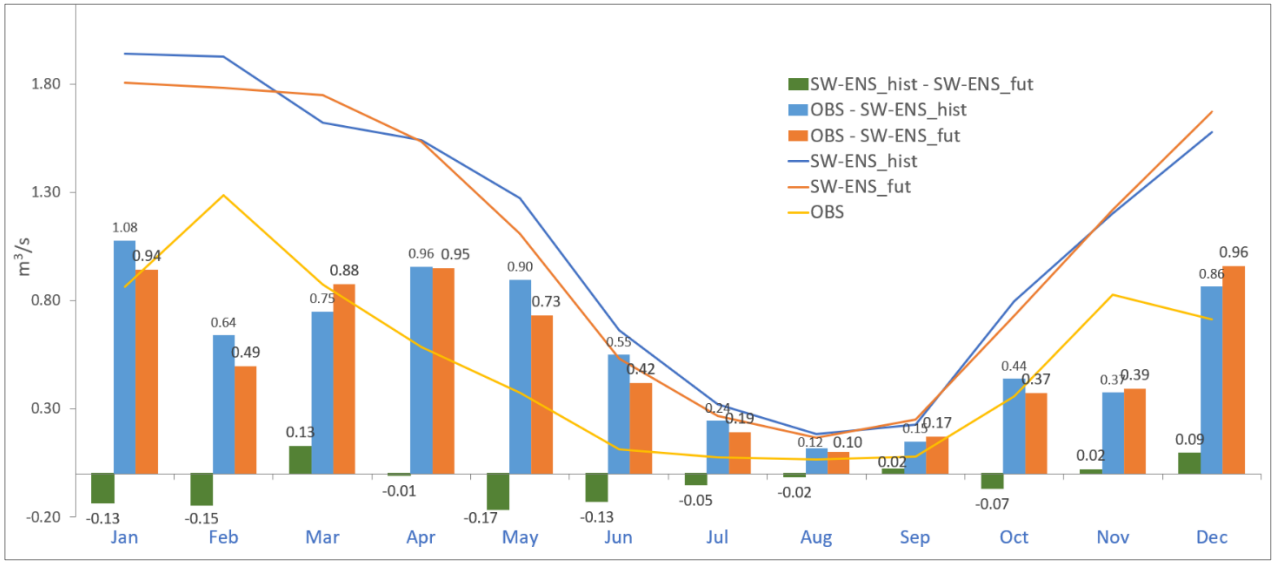

Figure 68 - SW-ENS outflow for historical (1978-2005) and future (2033-2060) and differences between SW-ENS_hist and SW-ENS_fut (green bars), between observed outflow and SW-ENS_hist (blue bars) and between observed outflow and SW-ENS_fut (orange bars)

Analyzing the Rio San Giorgio catchment (see FIGURE 53), the outflow for historical (SW-ENS_hist) and future (SW-ENS_fut) period present a relatively small reduction, probably depending on the 2 point sources, mentioned above, that constantly discharge wastewater. In dry periods this contribution represents the only inflow in the Rio San Giorgio.

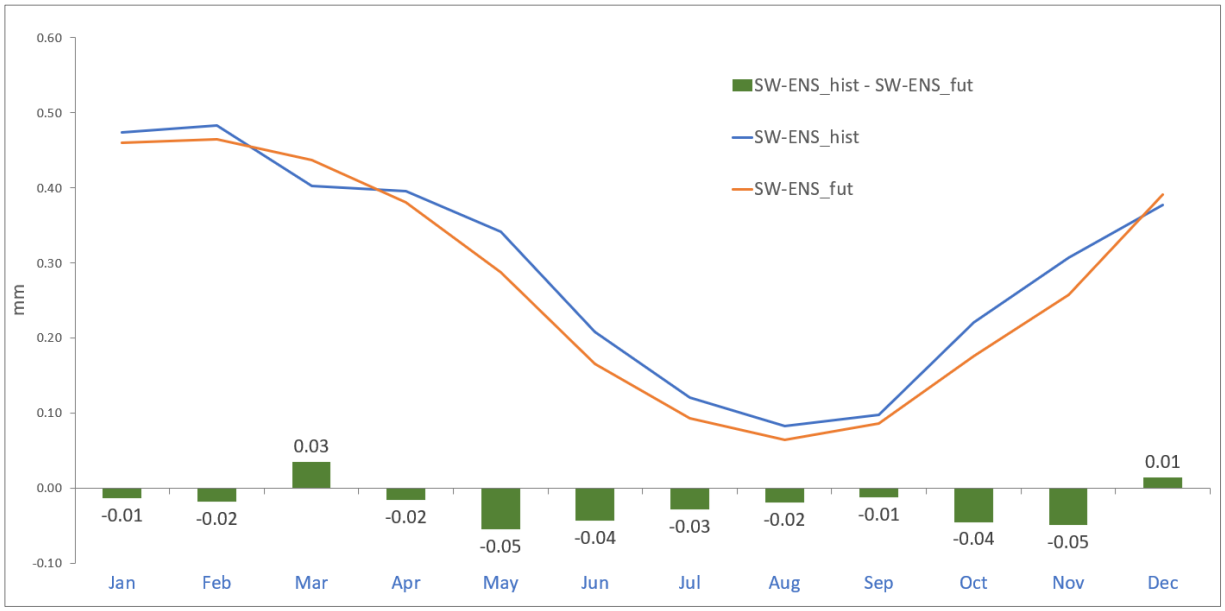

Figure 69 - Comparison between annual streamflow cycle for past (SW-ENS_hist) and future (SW-ENS_fut) and relative differences for San Giorgio basin.

In fact, considering mean surface-runoff values, a very significant reduction is projected for the future by the SW-ENS, as shown in FIGURE 70.

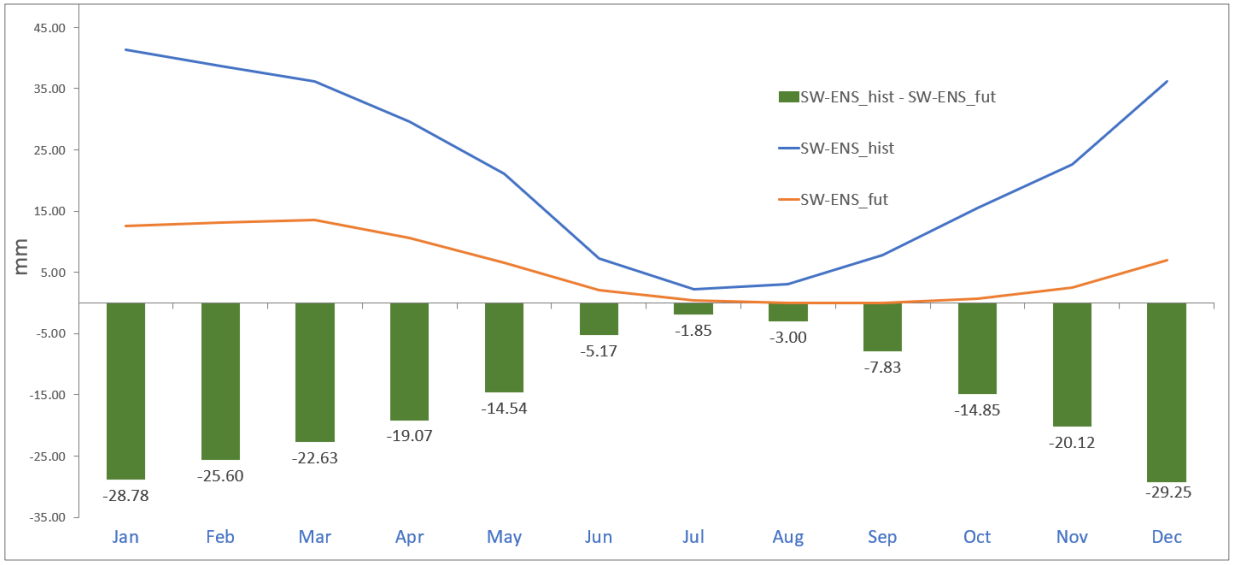

Figure 70 - Comparison between monthly mean surface runoff calculated over Rio San Giorgio basin for past (SW-ENS_hist) and future (SW-ENS_fut) and relative differences (geen bar)

Taking in account only for models that, compared to the observed annual cycle, have best performances (SW-MPI, SW-CLM1, SW-CLM3, SW-CLM4 and SW-KNM1) is notable that all the models predict (FIGURE 71) a decrease for spring season, except SW-KNMI for March and April and SW-CLM1 for April.

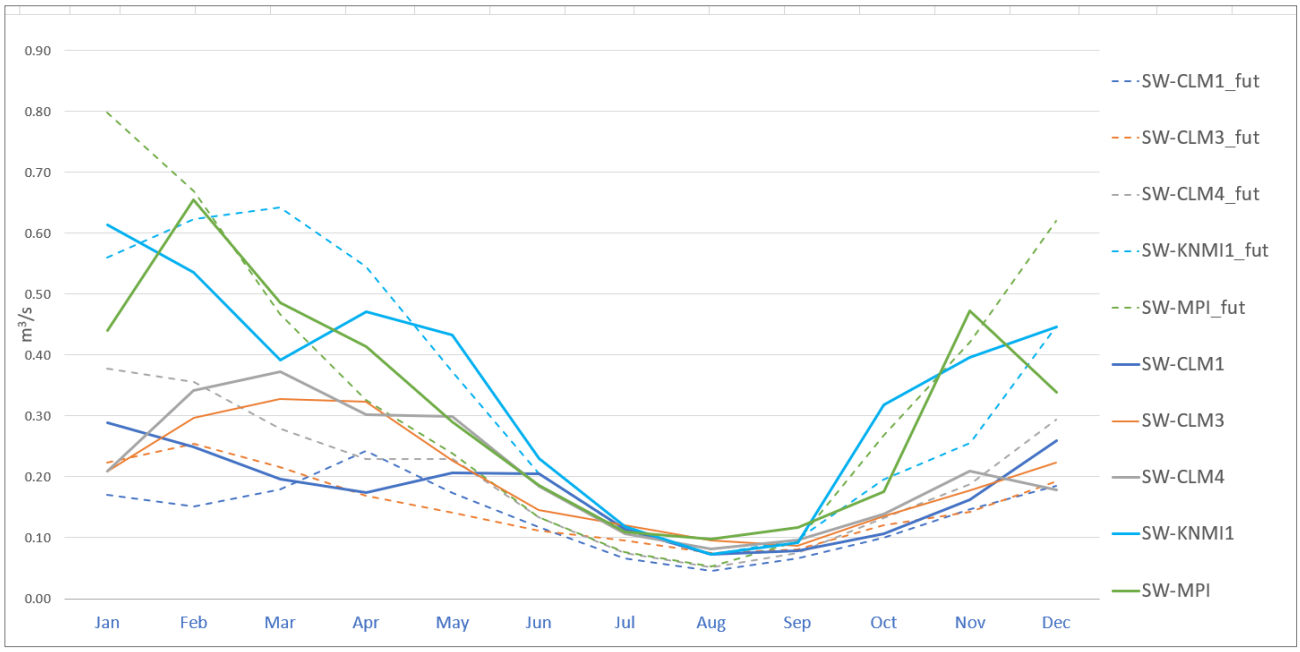

Figure 71 - Monthly mean outflow comparison between SWAT simulations, forced by the best performing SWAT/Euro-CORDEX coupled models, for historical period (1978-2005, continuous lines) and future (2033-2060, dashed lines)

Summer and autumn are expected to be dryer, except for SW-MPI that predicts an increase of the precipitation for October, probably related to extreme events. Nevertheless, it should be taken in account that MPI climate model was the less performing model within the ENS, while it showed a very good agreement in resulting outflow when coupled with SWAT model. Hence, this model has to be carefully considered for future projections, tanking in account its signal of overestimating the precipitation in the south west of the island, as highlighted in FIGURE 60. The Nash-Sutcliffe (NS) index was also calculated for the different SWAT combinations.

Table 17 – NS scores of SWAT model forced by the climate models

	SW-CLM3	SW-CLM1	SW-CLM4	SW-MPI	SW-KNMI1	SW-SMHI3	SW-DMI	SW-SMHI1	SW-SMHI4
NS	0.04	0.03	0.01	-0.30	-0.58	-15.80	-19.37	-19.61	-20.76

This analysis shows a limited reliability for future hydrological projections, due to the high number of uncertainty sources and model capabilities that could be improved with the collection of more

accurate data, in particular precipitation and streamflow discharge at the Rio San Giorgio's outlet. However, the different domains of the climate model analysis, that was done for the whole island, and the SWAT models simulations, limited to 2 small catchments, has to be taken in account when evaluating the performances.

Conclusions

In this study, a weighted multi-model ensemble, composed of different climate models of the Euro-CORDEX experiment was built and used as climate forcing for the SWAT hydrological model. Firstly, a climate model analysis was performed through the comparison between modeled and observed rainfall for a historical reference period (1979-2008), using several statistical indexes, such as Bias%, MAPE, Normalized Standard Deviation, Wilmott-D Score, Spatial Correlation, S score and Yule-Kendall index. This analysis allowed to build a weighted multi-model ensemble (ENS) through model ranking based on their performances against observed rainfall. The analysis of historical simulations revealed that the capacity of RCM models to reproduce local precipitation, such as the precipitation at small scales in regions with complex-orography, is still a bit limited, as also reported by Mascaro et al. (2018). KNMI2, KNMI1 and CLM4 resulted the best performing models. Future climate change signals predict a general decrease of mean precipitation up to -20 / -25% in particular for the southwest area, while in summer and autumn a small increase of precipitations is projected for the east and south east regions. An increase of precipitation events above 20 mm and extreme events is projected, with different patterns: events above 20 mm regard mainly the north-west and the Campidano plain, while an increase in extreme events is more pronounced in the east side and in the southern capes, with values of +30%.

The SWAT model was firstly run using observed rainfall, calibrated and validated against observed streamflow; subsequently SWAT was forced by the EURO-CORDEX models for the analysis of future hydrological variables. A general disagreement between the performances of climate models and SWAT-climate models' chain was noticed: in fact, models that showed best performances in reproducing precipitation patterns and seasonal variability not always showed the ability to force SWAT model to reproduce observed outflow and vice-versa. This reflects well the uncertainty caused by low-quality observations, SWAT model implementation/calibration and in Euro- CORDEX models' capabilities. Future projections highlight a general decrease in streamflow discharge, which

is not very significant due to the presence of continuous wastewater inflows from urban areas. The decrease of overland flow is pronounced if we take in consideration surface runoff that is predicted to be very high for the period 2033-2060. However, the reliability of these projections is low; more accurate predictions can only be reached by reducing the incoming uncertainties in the hydro-climate model chain, which could hence, become a very powerful tool for water and basin management decision-making.

Bibliography

Alpert P et al (2002) The paradoxical increase of Mediterranean extreme daily rainfall in spite of decrease in total values. Geophys Res Lett 29(11):311–314Aristeidis G. et al 2018

Arnold, J.G., Srinivasan, R., Muttiah, R.S., Williams, J.R., 1998. Large area hydrologic modeling and assessment — Part 1: model development. J. Am. Water Resour. Assoc. 34, 73–89

Casanueva, A., Kotlarski, S., Herrera, S., Fernández, J., Gutiérrez, J. M., Boberg, F., Colette, A., Christensen, O. B., Goergen, K., Jacob, D., Keuler, K., Nikulin, G., Teichmann, C., and Vautard, R.: Daily precipitation statistics in a EURO-CORDEX RCM ensemble: added value of raw and bias-corrected high-resolution simulations, Clim. Dynam., 47, 719–737, 2016

Dubrovsky M., Hayes M., Duce P., Trnka M., Svoboda M., Zara P., 2013; Multi-GCM projections of future drought and climate variability indicators for the Mediterranean region. Reg Environ Change (2014) 14:1907–1919. DOI 10.1007/s10113-013-0562-z

Gao X, Pal JS, Giorgi F (2006) Projected changes in mean and extreme precipitation over the Mediterranean region from a high resolution double nested RCM simulation. Geophys Res Lett 33:L03706. doi:10.1029/2005GL024954

Christensen JH, Kjellström E, Giorgi F, et al (2010) Weight assignment in regional climate models. Clim Res 44:179–194. doi: 10.3354/cr00916

Ferro CAT, Hannachi A, Stephenson DB (2005) Simple nonparametric techniques for exploring changing probability distributions of weather. J Clim 18:4344–4354. doi: 10.1175/JCLI3518.1

Giorgi F, Jones C, Asrar GR (2009) Addressing climate information needs at the regional level: The CORDEX framework. WMO Bull 58:175–183

Jacob, D., et al. (2001), A comprehensive model inter-comparison study investigating the water budget during the BALTEX-PIDCAP period, Meteorol. Atmos. Phys., 77(1–4), 19–43, doi:10.1007/s007030170015.

Katragkou E, García-Díez M, Vautard R, et al (2015) Regional climate hindcast simulations within EURO-CORDEX: evaluation of a WRF multi-physics ensemble. Geosci Model Dev 8:603–618. doi: 10.5194/gmd-8-603-2015

Kotlarski S, Keuler K, Christensen OB, et al (2014) Regional climate modeling on European scales: a joint standard evaluation of the EURO-CORDEX RCM ensemble. Geosci Model Dev 7:1297–1333. doi: 10.5194/gmd-7-1297-2014

Mascaro, G., Viola, F., Deidda, R., 2018. Evaluation of precipitation from EURO-CORDEXregional climate simulations in a small-scale mediterranean site. J. Geophys. Res.: Atmos. 123 (3), 1604–1625.

Nerantzaki, S.D., G.V. Giannakis, N.P. Nikolaidis, I. Zacharias, G.P. Karatzas and I.A. Sibetherous, 2016. Assessing the impact of climate change on sediment loads in a large Mediterranean watershed. Soil Science, volume 181(7). 306–314. DOI:10.1097/SS.0000000000000164

Perkins SE, Pitman AJ, Holbrook NJ, McAneney J (2007) Evaluation of the AR4 Climate Models' Simulated Daily Maximum Temperature, Minimum Temperature, and Precipitation over Australia Using Probability Density Functions. J Clim 20:4356–4376. doi: 10.1175/JCLI4253.1

Perra, E., M. Piras, R. Deidda, C. Paniconi, G. Mascaro, E.R. Vivoni, P. Cau, P.A. Marras, R. Ludwig and S. Meyer, 2018. Multimodel assessment of climate change-induced hydrologic impacts for a Mediterranean catchment. Hydrology and Earth System Science. Volume: 22(7). 4125-4143. DOI: 10.5194/hess-22-4125-2018

Piras M., G. Mascaro, R. Deidda, E.R. Vivoni, P. Cau, P.A. Marras, S. Meyer and R. Ludwig (2015), Assessment of climate

change effects in a Mediterranean basin with different hydrologic models. In:"SWAT 2015 Book of abstracts", p. 123, International Soil & Water Assessment Tool Conference, Pula (CA), Italy, 24-26 June 2015

Rajczak J, Pall P, Schär C (2013) Projections of extreme precipitation events in regional climate simulations for Europe and the Alpine Region. J Geophys Atmos 118:3610–3626. doi:10.1002/jgrd.50297

Riahi K, Rao S, Krey V, et al (2011) RCP 8.5—A scenario of comparatively high greenhouse gas emissions. Clim Change 109:33–57. doi: 10.1007/s10584-011-0149-y

Rockel B, Will A, Hense A (2008) The regional climate model COSMO-CLM (CCLM). Meteorol Z 17:347–348. doi:10.1127/0941-2948/2008/0309

Samuelsson P, Jones CG, Willén U, Ullerstig A, Gollvik S, Hansson ULF, Jansson C, Kjellström E, Nikulin G, Wyser K (2011) The Rossby Centre Regional Climate Model RCA3: model description and performance. Tellus Ser A 63(1):4–23

Sánchez E, Gallardo C, Gaertner M, Arribas A, Castro M (2004) Future climate extreme events in the Mediterranean simulated by a regional climate model: a frst approach. Global Planet Change 44(1–4):163–180. doi:10.1016/j.gloplacha.2004.06.010

Sillmann J, Kharin VV, Zwiers FW, Zhang X, Bronaugh D (2013b). Climate extremes indices in the CMIP5 multimodel ensemble: part 2. Future climate projections. J Geophys Res Atmos 118:2473–2493. doi:10.1002/jgrd.50188

Soares PMM, Cardoso RM, Ferreira JJ, Miranda PMA (2015) Climate change impact on Portuguese precipitation: ENSEMBLES regional climate model results. Clim Dyn 45:1771–1787. doi:10.1007/s00382-014-2432-x

Soares PMM, Cardoso RM, Lima DCA, Miranda PMA (2017) Future precipitation in Portugal: high-resolution projections using WRF model and EURO-CORDEX multi-model ensembles. Clim Dyn 49:2503–2530. doi: 10.1007/s00382-016-3455-2

Von Trentini F., Leduc M., Ludwing R., 2019 Assessing natural variability in RCM signals: comparison of a multi model EURO-CORDEX ensemble with a 50-member single model large ensemble

Willmott CJ, Robeson SM, Matsuura K (2012) A refined index of model performance. Int J Climatol 32:2088–2094. doi: 10.1002/joc.2419

Chapter 5: First simulations of metal dispersion processes in Rio San Giorgio watershed

Introduction

This chapter presents simulations of the Zn and Pb transport in surface waters, performed with a SWAT model coupled with SWAT-HM module. Before analyzing the metals fate and transport simulation, an analysis of the hydrological cycle of the Rio San Giorgio basin has been done for the historical period.

Results of the numerical models

The simulations of SWAT-HM were run at monthly and daily time-steps for the historical period, while the future projections were run at monthly time-steps only. The historical period goes from 2001 to 2016, with 2 years of warm-up for the model (warm-up timespan 1999-2000 will be not considered for the final output in this work). Warm-up period is an initial time range in which the simulation is run before producing the output, to get into conditions that are typical of normal running conditions in the simulation of the watershed.

Projections of future scenarios were carried out using the climate models, described in the previous chapter. These provided daily records of rainfall and temperatures for the period 2031-2060, 2 years (2031-2032) of which covered the warm-up of SWAT-HM. Rio Mannu of Fluminimaggiore basin was previously used for model calibration; only Rio San Giorgio's catchment will be considered in the discussion hereafter.

Water balance of the Rio San Giorgio.

Water balance was calculated for the Rio San Giorgio basin at monthly time-steps. The annual cycle is resumed in the following figure (FIGURE 72) which represents the mean monthly value of the water balance terms for the period 1981-2016.

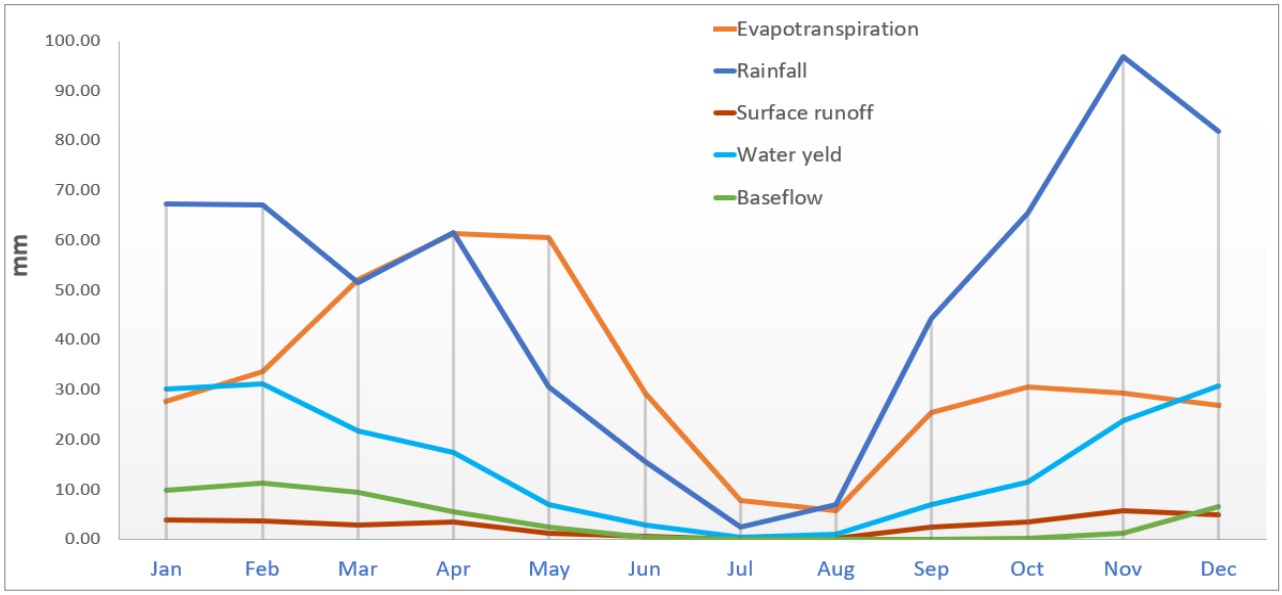

Figure 72 - Water balance terms for the Rio San Giorgio basin

Mean annual rainfall for the Rio San Giorgio basin is 591 mm (TABLE 18), 66% of which is lost through evapotranspiration that is on average 390 mm, and 6% through surface runoff at around 32 mm. Averaged baseflow is 47 mm with water yield, which is the amount of water effectively transformed in streamflow, accounting for the channel transmission losses, is 185 mm.

Table 18 - Monthly water balance and annual averages in Rio San Giorgio basin

	Rainfall	ET	Surf. runoff	Water yield	Baseflow
Jan	67.37	27.79	3.81	30.14	9.88
Feb	67.06	33.64	3.66	31.16	11.28
Mar	51.50	52.09	2.79	21.78	9.54
Apr	61.54	61.25	3.52	17.35	5.61
May	30.52	60.43	1.32	6.93	2.39
Jun	15.56	29.42	0.72	2.82	0.46
Jul	2.37	7.86	0.06	0.52	0.03
Aug	7.03	5.72	0.31	1.09	0.00
Sep	44.34	25.46	2.42	6.98	0.04
Oct	65.48	30.59	3.59	11.47	0.14
Nov	96.92	29.42	5.67	23.89	1.24
Dec	81.94	26.92	4.87	30.72	6.52
Total	**591.62**	**390.60**	**32.73**	**184.85**	**47.13**

Streamflow (FIGURE 73) has typically low regimes, with mean discharge ranging from 0.40-0.45 m^3/s in winter to less than 0.05 m^3/s in August. Usually, due to the scarce or total absence of precipitation,

flow in summer is mainly from urban wastewater point sources, described in the SWAT model setup section, that release respectively 2450 m^3/day and 300 m^3/day (around 0.032 m^3/s).

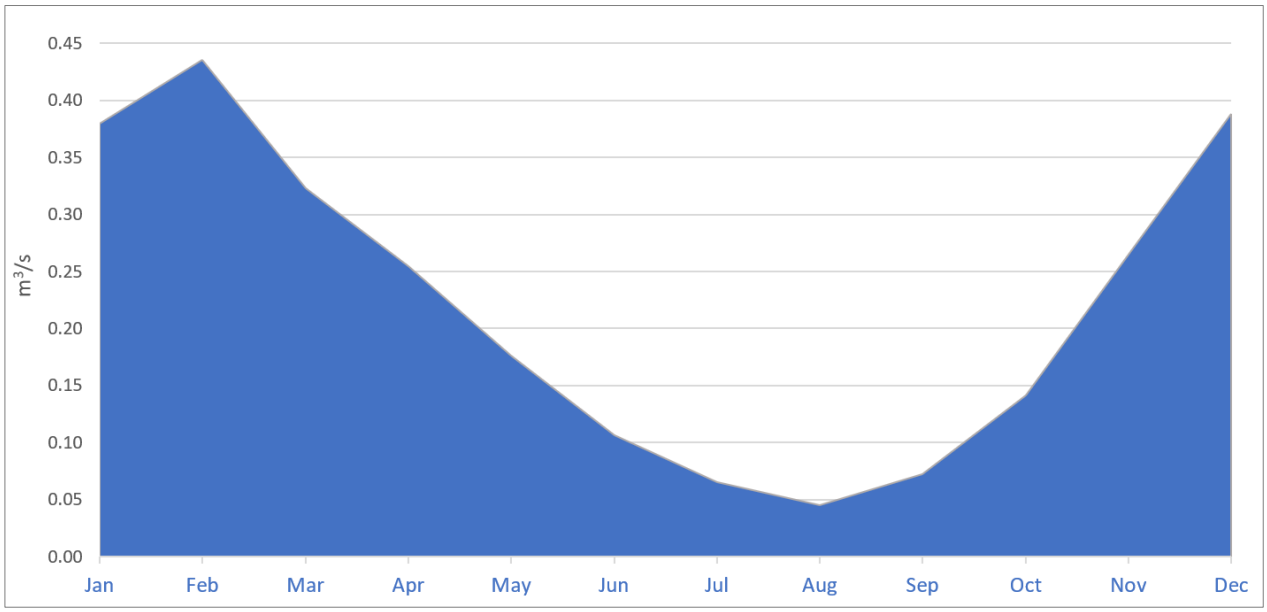

Figure 73 - Monthly mean streamflow (m^3/s) at Rio San Giorgio outlet calculated from 1981 to 2016

FIGURE 74 shows the streamflow response of the catchment to rainfall at daily time-steps for the period January 2001 – December 2006. The response is rapid, as indicated by the high steepness of the flow curve descent after significative rainfall events.

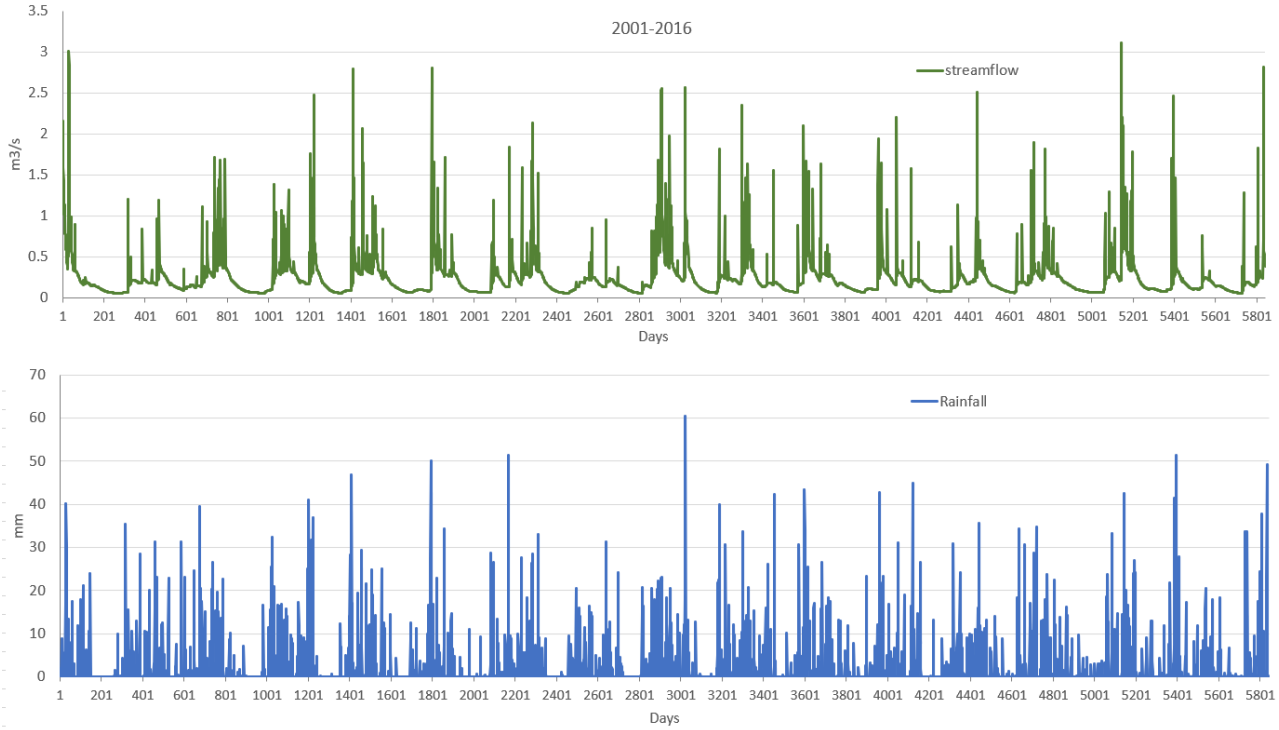

Figure 74 – Daily streamflow (green curve) and rainfall values (blue bars) of the Rio San Giorgio from 2001 to 2016

FIGURE 75 shows yearly mean outflow from 1981 to 2016 is 0,22 m3/s, a minimum mean discharge of 0.09 m3/s in 1985 and a maximum mean discharge of 0.36 m3/s in 1986 can be observed. The simulation was conducted assuming constant values of wastewater discharge over time.

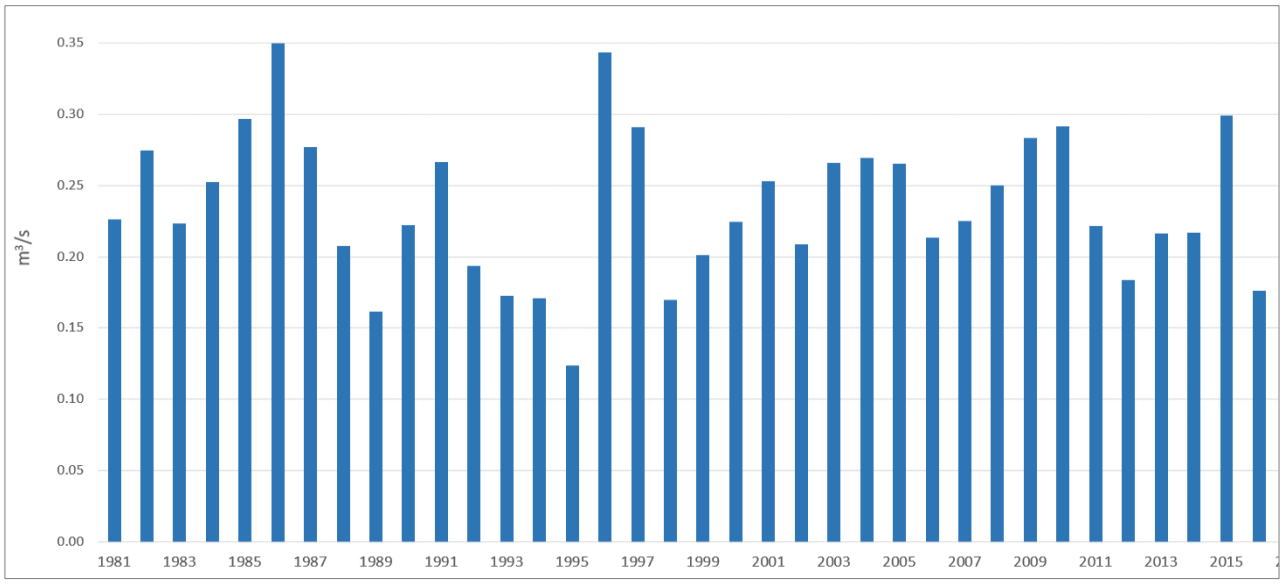

Figure 75 - Yearly mean flow (1981-2017) at Rio San Giorgio outlet

Heavy metal transport simulations

The SWAT-HM simulation was calibrated against measured concentration of Zn and Pb in stream water, in different points of the watershed. However, as mentioned in Chapter 2, the calibration process is not satisfactory and needs to be improved with further data collection. Data such as continuous and regular sampling of the stream water, loads estimations in different hydrological conditions and streamflow measurements could provide valuable information to the model, and improve its reliability. The results that will be described hereafter, show an overestimation of the metal loads when intense precipitation and high streamflow occur, while displaying an underestimation in dry periods of low flow. Hence, in a future phase, the model calibration will be possibly improved.

The parameters simulated by SWAT-HM that will be described are the dissolved metals load and total metal load (dissolved + particulate) expressed in kg per day, and the sediment loads expressed in tons per day.

Historical simulations

This paragraph illustrates results from Zn and Pb simulations for the historical period from 2001 to 2016. **FIGURE 76** shows the simulation with daily resolution of Zn load (Kg/day). Zn load is compared to rainfall, streamflow and sediment loads simulated at the Rio San Giorgio's outlet.

Figure 76 - Comparison between rainfall, streamflow, total load of Zn, dissolved Zn and sediment load at the Rio San Giorgio outlet (daily time-step)

Total Zn load has an average of 70 kg/day with mean discharge of 0,23 m^3/s. Total Zn load attains a maximum value of 4697 kg/day in November 2005 for a simulated streamflow of 2.8 m^3/s, suggesting there is a large overestimation of the peak loads. Minimum values of total load are below

1 mg/day for streamflow values ranging from 0.059 m^3/s to 0.065 m^3/s, with large underestimation. Dissolved Zn load is, in average, 0.17 kg/day, with peaks of 30 kg/day and values below 1 kg for big part of the simulation period. The minimum values of dissolved Zn are below 1 mg/day for streamflow of around 0.05 m^3/s, suggesting that the model is not capable of reproducing real conditions, in which, for this flow regime, loads of 5 kg/day were reported by De Giudici et al. (2017). It is worth noting that dissolved and total Zn loads are strictly related to the watershed rapid response to rainfall and sediment transport, with a strong correspondence of the peaks. Interesting for assessing the temporal evolution of the pollutant dispersal processes, FIGURE 76 indicates a very clear decreasing trend for dissolved Zn in time.

Zn annual loads for the historical period are shown in FIGURE 77. Loads show wide variations, ranging from peaks above 40 tons in 2001 and 2003 to a minimum load of around 10 tons in 2012. The average yearly load is ~26 tons/year.

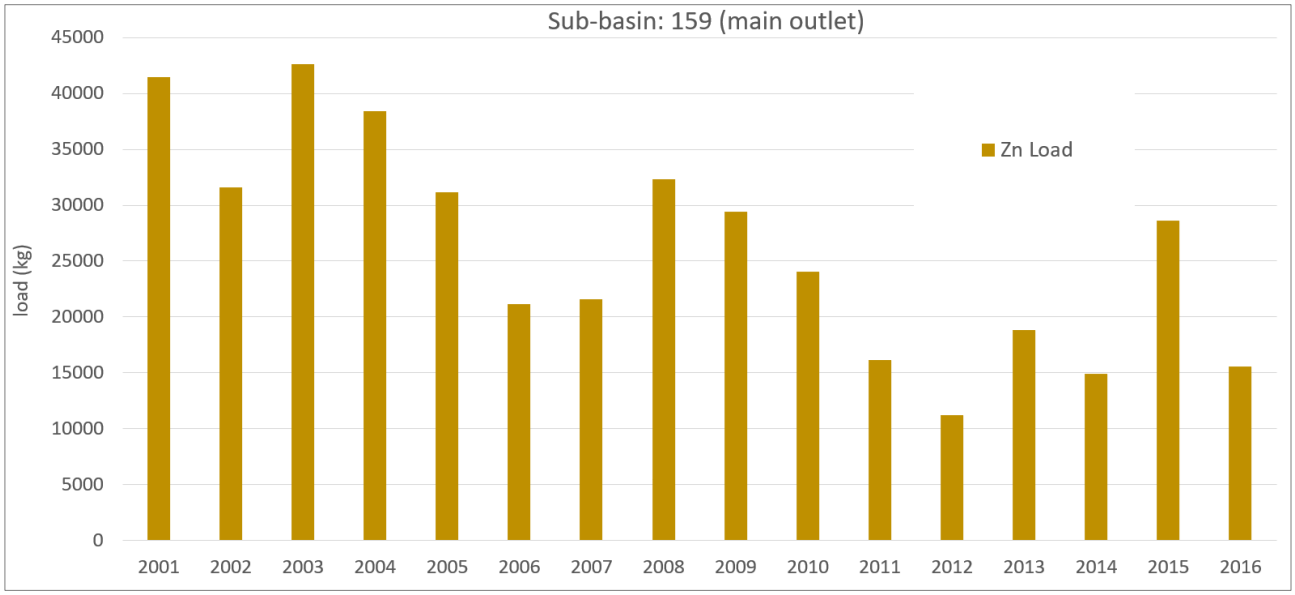

Figure 77 - Annual loads of Zn at the Rio San Giorgio outlet

FIGURE 78 illustrates the simulation of the Pb load at daily resolution for the historical period. Pb loads have values significantly lower than the ones observed for Zn. Dissolved and total loads do not show the decreasing trend observed in Zn simulations. Pb total load has an average of 23.95 kg/day and a maximum value of 1649 kg/day simulated in April 2009 in correspondence to an extreme rainfall event. Minimum values of around 2 mg/day for low flow days (~0.05 m^3/s) were obtained by simulations. As already argued for Zn, the results indicate that the adopted model largely

underestimates metal loads in occurrence of low flow regimes, and likely overestimates Pb load for high flow regimes.

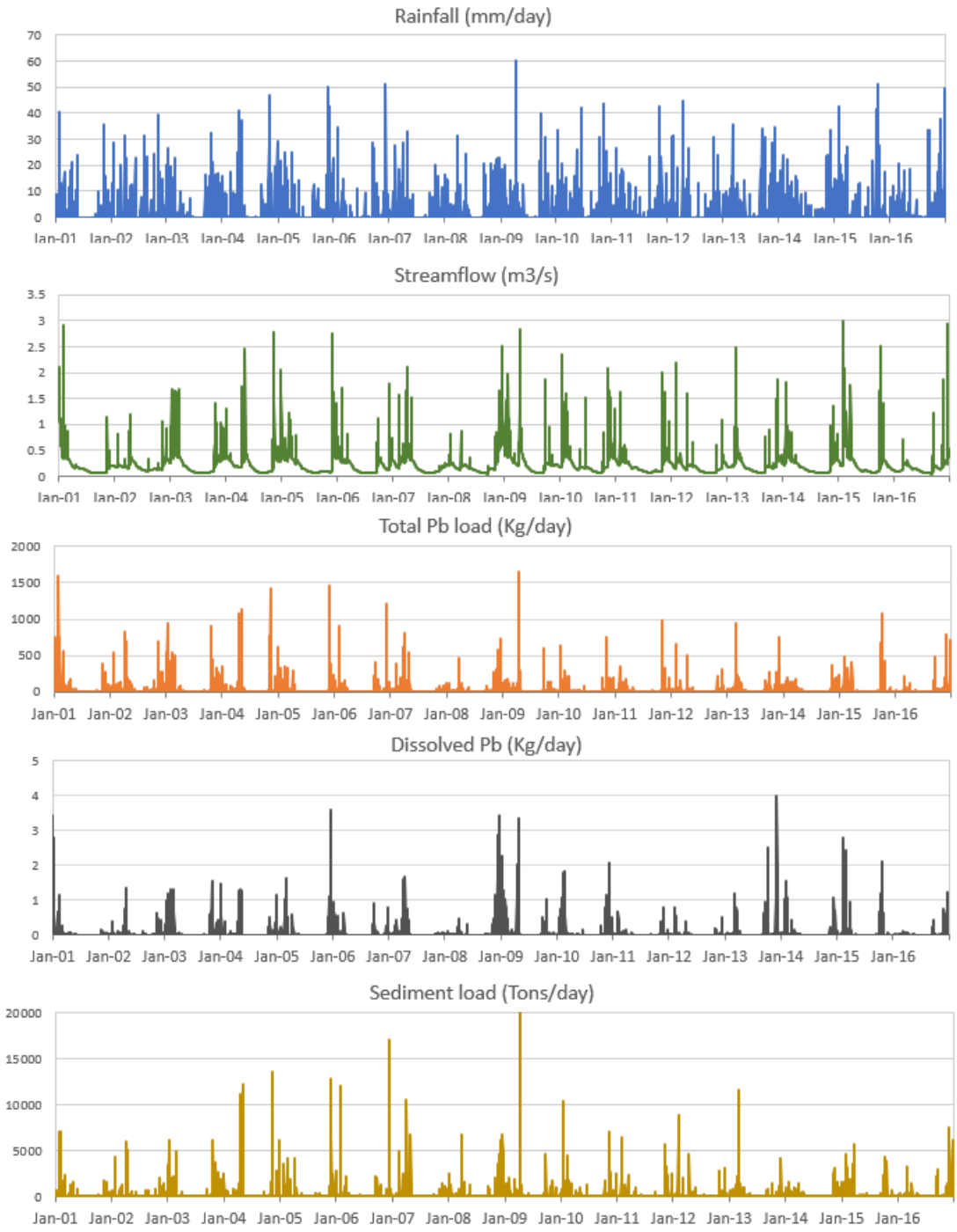

Figure 78 - Comparison between rainfall, streamflow, total load of Pb, dissolved Pb and sediment load at the Rio San Giorgio outlet (daily time-step)

Pb yearly total loads (FIGURE 79) show less variations, ranging from a maximum value around 15 tons in 2003 to a minimum of around 4 tons in 2012, which was a very dry year, with an average of 8.7 tons/year.

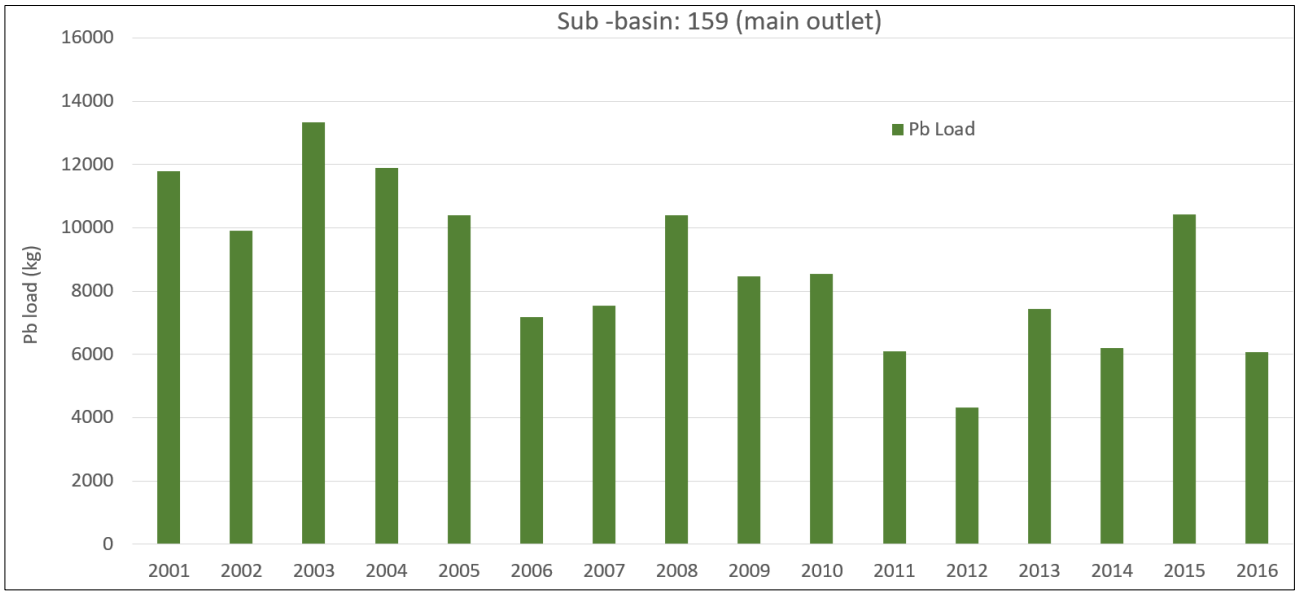

Figure 79 - Annual loads of Pb at the Rio San Giorgio outlet

Historical simulations confirm that the calibration of SWAT-HM should be improved to reproduce the metal balance of the watershed.

Future projections

Simulations of metal loads for the future period (2033-2060) were run forcing SWAT-HM with the different climate models analyzed in the previous chapter. From now on, different combinations of SWAT-HM and climate models will be simplified as HM-acronym of the climate model (e.g. combination between SWAT-HM and CLM1 climate model for Zinc will be Zn-HM-CLM1). The Zn/Pb-HM-ENS is the resulting load obtained by weighting the different outputs, merged in one signal using the climate model's weights (TABLE 19). Only total load at the watershed outlet will be discussed for future simulations.

Table 19 - Weights of the different combinations between SWAT-HM and climate models, used to build a weighted output (HM-ENS)

HM-CLM1	HM-CLM3	HM-CLM4	HM-DMI	HM-KNMI1	HM-MPI	HM-SMHI1	HM-SMHI3	HM-SMHI4
0.16	0.07	0.22	0.10	0.29	0.02	0.08	0.03	0.03

FIGURE 80 represents Zn-HM-ENS obtained weighting the total Zn load simulated by the different HM combinations for the future period at the monthly time-step. The mean simulated load is ~2500 kg/month, showing a small increase in comparison to the historical period, that was ~2100 kg/month. A minimum of around 0.5 kg is simulated in July 2040, for which a very dry regime of precipitation is projected. The highest peak of load values is projected for the first year of simulation (18659 kg), while the peak loads for the rest of the simulation range from 8000 and 11000 kg, mostly for the winter months.

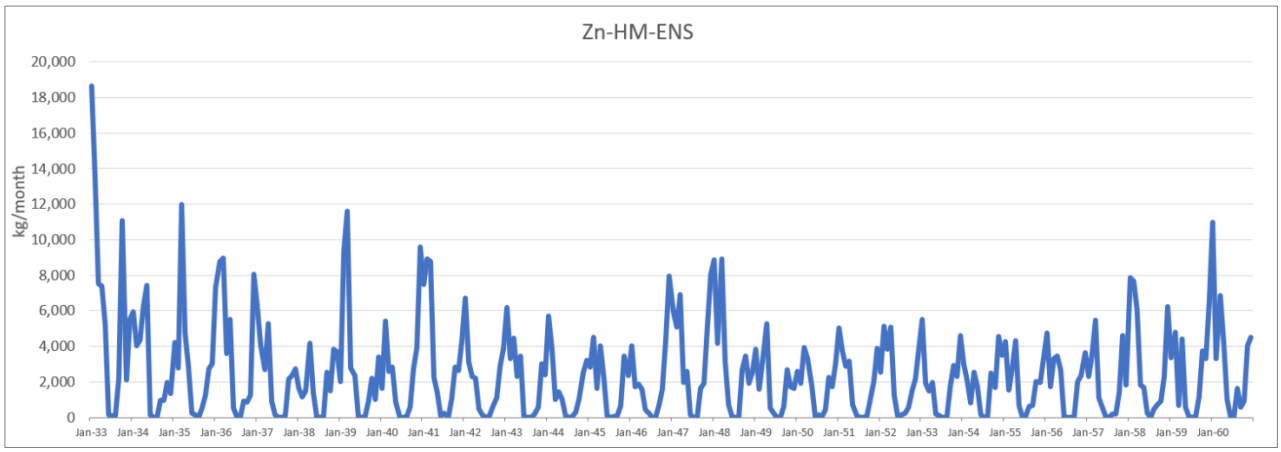

Figure 80 - Zn monthly load simulated in Rio San Giorgio's outlet (Zn-HM-ENS) obtained by weighting the outputs of the different HM-climate models combinations.

The comparison between the Zn-HM-ENS signal and its single components is shown in FIGURE 81. The different precipitation changes projected by the different climate models are well reflected in the monthly Zn load. Some models, such as HM-SMH1 and HM-MPI, predict an average load around 1500 kg/month (Zn-HM-CLM1 and Zn-HM-CLM3) while Zn-SMHI4 estimates an average load of 3500 kg/month.

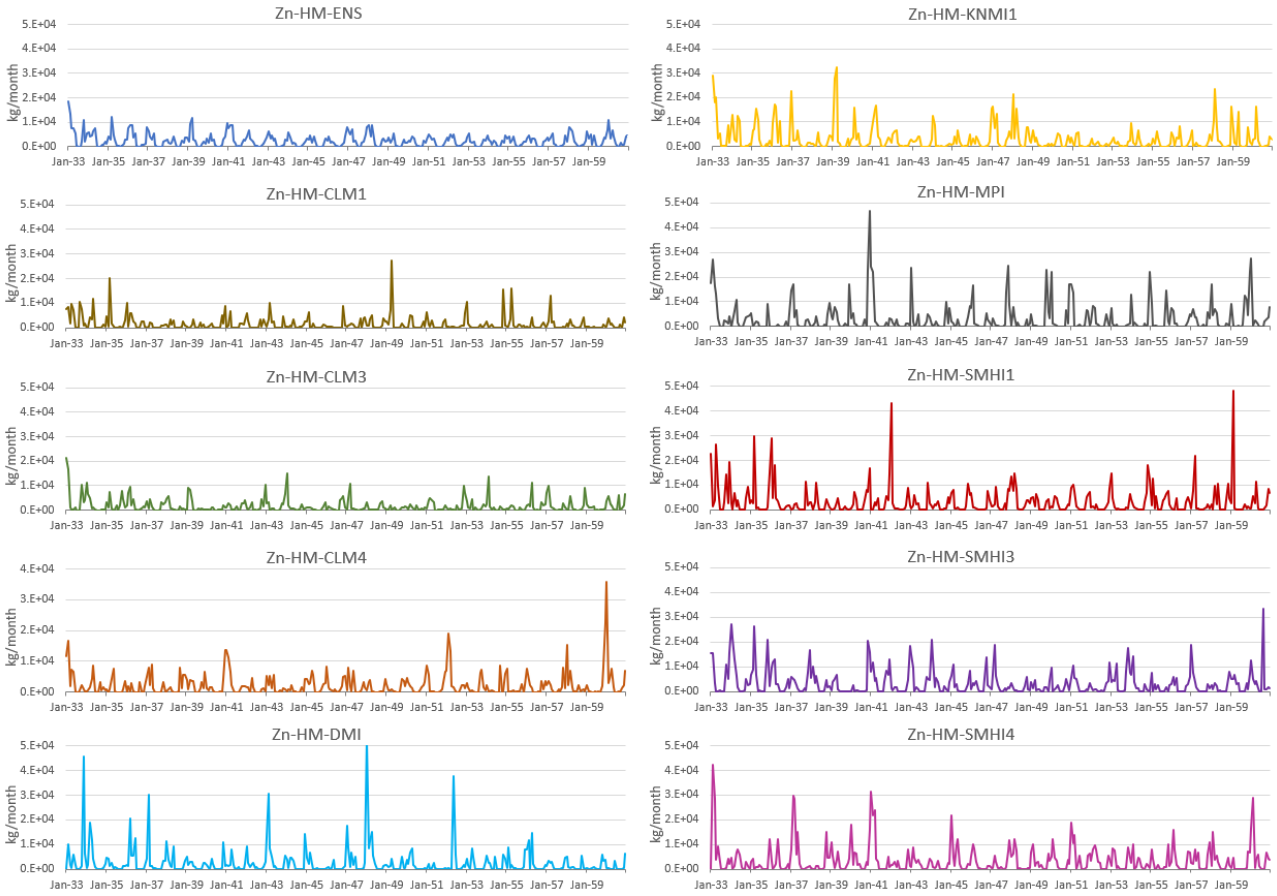

Figure 81 - Monthly Zn load for period 2033-2060 resulting from the combination between ENS and SWAT-HM.

The yearly variation of load predicted by the Zn-HM models (FIGURE 82) delineates the different trends. The Zn-HM-ENS project a mean load around 30 tons/year, which is higher than the mean load predicted for the historical period (26 tons/year). A small decrease of the loads well notable in Zn-HM-ENS from 2049 was followed by a significant increase, from 2057 to 2060. In fact, the single signals of the most influential models within the Zn-HM-ENS, namely Zn-HM-KNMI1 and Zn-HM-CLM4, show some extremes in the last years of the simulation. Zn-HM-MPI, Zn-SMHI1 and Zn-HM-SMHI3 vary in a similar range of annual loads between 20 tons and 60 tons per year.

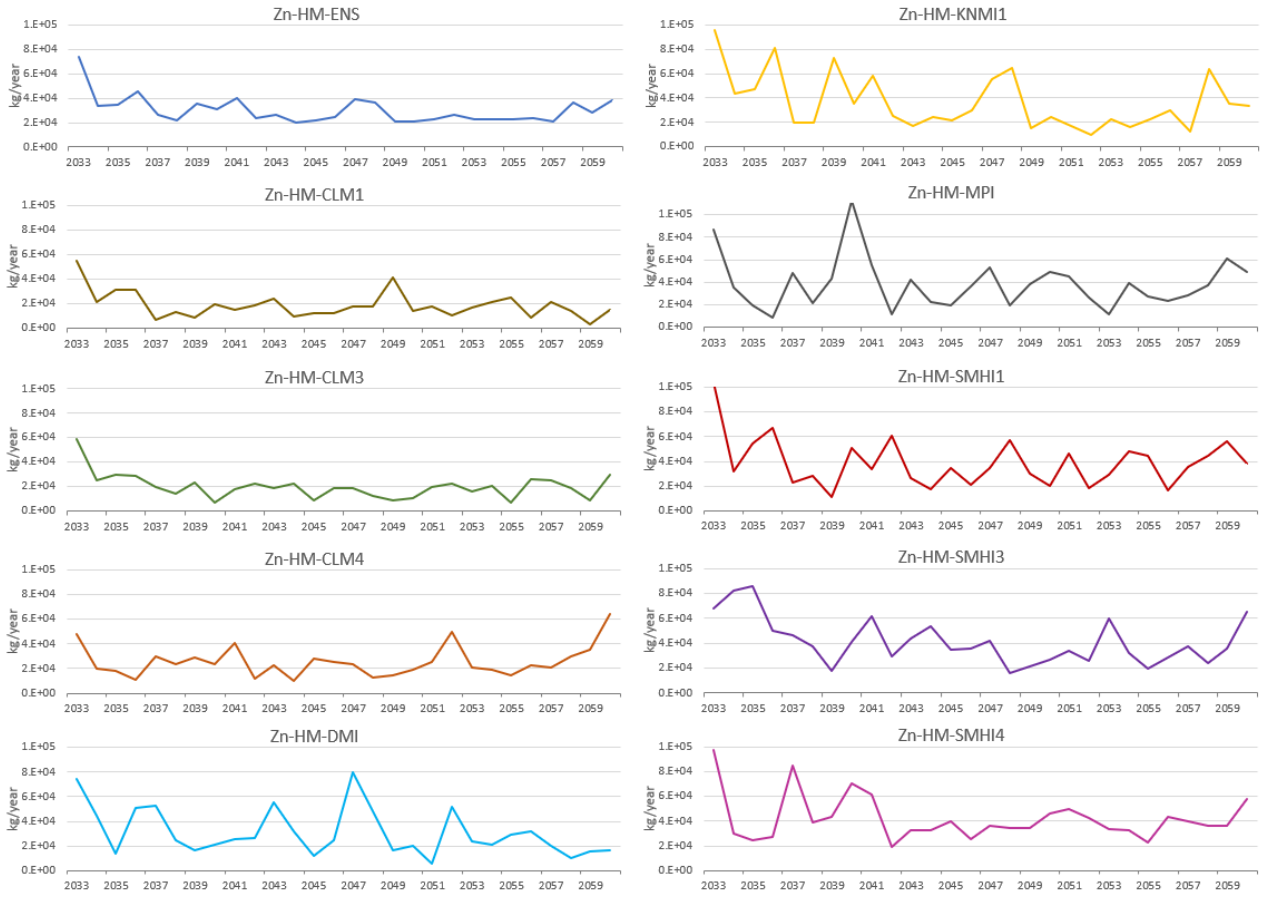

Figure 82 - Zn total yearly load simulated in Rio San Giorgio's outlet using different climate forcing models by SWAT-HM

Pb monthly load predicted by the Pb-HM-ENS at the Rio San Giorgio outlet for the future period 2033-2060 is shown in **FIGURE 83**. The mean estimated load is 475 kg/month, with maximum peaks above 2500 kg/month and minimum values below 1 kg/month in very dry periods. The mean monthly load is significantly lower compared with the historical simulation (~800 kg/month).

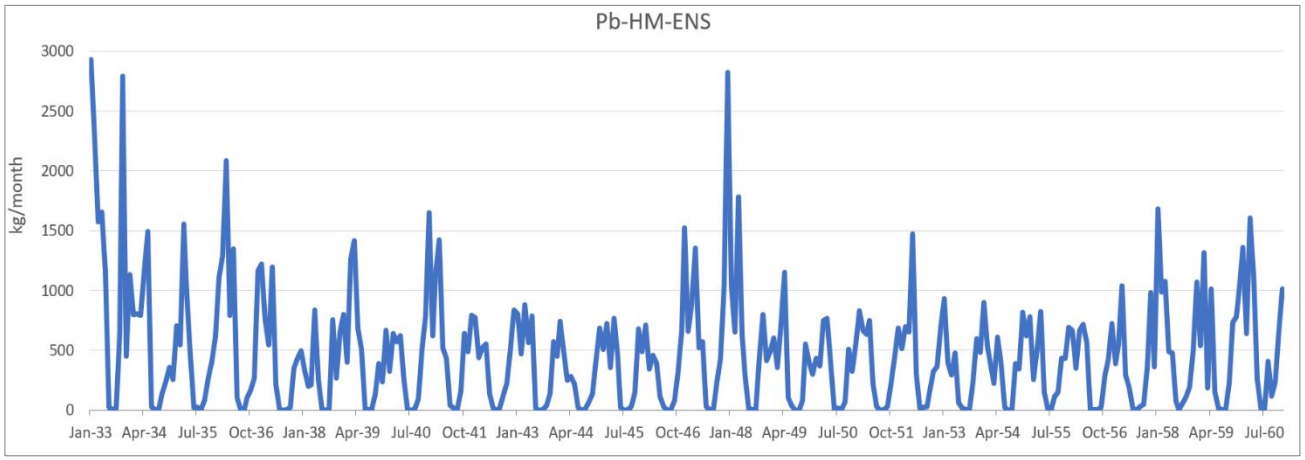

Figure 83 - Pb monthly load (Pb-HM-ENS) simulated in Rio San Giorgio's outlet obtained by weighting the outputs of the different HM-climate models combinations.

To better understand the Pb-HM-ENS curve, a comparison between the different HM models is depicted in FIGURE 84. Some models, such as Pb-HM-CLM1, Pb-HM-CLM3 and Pb-HM-CLM4 keep almost the same trend throughout the simulation, below 5000 kg/month, with some increase at the end of the period. The rest of the models predict higher peaks related to extreme precipitation events, such as Pb-HM-MPI and Pb-HM-DMI.

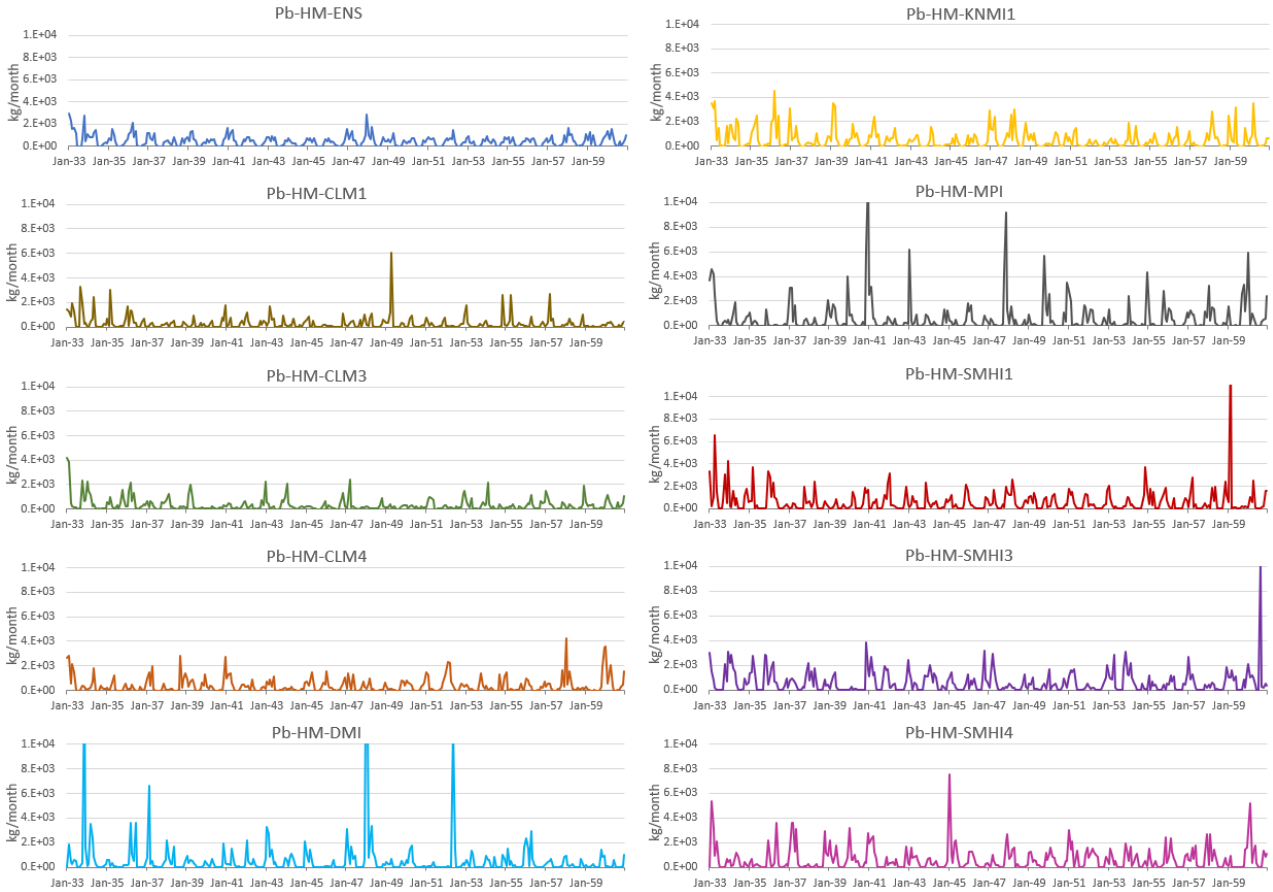

Figure 84 - Pb total yearly load simulated in Rio San Giorgio's outlet using different climate forcing models by SWAT-HM

FIGURE 85 illustrates the general trend of the Pb yearly load for the future simulation, delineating the differences between the combination of HM/climate models. Despite the extremes, the mean Pb load is 5700 kg/year against the 8700 kg/year simulated for the historical period. It is notable how the high peaks, related to the increase of extreme rainfalls projected for the future, strongly influence the total yearly load, in particular for Pb-HM-DMI, Pb-HM-KNMI1, Pb-HM-MPI and Pb-HM-SMHI1, which show extreme loads of 25 tons/year.

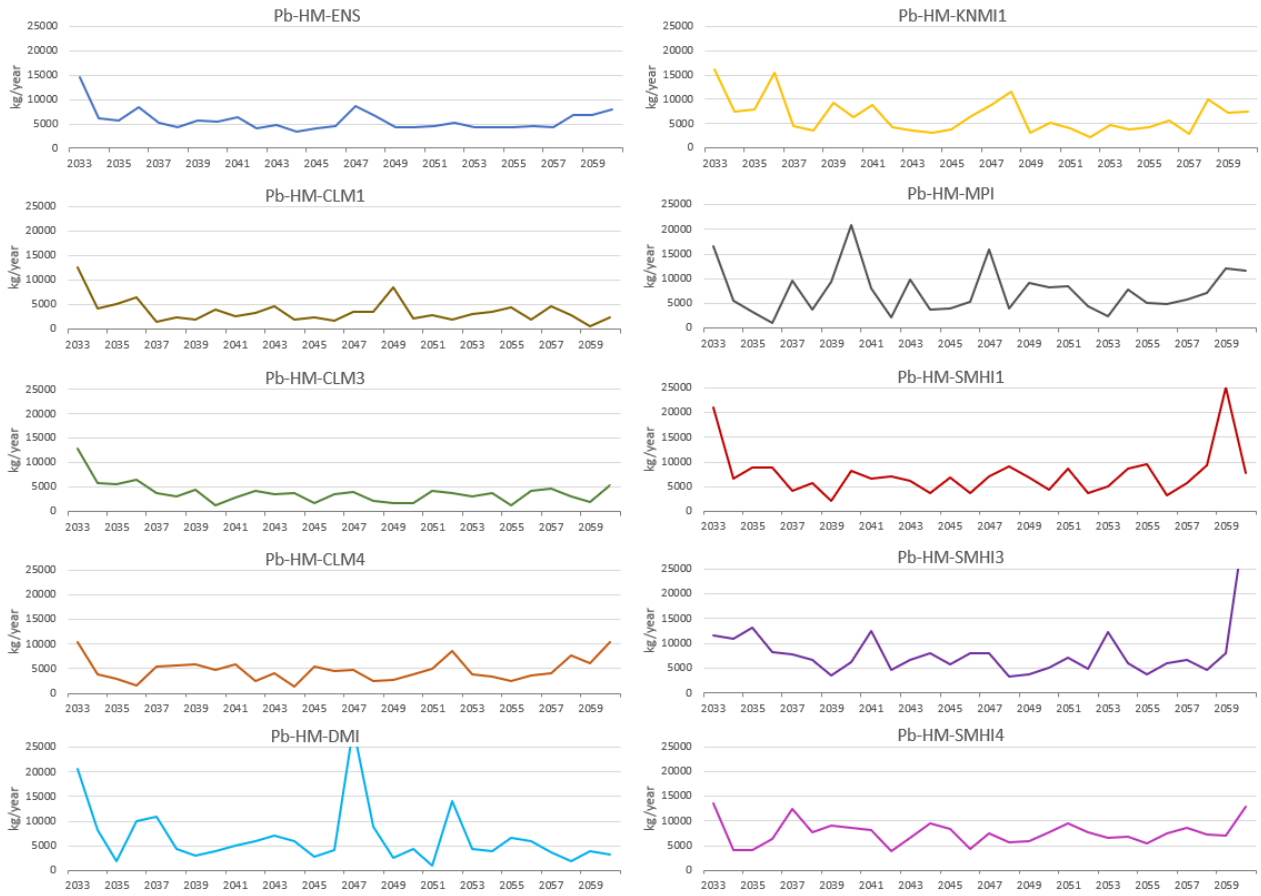

Figure 85 - Pb yearly load simulated in Rio San Giorgio's outlet using different climate forcing models by SWAT-HM

It is worth noting that Zn and Pb loads show opposite trends in temporal projections. Compared with historical simulation, the Zn load tends to augment, due to the precipitation extremes predicted by the climate models, while for Pb, despite the precipitation extremes, a significant general diminution is projected.

Waste removal scenarios

In order to assess different management scenarios of Rio San Giorgio, simulations were conducted to evaluate the impact of metal dispersion from some of the tailings in the in Rio San Giorgio valley. Specifically, the aim is to conduct first tests of the capability of HM simulations to be used as a decisional tool for assessing the impact of individual waste bodies and the priorities for reclamation. FIGURE 86 represents the monthly load of total Zn based on HM-ENS at the Rio San Giorgio's outlet for the period 2033-2060 under two different conditions: the blue curve represents the Zn load if no changes occur on the mine wastes, while the orange curve represents the Zn load assuming

removal of the whole Fanghi Rossi waste. The latter has a volume of around 2 million of cubic meters and a mean Zn concentration of 8%. This waste is considered the major source of water pollution in the watershed (Cidu & Fanfani, 2002; De Giudici et al. 2017). **FIGURE 86** shows that the estimated decrease of total Zn load attains 40% after the waste removal. that is a considerably high percentage.

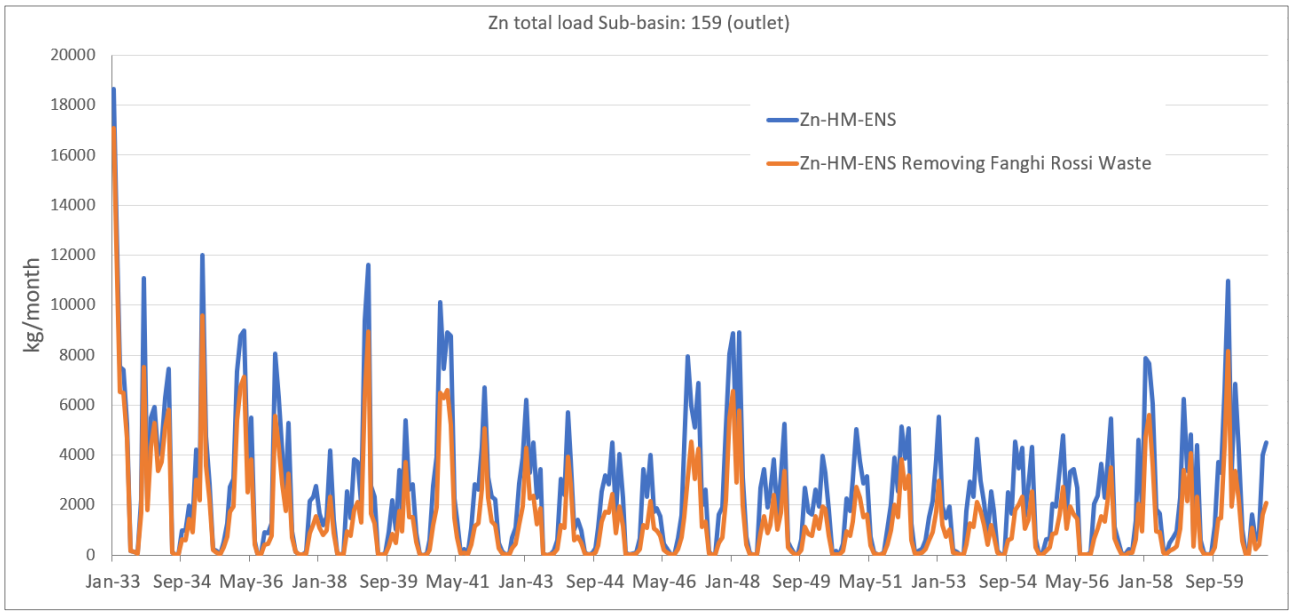

Figure 86 - Simulation of the effect of Fanghi Rossi waste removal on the total Zn load at the Rio San Giorgio's outlet (2033-2060)

Figure 37 shows the decrease of Pb load after removal of Fanghi Rossi. In the simulated scenario, the environmental benefit is considerably high, with a decrease of around 34%.

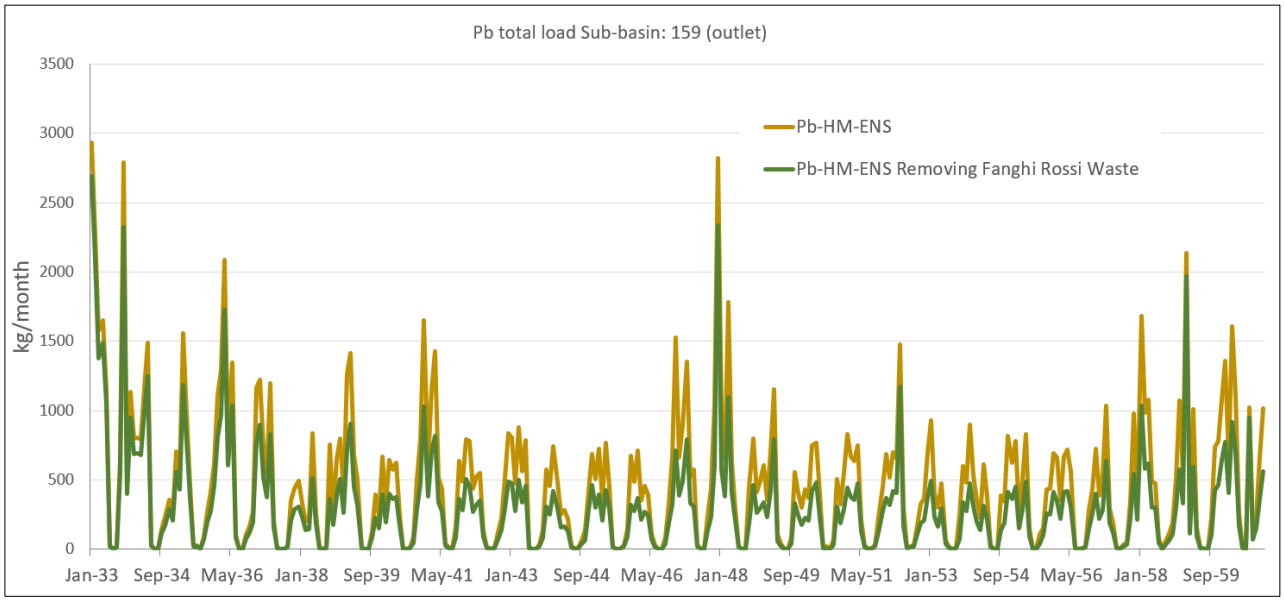

Figure 87 - Simulation of the effect of Fanghi Rossi waste removal on the total Pb load at the Rio San Giorgio's outlet (2033-2060)

A second scenario (FIGURE 88) simulates the changes in load of Pb for the period 2033-2060 assuming removal of Campo Pisano mine waste. The red line represents the Pb load estimated by the HM-ENS at the Rio San Giorgio outlet with no changes in the watershed, the green line sows the predicted Pb loads after removal of Campo Pisano waste. The reduction in Pb load estimated by the Pb-HM-ENS in 30 years would be approximatively -35%.

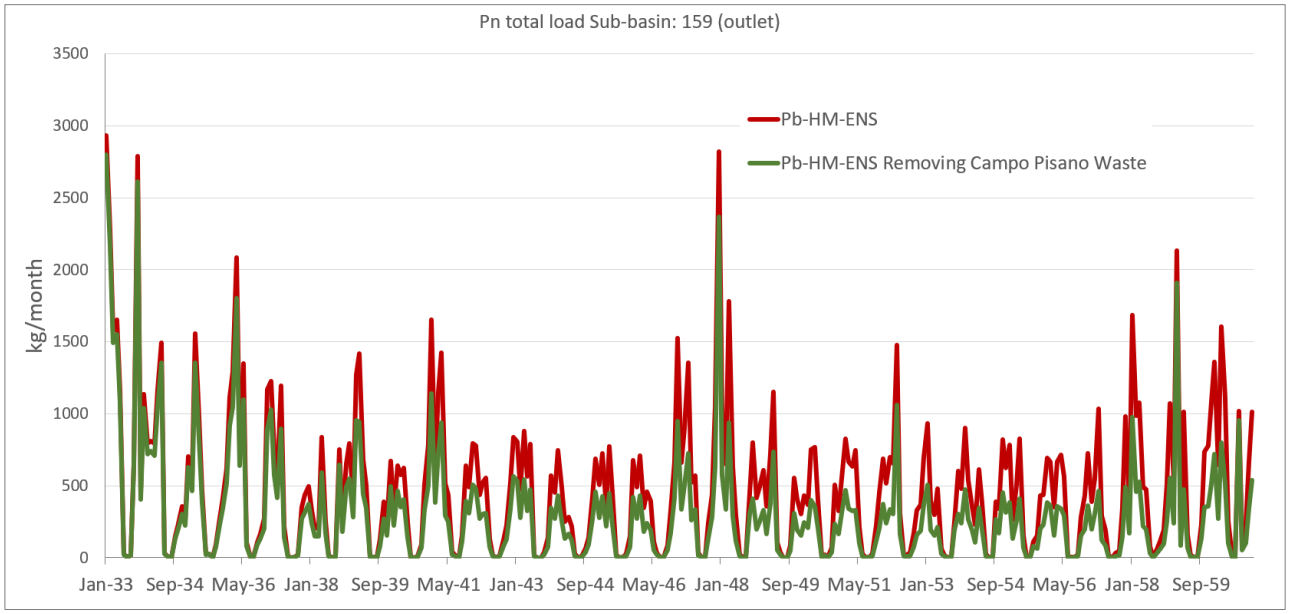

Figure 88 - Simulation of the effect of Campo Pisano waste removal on the total Pb load at the Rio San Giorgio's outlet

The effect Campo Pisano waste removal is less pronounced for Zn load (**FIGURE 89)** that shows a diminution of around 9% in 30 years.

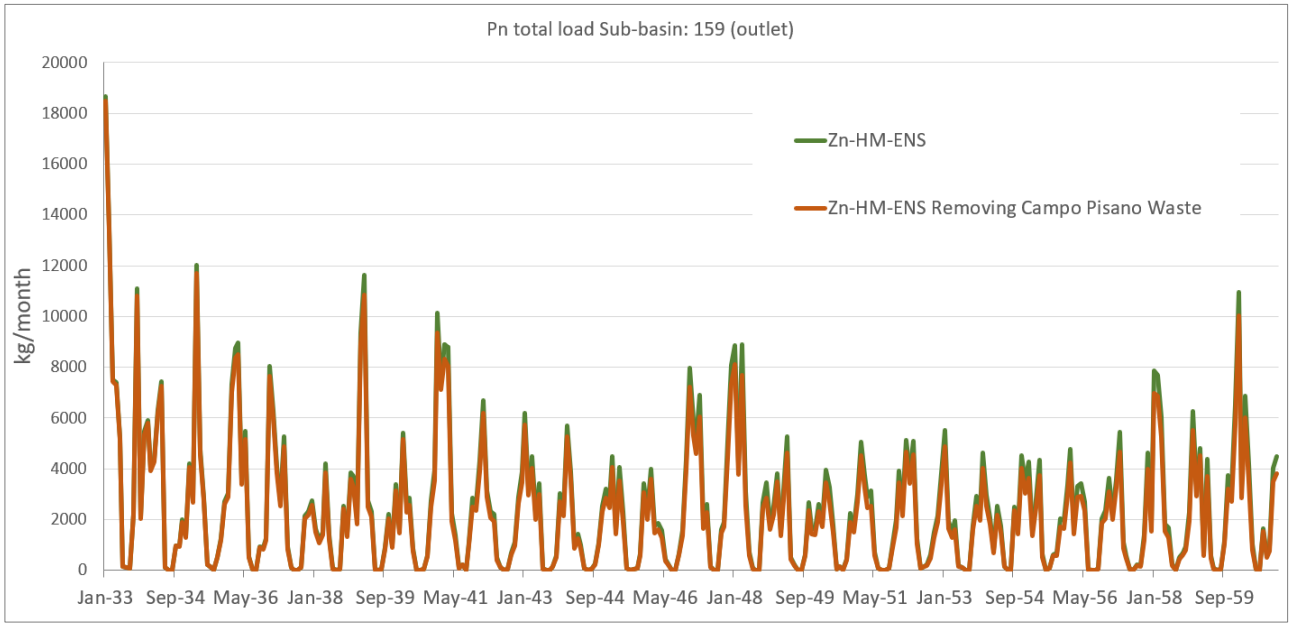

Figure 89 - Simulation of the effect of Campo Pisano waste removal on the total Zn load at the Rio San Giorgio's outlet

These simulations indicate that the multi-model tool could be used to assess priorities and targets for the remediation actions evaluating different scenarios. The results must still be considered qualitative and there is a need for better reliability that, in turn, can be fixed by a second process of

calibration using high density of data. Despite this, the tool is potentially very useful in environmental scenario assessment. In fact, simulating the effect of different waste management in the future, could give very important information to researchers and decision makers, helping to identify the major sources of pollution.

Resume and conclusions

The product of this research is a toolkit, composed by a set of numerical models and a web application, which allow simulating the fate and the transport of heavy metals along a watershed.
The numerical models are the well-known SWAT hydrological model and SWAT-HM, a new experimental metal transport model recently developed by researchers of the Beijing Normal University (Meng et al., 2018).
SWAT was calibrated comparing the simulated streamflow with observed streamflow in the nearest basin with a measurement station (Rio Mannu di Fluminimaggiore), performing well at daily (NS=0.66) and monthly (NS=0.88) time-step. The lack of a streamflow measurement station in Rio San Giorgio, which lead to calibrating the model to a nearby basin, was a primary uncertainty source in this study, considering the crucial role of the streamflow in metal transport. Starting from the hydrological cycle of SWAT, SWAT-HM simulated the processes that cause the metals' spread, such as weathering, erosion, leaching and interactions between the dissolved phase and the particulate phase in stream water. The SWAT-HM performances were evaluated on the capabilities of the model to reproduce observed concentration in stream water. The observed and simulated concentrations showed a reasonable agreement for some sub-basins, but still a large mismatch for some others, especially for Pb that resulted to be largely underestimated, while Zn simulations performed better results.
In order to run future projections of the metal transport, climate models of the Euro-CORDEX project (Giorgi et al., 2009) were used to force the transport model. First, a statistical analysis of the Euro CORDEX RCMs was performed, comparing the climate models with observed rainfall for a reference period (1979-2008) showing differences in the model performances. KNMI2, KNMI1 and CLM4 resulted to be the best performing models. Based on the performances of the climate models, a weighted multi-model ensemble was built-up. Once forced by the RCMs, the results of the SWAT hydrological model were analyzed, both for historical and future periods. SWAT future projections reflect the changes in precipitation predicted by the RCMs, showing a decrease of mean streamflow discharge and an increase of extreme outflows in occurrence of extreme precipitation events.
Simulations of the metal transport were run for historical (2001-2016) and future periods (2033-2060) for two of the main pollutants of the Rio San Giorgio catchment, namely Zn and Pb. Analyzing the historical simulations, SWAT-HM model tends to overestimate the loads for Zn and Pb when

high rainfall events occur, while largely underestimating loads during low flow periods if compared to measurements conducted by De Giudici et al. (2017) conducted in low-flow regimes. Zn shows a decreasing trend in time during simulation. As SWAT-HM has been recently developed, further studies should be conducted to prove its skills to simulate the metals' transport under different hydrological conditions, in particular for basin with low flow regimes and fast response to precipitation.

Future simulations, resulting from the combinations between the SWAT-HM model and the different climate models, project different trends. The Zn load projections depict an increase, if compared with the historical simulation, both at monthly (from ~2100 to ~2500 kg/month) and yearly scale (from ~26 to ~30 tons/year). The mean Pb load is expected to decrease significantly compared to the historical period, from ~800 to ~470 kg/month and from ~8700 to ~5700 kg/year. Two different scenarios of waste management were simulated for the future period: the removal of Fanghi Rossi waste and the removal of Campo Pisano waste. The results of these scenarios were compared to the "normal" scenarios, namely future scenarios with no changes in the watershed management that were previously analyzed. In the first scenario, the removal of Fanghi Rossi produces a diminution of -40% for the Zn total load and -34% for the Pb total load. In the second scenario, with the removal of Campo Pisano waste, only Pb has a significant diminution of the total load (-35%), while Zn decreases of -9%.

The results of the previous environmental monitoring and the SWAT and SWAT-HM simulations are available in the CESApp web application. CESApp allows to report measured and simulated loads, concentrations of the metals for each sub-basin in the Rio San Giorgio watershed. CESApp adds value to the models' results, giving the chance to analyze the spatial distribution of the pollution through dynamic maps, a very important component when assessing the sources of contamination. From this first analysis, this toolkit shows good potential to help in the context of mine reclamation. In particular, the multi-model approach used to simulate future scenarios could describe the possible evolution of the system in time, and it deserves further efforts to be improved.

Field analysis, that produces very accurate and detailed measurements, requires several years of sampling to delineate the trend and the behavior of a polluted watershed, with high costs in terms of time and money. Moreover, field analysis often lacks in terms of spatial distribution of the measurements, considering that the concentration of the metals can have a huge variation in space, while the models can better take in account this factor.

The toolkit is still limited when estimating pollutant loads, which could be improved with a more accurate calibration of both hydrological and metal model in a follow-up of the research project.

Furthermore, the multi-model tool is affected by the propagation of uncertainties and errors in input and output of the climate models, of the hydrological model and the metal transport model, which must be further reduced.

More detailed observations of streamflow discharge, concentration of the metals in stream water and loads under different hydrological conditions should be used to obtain a more satisfactory calibration and model reliability. Modelling the transport of metals, once the calibration has a strong basis and the uncertainty of the model is well defined, can produce useful information on the pollution status over time, with a significantly smaller time cost and economical effort compared to traditional methods.

Bibliography

Cidu, R., Fanfani, L., 2002. Overview of the environmental geochemistry of mining districts in southwestern Sardinia. Italy. Environ. Geol. 2, 243e251.

De Giudici G., Pusceddu C., Medas D., Meneghini C., Gianoncelli A., Rimondi V., Podda F., Cidu R., Lattanzi P.F., Wanty R.B., and Kimball B.A., 2017. The role of natural biogeochemical barriers in limiting metal loading to a stream affected by mine drainage. Applied Geochemistry 76. DOI: 10.1016/j.apgeochem.2016.11.020

Giorgi F, Jones C, Asrar GR (2009) Addressing climate information needs at the regional level: The CORDEX framework. WMO Bull 58:175–183

Meng Y., Zhou L., He S., et al., 2018. A heavy metal module coupled with the SWAT model and its preliminary application in a mine-impacted watershed in China. Science of The Total Environment, 613-614:1207-12